UNDERSTANDING MAGNETIC FLUX LEAKAGE (MFL) SIGNALS FROM MECHANICAL DAMAGE IN PIPELINES – PHASE II

Final Report
June 2008

Contract DTPH56-05-T-0001

Prepared by

L. Clapham, V. Babbar, K. Marble
and P. Weyman

Prepared for

United States Department of Transportation
Pipeline and Hazardous Materials Safety Administration

Table of Contents

Table of Figures

Table of Tables

UNDERSTANDING MAGNETIC FLUX LEAKAGE (MFL) SIGNALS FROM MECHANICAL DAMAGE IN PIPELINES – PHASE II

1.0 Introduction and Overall Project Objective

Pipeline inspection tools based on Magnetic Flux Leakage (MFL) principles represent the most cost-effective method for in-line detection and monitoring of pipeline corrosion defects[1]. These tools have been in commercial use for over three decades. Mechanical damage produces MFL signals, but as yet these signals are not sufficiently well characterized and understood to be used for reliable mechanical damage detection and characterization. The objective of this project is to accurately model MFL signals produced by mechanical damage in pipelines using Finite Element Analysis (FEA) and magnetic modeling techniques. The final, validated magnetic model, along with corresponding experimental measurements, will be used to produce a comprehensive dent/gouge MFL signal library made accessible to inspection vendors and pipeline operators for use in interpreting MFL signals from mechanical damage defects.

MFL signals from dents include a geometry component in addition to a component due to residual stresses. If gouging is present, then there may also be an additional magnetic contribution from the heavily worked material at the gouge surface. The relative contribution of each of these components to the MFL signal depends on the size and shape of the dent in addition to other effects such as metal loss, wall thinning, corrosion, etc. In this project, magnetic Finite Element Analysis (FEA) is used to model MFL signals from mechanical damage 'defects' having various sizes, shapes, and configurations. These models can include geometry effects, residual stress contributions and also magnetic behavior changes due to severe deformation. The modeled results are then compared with experimental MFL signal measurements on dents and gouges produced in the laboratory as well under 'field' conditions.

The Applied Magnetics Group (AMG) at Queen's University began working on mechanical damage in 2002. In 2002 and 2003, mechanical damage investigation formed a relatively small part (~30%) of a larger Gas Research Institute (GRI)-funded AMG project involved with examining stress effects on MFL signals (GRI Contracts # 5093-260-2605 and 5093-260-8682[2]). At that early stage, the magnetic modeling software* was limited in its geometric modeling capabilities; i.e., the dent shape could not be accurately modeled. In 2004, a new version of the software was released with improved geometrical modeling capability. This capability, combined with our GRI-funded experience in modeling stress effects, enabled construction of magnetic MFL models to account for both the dent geometry and associated stress distribution. GRI funding in 2004 enabled further work on modeling and corresponding experimental efforts on simple circular dents in steel plate samples[3].

The current 2006/07 study (year-end June 30, 2007) is the second year (Phase II) of a 4-year project that includes the following tasks:

* AMG uses Infolytica MagNet magnetic modeling software, which is the only magnetic modeling software that allows for the incorporation of "stresses" into the magnetic model via local modifications of the magnetic permeability functions.

- Year 1 (Phase I April 2005-March 2006): Magnetic modeling of MFL signals from simple dents (without gouges) in steel plate. Elongated dents with a 2:1 aspect ratio and long axis oriented in either the axial or circumferential directions were considered, Corresponding experimental work was conducted to verify magnetic models and examine dent depth effects.
- Year 2 (the current year – Phase II: July 2006-June 2007): Extension of Year 1 work on plain dents (dents without gouges) to a modeling and experimental study of backhoe-created dents in pipeline sections. Samples were produced by Gaz de France using their Pipeline Aggression Rig (PAR) – a simulated laboratory backhoe device that creates dents and gouges in sections of pressurized pipe.
- Year 3 (Phase III: July 2007- June 2008): Modeling and experimental work on gouges and dents+gouges. Work will involve magnetically characterizing severely damaged material typical of that found in a gouge region. Experimental and MFL modeling studies will be conducted primarily on gouges with little or no corresponding dent. MFL measurements on gouged samples from Gaz de France will be used to validate MFL models.
- Year 4 (Phase IV: July 2008 – June 2009) Sensitivity analysis (modeling and experimental) of MFL signal to changes in a number of dent characteristics – dent depth, length, wall thinning, dent sidewall slope, dent base shape.

2.0 Summary of All Previous Work

2.1 MFL and Stress Effects: Key Features

2.1.1 General description of samples and testing procedure

The MFL inspection technique involves applying a direct current (DC), axially-oriented magnetic field to the pipe wall using a set of large permanent magnets. The pipe wall is magnetized to near-saturation. Therefore, in regions of metal loss (such as a corrosion pit), some of the magnetic flux is forced (or 'leaks') into the surrounding air. A Hall probe or detector coil mounted between the magnet pole pieces detects this "leaking" flux as an MFL signal.

In corrosion detection, the size of the MFL signal correlates to the size of the corrosion region. However, a complicating factor in corrosion signal interpretation is the influence of stress. This is due to the fact that magnetism is strongly stress dependent, and that there are many different 'sources' of stress in an operating pipeline – applied (pressurization) stresses, residual stresses introduced during manufacturing and installation, in addition to stress concentrations around the defects themselves. In what is now recognized as a classic paper in the field[1], David Atherton (the founder of the Applied Magnetics Group at Queen's University) focused attention on the effects of stress on MFL corrosion signals, illustrating that stress may affect the magnitude of these signals by up to 50%. From 1998-2002, the AMG conducted an extensive GRI-funded study to characterize elastic and plastic deformation effects on MFL signals using both experimental and FEA techniques. This work provided an invaluable database of knowledge in this area, which is summarized in GRI reports[2,3] and a number of technical papers[4-7].

The understanding of stress effects gained in this earlier GRI-funded study is the foundation of the present MFL mechanical damage study. The following selected results from this earlier work are of particular importance:

- Elastic tensile strain creates an increase, and compressive elastic strain a decrease, in the magnetic permeability* of a pipeline wall. Therefore, local pipe wall elastic strain such as that associated with dents can enhance or decrease MFL signals depending on their sign, magnitude and orientation with respect to the applied MFL field.
- Earlier work has shown that magnetic properties are highly dependent on elastic strain, but very much less sensitive to plastic strain up to about 20% total deformation[8]. Therefore, for a plain (ungouged) dent only the elastic (residual) strain is expected to contribute to the MFL signal. It should be noted that gouges include much higher deformation levels, and that the plastically deformed material associated with gouges is expected to have an associated MFL signal. The effect of gouges will be considered in Phase III of this project.
- Because most of the effects on MFL signals arise from elastic (residual) strain, these effects can be largely removed in laboratory samples by using standard 'stress relieving' heat treatments.
- Working closely with the Infolytica MagNet FEA software[9] company, magnetization functions were developed by the AMG and implemented within the magnetic modeling software to allow the magnetic permeability to be varied both locally and anisotropically (i.e., in the three orthogonal directions). This enabled our group to conduct magnetic modeling of the multi-axial effects of stress on MFL signals.
- Extensive experimental testing of samples under stress and applied field conditions provided the critical magnetization function data needed for FEA modeling of stress effects on MFL signals.

2.2 Summary of 2004 GRI-Funded Study[3]: MFL Signals from Circular Dents (Modeled and Experimental)

In 2003, improvements in the Infolytica MagNet FEA modeling software [9] made it possible to more accurately represent dent geometries, and in 2004, this capability was extended to model MFL signals from simple circular dents (note 'simple' implies no gouge is present). Figure 1 shows the magnetic model used in the 2004 study[1]. A detailed description of the magnetic MFL modeling process is provided in Section 5. The discussion that follows provides only a brief background relevant to a description of the 2004 study.

* Magnetic permeability is the proportionality constant between applied field and induced flux density in a material. It is not constant, but is a function of applied field and the local stress level.

[1] A detailed summary of this work can be found in reference 6.

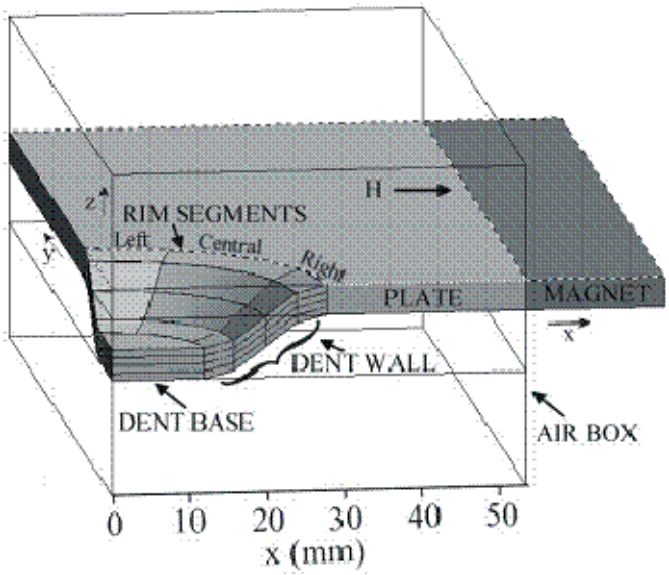

Figure 1: Magnetic FEA model used in the 2004 GRI-funded study of MFL signals from circular dents. Only a quarter-model is used because of symmetry considerations. The air box is the rectangular parallelepiped lying between the topmost horizontal surface and lowermost horizontal surface of the model.

As shown in Figure 1, the circular dent model is divided into 'dent rim' and 'dent base' regions, and these regions are further subdivided into blocks through the thickness of the wall. Different blocks can be assigned different anisotropic permeability functions, depending on the stress level in each block. The stress levels were determined using structural FEA modeling.

Additionally, it is worth noting that the result of the modeling process is a 3D magnetic vector field. The MFL signal itself is represented by either the radial, axial or circumferential component of this field. Experimentally, each of these MFL signal components can be measured separately through appropriate orientation of the detector (usually a Hall probe). Traditionally, pipeline inspection vendors have used the axial component of the MFL field (MFL_{axial}) however our experimental work typically involves obtaining all three signal components.

The overall FEA-modeled MFL_{radial} signal (radial component), incorporating both geometry and stress contributions, is shown in Figure 2 (note that this is a quarter-model representing the upper right quadrant). Figure 3 shows the experimental MFL_{radial} signal obtained from laboratory measurements on a 40-mm diameter circular dent of 7mm depth. The experimental (Figure 3) and modeling (Figure 2) results match very closely. Furthermore, since stress effects could readily be turned 'on' or 'off' in the magnetic FEA model, it was possible to identify the individual effects of stress and dent geometry. These modeling results enabled determination of the origin of each specific feature in the experimental result of Figure 3, specifically:

- The circular dent geometry gives rise to two central peaks (labeled 'geometry peaks' in Figure 3) of opposite polarity.
- The stresses in the dent rim create a significant shoulder peak (labeled 'rim stress peak' in Figure 3). This appears to combine with the similar polarity outer geometry peak, creating what appears to be a "halo" effect.

- An additional stress peak is also associated with the dent base (labeled "dent base stress peak' in Figure 3), but this peak is obscured by the main geometry peak.

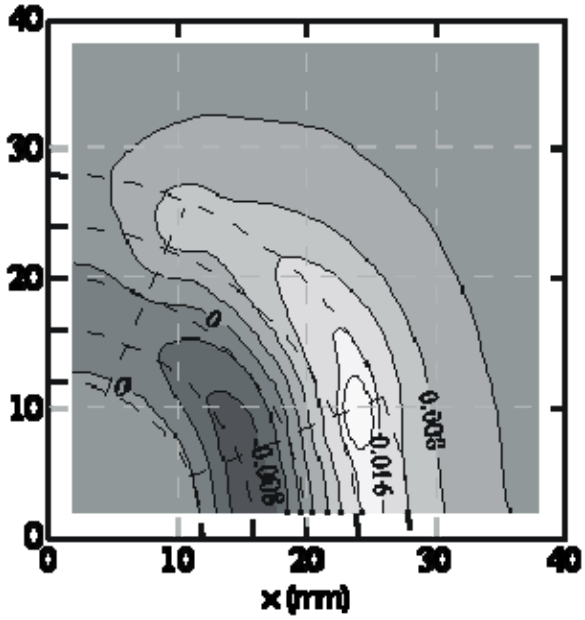

Figure 2: Quarter-model magnetic FEA result for the MFL signal (radial component) shown as a contour plot. This corresponds to the upper right-hand quadrant of the experimental signal shown in Figure 3. Both stress and geometry contributions to the MFL signal are included.

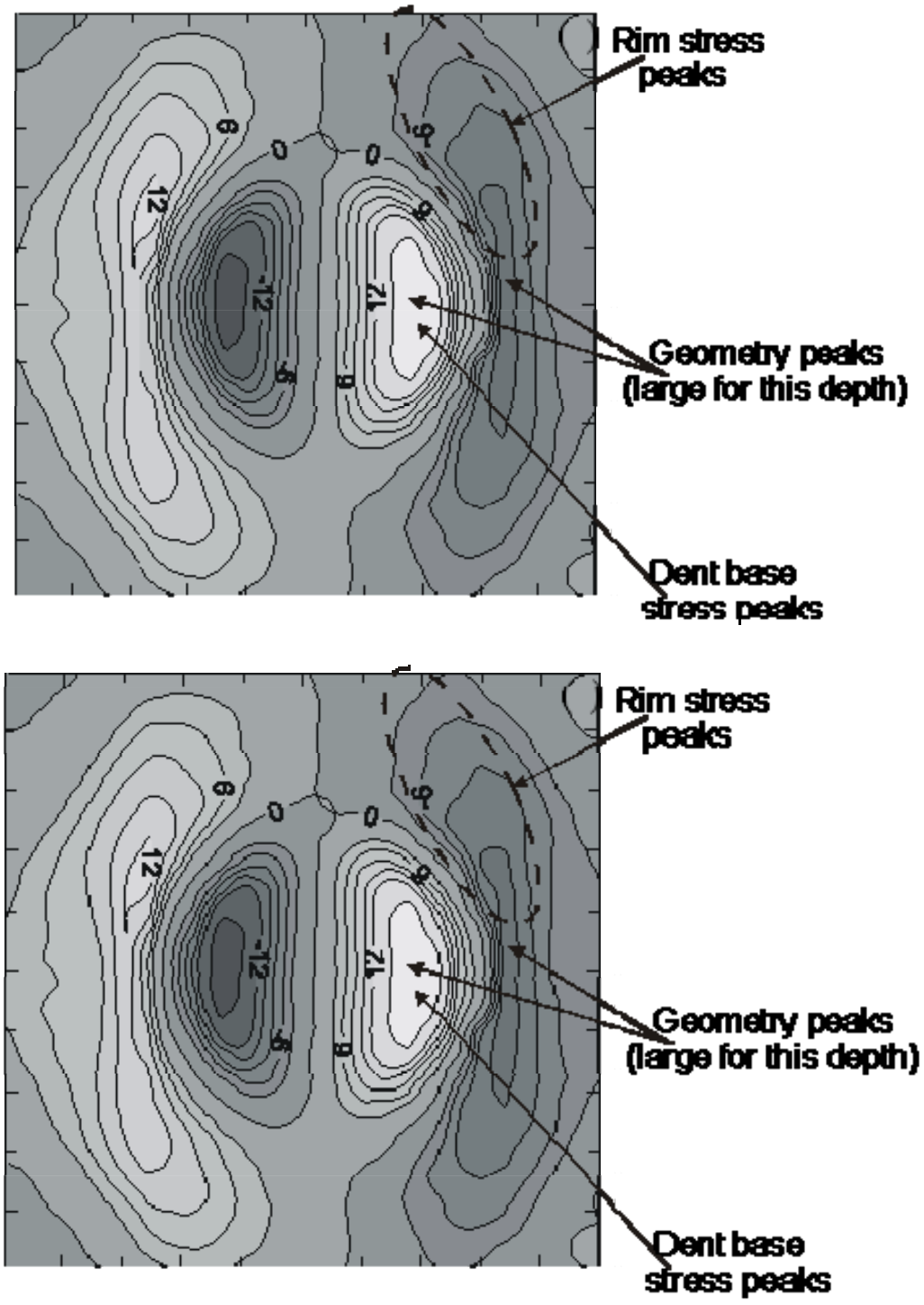

Figure 3: Experimental MFL radial component contour plot for a 40-mm diameter circular dent. The FEA modeled result shown in Figure 2 enabled the individual features of this MFL result to be associated with either geometry or stress as indicated in the diagram. (Note that the peak polarity is reversed compared with Figure 2 because the field is applied in the opposite direction.)

2.3 Summary of work in PHASE I (April 2005-March 2006) of the current project

As noted in section 2.2, work conducted prior to the current DOT PHMSA/PRCI contract involved preliminary experimental work and modeling studies of circular plain dents in plate samples, with the dents created using a hydraulic press. In Phase I of the current contract (which began April 2005) this work was extended to include 2:1 aspect ratio elongated dents, oriented in both the axial and circumferential directions. As with the study of circular dents, the work involved a combination of modeling and experimental studies. On the modeling side, structural finite element analysis (FEA) modeling was used to evaluate the stress distribution around a dent. The elastic strain information from these structural FEA models was used to assign permeability functions within the magnetic models. As in the circular dent study, both MFL signal effects of dent geometry and local stress were examined.

Experimental work paralleled that of the modeling work. 2:1 aspect ratio dents of varying depths (3mm-8mm) were produced in 3mm thick steel plate samples. Full contour plots of MFL signals from these dents were then obtained in each of the radial, axial, and circumferential component directions. Selected dents were stress-relieved using standard annealing treatments, and then re-measured to examine the difference between the 'geometry+stress' and 'geometry-only' MFL signals. These experimental signals were then compared to the modeling results in order to verify and further refine the models.

The matrix of samples studied and MFL results obtained from this study are summarized in Table 1. It should also be noted that numerous 4:1 aspect ratio samples were also produced and measured; however these results were not included in the report except for comparison purposes.

Table 1: The matrix of samples studied and MFL results obtained from this study

Location	2:1 Dent Orientation	Dent Depth (mm)	Metal Condition	Measurement Orientation	Number of Contour Plots Produced
Topside	Circumferential	3, 4, 5, 6, 7	Before annealing; After annealing	MFL_{radial} MFL_{axial} MFL_{circ}	30
Topside	Axial	3, 4, 5, 6, 7	Before annealing; After annealing	MFL_{radial} MFL_{axial} MFL_{circ}	30
Underside	Circumferential	3, 4, 5, 6, 7	Before annealing; After annealing	MFL_{radial} MFL_{axial} MFL_{circ}	30
Underside	Axial	3, 4, 5, 6, 7	Before annealing; After annealing	MFL_{radial} MFL_{axial} MFL_{circ}	30

The results of the Phase I study are briefly summarized below.

2.3.1 Axially-elongated 2:1 aspect ratio dents: modeling and experimental studies

Figure 4 shows a typical MFL_{radial} result for an axial 2:1 dent, in this case depth of 6mm. The three color photos show the modeled result – the two at the top are the separate MFL signal contributions of geometry and stress, respectively, and the bottom left plot is the combined stress + geometry modeled result. The experimental result is shown on the bottom right, with good agreement shown.

As seen in Figure 4, both geometry and stress have considerable and interesting effects on the axially elongated dent signals:

- The geometry signal displays a characteristic '4 peak' MFL_{radial} signature along the line of the dent in the applied field direction. The two outside peaks are associated with the outer dent rim 'corner', while the two inner peaks originate from the corner at the dent base. This result is similar to that seen in circular dents – however as the dent aspect ratio increases the peaks migrate further away from the dent center.

- The main stress contribution to the MFL_{radial} signal is associated with the dent rim 'sidewall' – i.e. the rim along the long side of the dent. This produces a significant vertical peak which tends to be positioned approximately over the central dent geometry peak.

- The combined effect of geometry+stress on MFL_{radial} signals is very interesting in this case, since the dent sidewall stress contribution lies over the inner dent geometry peak but is of opposite polarity. This has two effects –
    1. to diminish the size of the inner geometry peak; and
    2. to 'create' an apparent additional peak in the centre dent sidewall rim region. This peak is actually a composite of geometry+stress effects. While this additional peak appears fairly slight in the 2:1 aspect ratio dent, studies on the 4:1 aspect ratio dent indicated that this produces a very evident 'additional peak' close to the center of the dent.

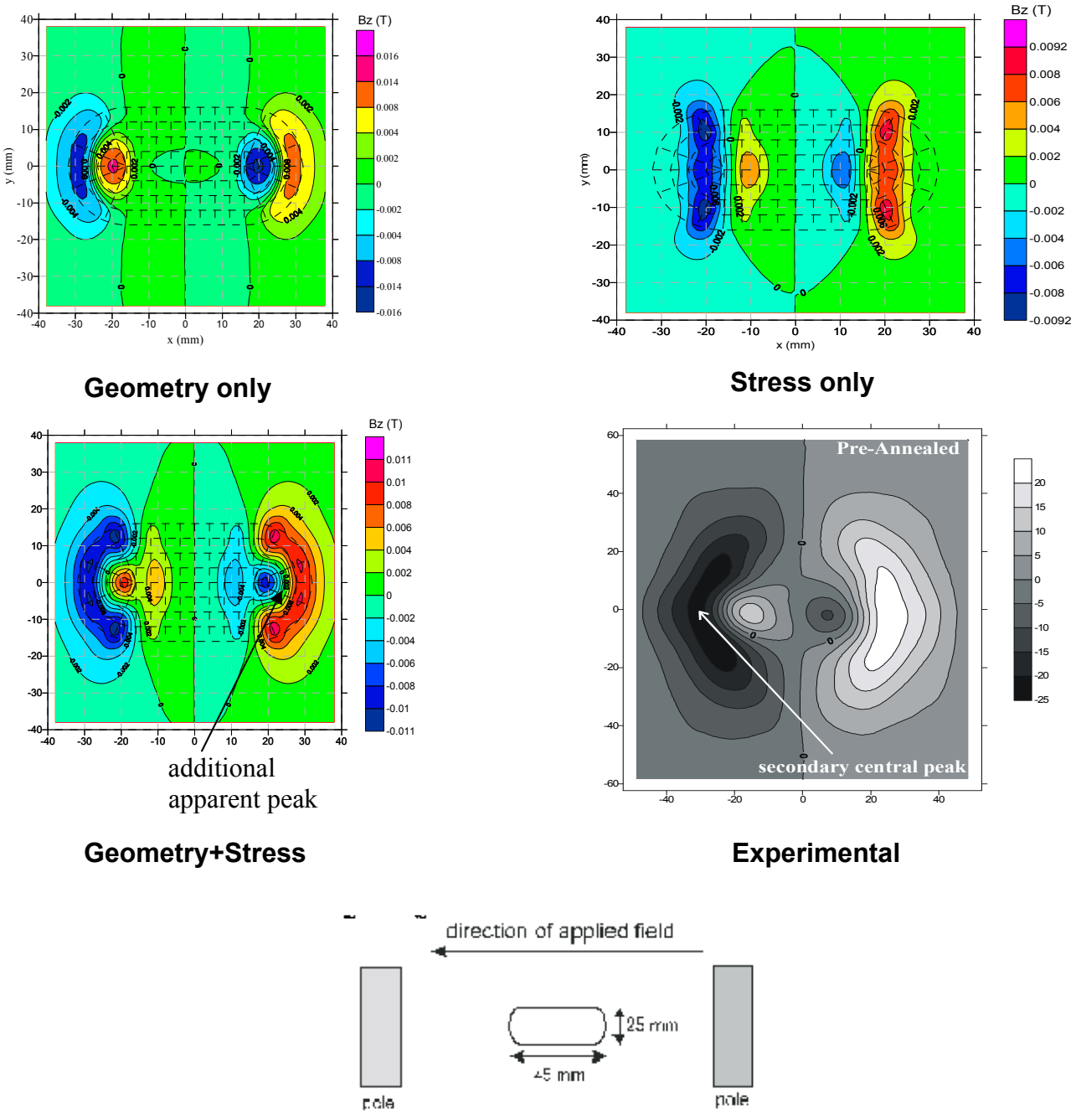

Figure 4: MFL_{radial} result for an axially elongated 2:1 dent, 6mm deep. The relative dent and applied field orientation are shown in the schematic at the bottom. The three color photos show the modeled result – the two at the top are the separate contributions of geometry and stress, respectively, and the bottom color plot is the combined modeled result. The experimental result is shown on the bottom right, with good agreement apparent.

2.3.2 Circumferentially-elongated 2:1 aspect ratio dents: modeling and experimental studies

Figure 5 shows a typical MFL_{radial} result for a circumferential 2:1 dent, in this case of depth 6mm. The three color photos show the modeled result – the two at the top are the separate contributions of geometry and stress, and the one at the bottom is the combined modeled result. The experimental result is shown on the bottom right, with good agreement shown.

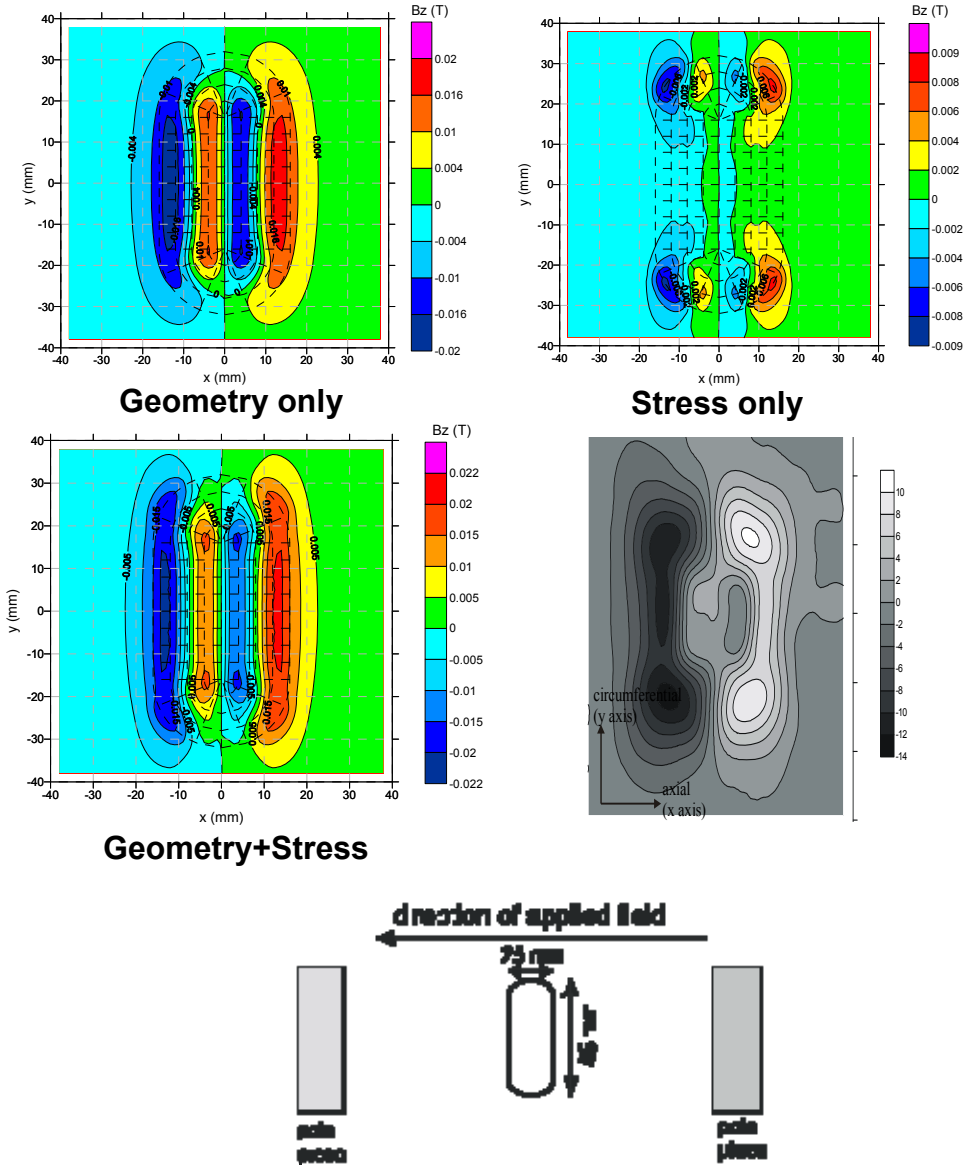

Figure 5: MFL_{radial} result for a circumferentially elongated 2:1 dent, 6mm deep. The relative dent and applied field orientation are shown in the schematic at the bottom. The three color photos show the modeled result – the two at the top are the separate contributions of geometry and stress, respectively, and the bottom color plot is the combined modeled result. The experimental result is shown on the bottom right, with good agreement apparent.

The experimental and modeled MFL_{radial} signal results for the circumferentially-oriented elongated dents are summarized below:

- The geometry signal consists of 4 peaks as with in earlier circular and axial dent cases, however due to the circumferential elongation of the dent these central peaks are much closer together and also elongated in the circumferential direction.
- Sidewall dent rim stresses have little effect on the MFL signal for this dent orientation. The stress effects on the signal are mainly in the form of shoulder peaks at the extreme ends of the signal (in the circumferential direction).

- Combined stress + geometry signals are relatively simple to interpret in this case and reflect a straightforward superposition of the two effects on the signal.

2.3.3 Experimental comparison of MFL_{radial}, MFL_{axial} and MFL_{circ} dent signals

Experimental studies examined both topside and also underside MFL signals from a range of depths, both in the axial and circumferential orientation. The following points were noted:

- The MFL_{radial} signal component consistently displays the largest and most detailed signals. This is due to the fact that the sensor lies closer to the surface in this orientation than in the other two.

- The MFL_{radial} and MFL_{circ} signals contain distinct stress-related and also geometry-related features (peaks). For both these components the central peaks tend to be geometry related, with dent rim stresses reflected in shoulder peaks. The MFL_{axial} component appears to have no specific stress-related features and also appears similar to signals produced by corrosion pits.

- All MFL signal features diminish slightly with stress-relief annealing, however the magnitude of the shoulder peaks is considerably affected by annealing, reinforcing the conclusion that they tend to be related to residual stress.

A major conclusion from this aspect of the work is that, for dent detection and sizing, inspection tools should measure all three components of the MFL signal, rather than just the MFL_{axial} signal as is typical in most cases.

2.3.4 Circular dents containing corrosion pits: modeling and experimental studies

In addition to extensive studies of elongated 'plain' dents, the Phase I study also included circular dents containing centrally located corrosion pits. Through-wall pits of 2, 4 and 24mm diameter were created in 40mm diameter circular dents. Both modeling and experimental work indicated that the MFL signals for the combined pit+dent were a simple superposition of the two signals. The pit was centered in the middle of the dent, so clear signals from pit and dent were seen when the dent was relatively small. In the 24mm diameter pit there was considerable overlap with signals and interpretation became more difficult.

2.3.5 Web-based database – preliminary work

The ultimate goal of this project is to produce modeled and experimental MFL signal results from dents of known shapes and stresses. With a very large number of results, effective presentation becomes an issue. In Phase I we presented a relatively simple proposed format for a web-based results spreadsheet which should allow for easy access to both modeled and experimental results of this study. Further expansion and development of this database continued in Phase II as described below.

3.0 Specific Objectives of Phase II

In Phase I of the project the experimental work consisted entirely of producing dents in samples of 3mm thick steel plate using a laboratory denting tool available at Queen's. In Phase II we were fortunate to gain access to samples created using the Gaz de France Pipeline Aggression Rig (PAR). The PAR is a laboratory backhoe simulation facility that is used to reproducibly introduce a variety of 'realistic' dents and gouges into pressurized pipeline sections. These dented and gouged samples are later cut out of the pipe section and saved as coupons for later use. The focus of the work in Phase II was to measure and model MFL signals from this selection of mechanically damaged coupons available at the Gaz de France facility in St. Denis, France. The main focus of this work was measurement of signals from dents; however since gouge samples were also available some preliminary gouge measurements were made in addition to the dent studies. Specifically, the project objectives for Phase II were as follows:

- To upgrade the existing laboratory MFL testing rig at Queen's to make it portable and more robust for travel to the Gaz de France facility in St. Denis, France.

- To upgrade the existing MagNet MFL FEA models to be able to accommodate larger, asymmetrical dents more typical of realistic pipeline dents.

- To travel to the Gaz de France facility to measure MFL signals from dented samples produced using their Pipeline Aggression Rig.

- To do preliminary modeling of 'realistic' gouges.

- To make preliminary MFL measurements on some of the gouged samples available at Gaz de France.

- To incorporate these results (modeled and measured) into the web-based MFL signal library database developed in Phase I of the study.

4.0 Work Plan for Phase II

Specific elements of the work plan for the project period starting July 1, 2006 and ending June 30, 2007 are outlined in task list (PHMSA payable milestones table) shown below. Details of the experimental procedures and FEA modeling methods are given in Section 5.

Table 2: Work plan for Phase II

Item #	Task #	Payable Milestone	Quarter	Date	Month Completed
19	**6.1**	**Renew finite element magnetic modeling software**	**VI**	**Sep-06**	**18**
20	**6.2**	**Upgrade magnetic models to accommodate (larger) backhoe dents**	**VI**	**Sep-06**	**18**
21	**6.3**	**Upgrade existing MFL testing rig to accommodate (larger) pipeline samples**	**VI**	**Sep-06**	**18**
22	**6.4**	**Stress FEA modeling of plain dents**	**VI**	**Sep-06**	**18**
23	**4**	**Sixth Quarterly Status Report & Technical Committee Mtg.**	**VI**	**Sep-06**	**18**
	4, 6	**Sixth Payable Milestone**	**VI**		**18**
24	**6.5**	**Modeling of MFL signals from plain dents in pipe geometries**	**VII**	**Dec-06**	**21**
25	**6.6**	**Measurement of MFL patterns (3 components) around plain dents**	**VII**	**Dec-06**	**21**
26	**4**	**Seventh Quarterly Status Report & Technical Committee Mtg.**	**VII**	**Dec-06**	**21**
	4, 6	**Seventh Payable Milestone**	**VII**		**21**
27	**5**	**Pipeline Safety Research Peer Review**	**VIII**	**Jan-07**	**22**
28	**6.7**	**Analysis of MFL patterns from measurements done in Task 6.8**	**VIII**	**Mar-07**	**24**
29	**7.1**	**Modeling of MFL patterns around gouged dents in pipes**	**VIII**	**Mar-07**	**24**
30	**7.2**	**Measure MFL patterns around gouged dents**	**VIII**	**Mar-07**	**24**
31	**4**	**Eighth Quarterly Status Report & Technical Committee Mtg.**	**VIII**	**Mar-07**	**24**
	4, 5, 6, 7	**Eighth Payable Milestone**	**VIII**		**24**
32	**7.3**	**Analysis of MFL patterns from measurements done in task 7.3**	**IV**	**Jun-07**	**27**
33	**8.1**	**Complete lab dent results database**	**IV**	**Jun-07**	**27**
34	**8.2**	**Complete pipeline dent results database**	**IV**	**Jun-07**	**27**
	8	**Ninth Payable Milestone**	**IV**		**27**

5.0 Work Performed During Phase II

This section summarizes the work completed in the current year, as follows.

5.1: Outline of the experimental technique and modifications to MFL equipment
5.2: Structural FEA modeling results from Gaz de France.
5.3: Magnetic FEA modeling
5.4: Gaz de France dented samples: Experimental and modeling results
5.5: Gaz de France gouged samples: Preliminary experimental and modeling results

5.1 Outline of experimental technique and modifications to MFL equipment

5.1.1 Upgrade of MFL testing rig to accommodate larger, curved pipeline sections

As mentioned earlier, we were fortunate to have the in-kind support of Gaz de France, who has a full sized 'laboratory' backhoe pipe denting facility. Over the past few years, Gaz de France has produced a number of dents and gouges of varying severity and dimensions in full pipeline sections. Typically the dent regions of these pipelines are removed as 'coupons' and then stored for future use. Gaz de France made these pipeline sample coupons available for MFL measurements by our Queen's group for the purposes of the current contract. However these samples were located in the St. Denis (Paris) facility of Gaz de France, meaning we had to transport our MFL measuring equipment there. Our original laboratory-based MFL system was not designed for portability; neither could it accommodate the curved nature of a pipeline sample, nor samples containing dents of very large dimension. Therefore experimental work early in Phase III involved modifying the components of our MFL stress rig to make them more robust, and appropriate for larger dents in pipeline geometries. The following modifications were made to the rig:

1. Replaced the CRT monitor with a flat screen monitor (lighter, more portable).

2. Upgraded the Labview system on the MFL computer. Initially we considered the possibility of replacing our desktop MFL computer system with a laptop. However a laptop containing the appropriate DAC (Data Acquisition card) for taking measurements and driving the XY scanner proved to be prohibitively expensive, and largely unnecessary. As a result we used the original MFL computer system, equipped with a transformer to accommodate the power requirements.

3. Upgraded and refurbished the XY scanner for use on larger samples. Many of the MFL scans that were done as part of the earlier work were conducted using salvaged XY plotter systems. However these systems are not sufficiently robust for transport. As a result, we upgraded an existing XY stepper-motor driven scanning system for use on these samples. This system had been in use for another project and needed repair and refurbishment. This work was completed successfully, plus we redesigned the MFL probe carriage. MFL probes are Hall probes, which measure a single component of a magnetic field. Three new housings were constructed for the circumferential, axial and radial-oriented probes. Quick connection electrical couplings were produced to facilitate

probe switching and each of the probe housings were fitted into a spring-loaded probe holder mounted at the end of the arm on the XY scanning system.

4. Modified the MFL circuit pole piece components. Earlier, magnetic circuit pole pieces were not appropriate for use on pipeline sections since the pipe surface was curved. Therefore, a number of different 'end sections' for the pole pieces were constructed. Each of these end sections has a curvature that will exactly match that of the dented sections available at Gaz de France, i.e. to accommodate 16", 20", 24" and 36" diameter pipe sample coupons.

Figure 6 below shows two views of the equipment during scans of the inside surface of a pipe coupon at the Gaz de France facility.

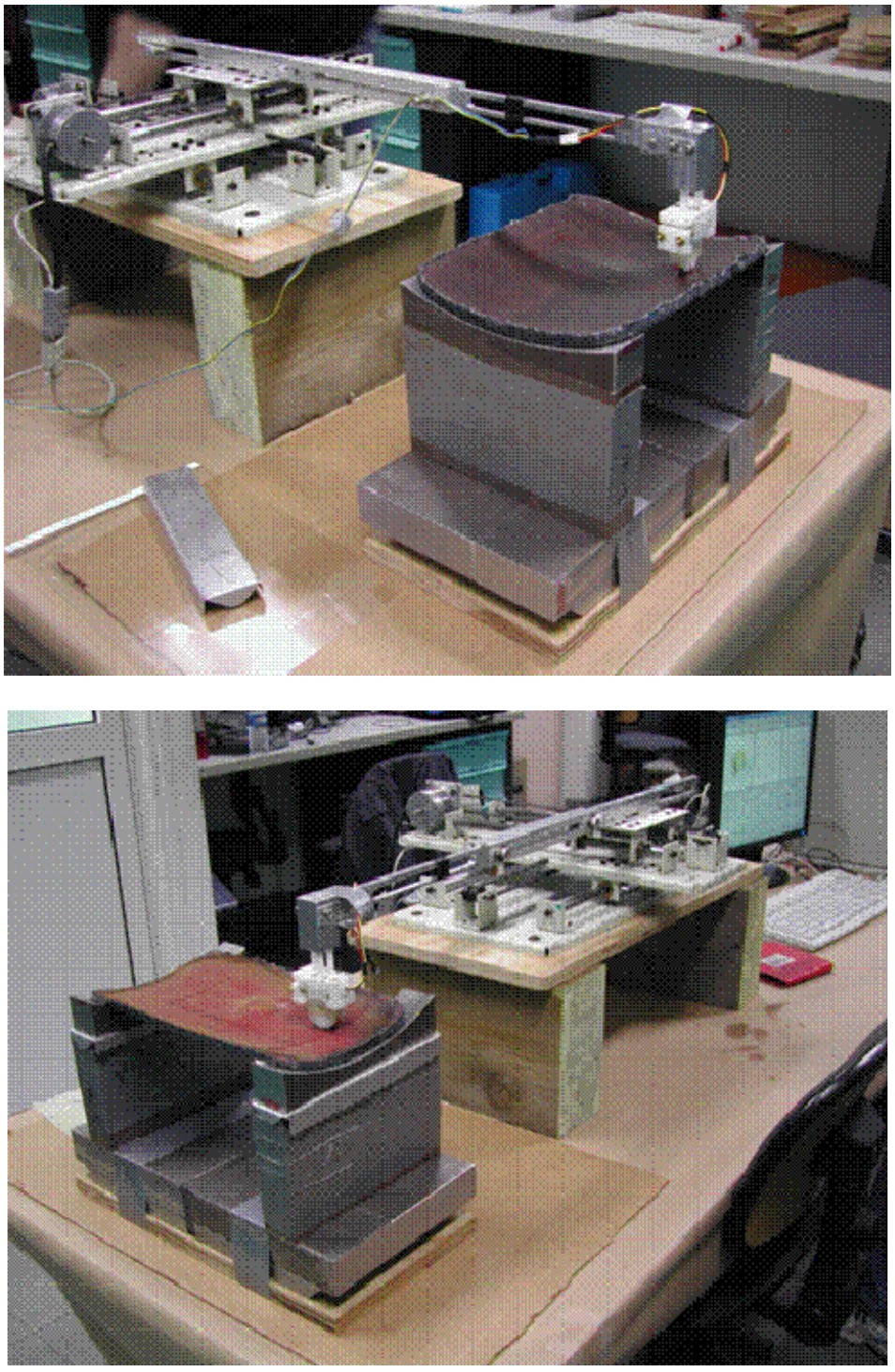

Figure 6: Two different views of the Queen's MFL testing rig, during scanning of a dented sample coupon at the Gaz de France facility.

5.2 Structural FEA modeling results from Gaz de France.

As noted earlier, the local **elastic strain** around a mechanically damaged region can significantly influence the MFL signal. Our magnetic models have the capability of incorporating the effects of elastic strain on magnetic properties, as will be described in later sections. Therefore it is necessary to first conduct **structural** FEA analysis in order to determine the local stress/strain levels. These strains are then used to calculate magnetic parameters for input into our models.

Structural modeling for a 'realistic' dent was conducted by Gaz de France, for the modeled case of pressurized pipe which was subsequently dented by a backhoe tooth. The pipe section containing the dent (at the right-hand top location) is shown in Figure 7. Symmetry conditions enabled only a half-pipe section to be considered.

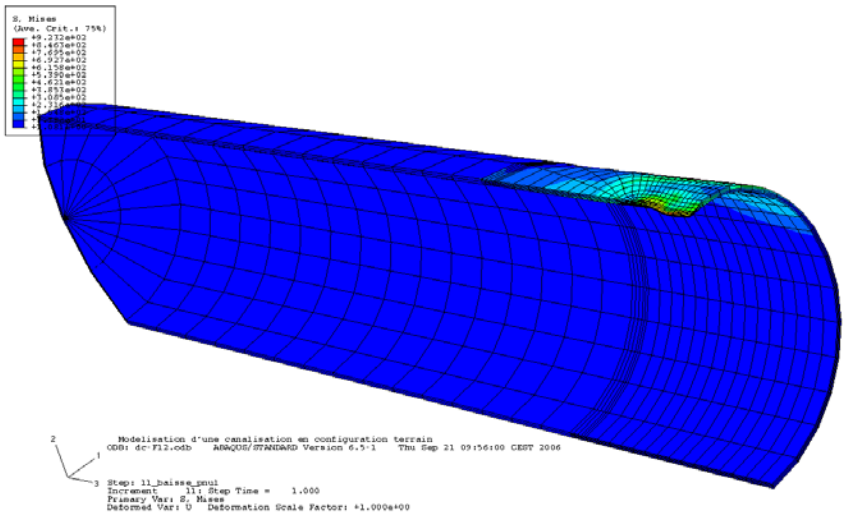

Figure 7: Half pipe section showing backhoe dent at closest end (at top).

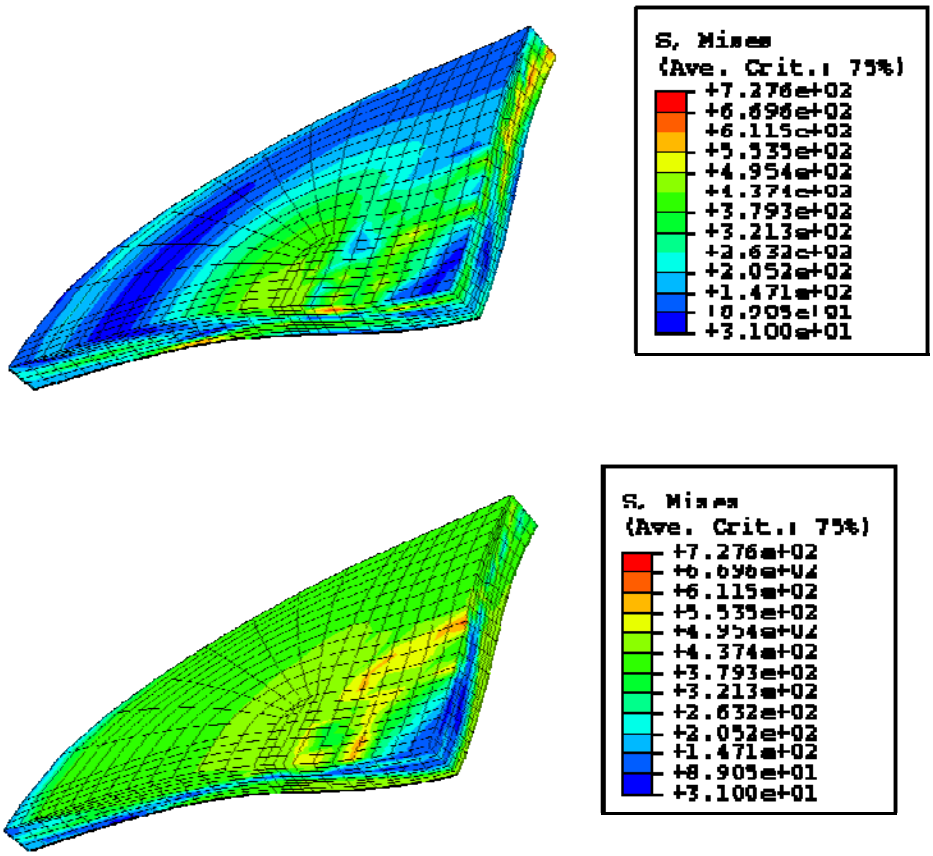

Figure 8: von Mises stress plots in the dent vicinity – before and after pressure cycling.

A large number of stress and strain plots were produced from this model. These are not documented in this final report, however Figure 8 shows a couple of examples of Von Mises stress results before and after pressure cycling.

It is important to note that local elastic stress levels will be highly dependent on the stress history of the pipe section. In the aforementioned model, a dent is introduced into a pressurized pipe, followed by some pressure cycling. However, the experimental dents available at the Gaz de France facility have a significantly different stress history than that represented by this particular model, since the pipe they were contained in was also pressure tested to failure, and then the region containing the dent was cut out of the pipe. As a result of the likely differences in local strains between the model and the sample coupons (on which MFL measurements were made), the stress influences on the MFL signal were NOT incorporated into the magnetic models at this point. This will be further discussed in a later section.

5.3 Magnetic FEA modeling techniques for dents in pipeline samples using Infolytica's MagNet 6.16.3

Real backhoe dents encountered in the pipeline industry are generally larger than the laboratory-produced dents studied in Phase I. Furthermore, they often lack axial or circumferential symmetry, in addition to experiencing wall thinning and non-uniform depth. The development of the relatively "simple" quarter-model dent geometry employed previously was challenging in itself. Introducing asymmetry and modeling 'true' dent geometry is at least an order of magnitude more difficult, and we have invested considerable time and effort in the current year on this task. Due to the challenges in geometrically modeling the dent, coupled with the fact that accurate local stress modeling of the local dent region are not yet available, the focus of the Phase II modeling effort was to investigate predominately the geometrically-induced MFL signals.

Within this section we discuss the progression of our modeling efforts in the past year. Initially, these effort involved attempts to model dent geometry using a 'direct manual' approach (section 5.3.1) – essentially measuring the dent manually and attempting to reconstruct the main features into the model geometry. These attempts were unsuccessful, and led to a "progressive asymmetry" approach (section 5.3.2) where the starting point was a completely symmetrical dent, with asymmetry gradually introduced. Finally at the end of the year we spent considerable time and effort developing a workable software interface to effectively 'import' laser scan data (available from Gaz de France for their dent samples) directly into the MagNet modeling software (section 5.3.3).

5.3.1 The Direct Manual Approach to producing Dent models in MagNet

It is worthwhile noting at the outset that the existing MagNet modeling software does not include the capability of importing a model geometry from any form of standard design software (e.g. AutoCad). The functionality is such that models must be built and modified within MagNet itself.

As such, our first attempt to develop a realistic dent model involved trying to directly 'build' a model by replicating the geometry of an actual pipeline backhoe dent. Although this attempt was unsuccessful and quite time-consuming, it was useful in that it enabled us to probe some of the limitations of the modeling software. The work is described below.

We procured a backhoe-dented pipeline sample from an industry source, and used it to develop a model using our magnetic modeling software MagNet 6.16.3. The sample was an X70 pipeline sample coupon of thickness 6.5 mm containing an elongated dent of length 145 mm, width varying from 20 mm to 27 mm, and depth varying from 0 to 13 mm. A detailed physical examination of the dent (Figure 9) helped us determine the following dimensional constraints for the initial modeling work:

1. The topside (outer pipe wall) cross-section of the dent is essentially rectangular except for a variation in the width. The topside edges are blunt and the inside corners are round along the

length of the dent. The underside (inner pipe wall) of the dent has an elongated round shape, which is quite similar to that of our earlier elongated laboratory dents of comparable size.

2. The plate thickness is non-uniform in the dented region; the variation in thickness is estimated to be ±1-2 mm.

3. The dent is broadly symmetrical across an axial plane normal to the pipe wall and dividing the width in two halves, thus making it possible to work with a half model with two-fold symmetry.

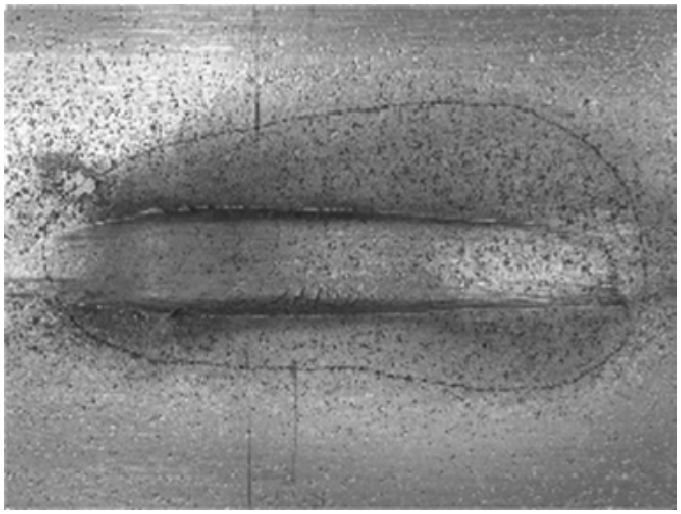

Figure 9: Photograph of the pipeline backhoe dent used from which the model dimension was derived. The dent was axially oriented, of length ~145mm (topside view).

Considering the large size and complex geometrical requirements, we first chose to build a quarter model with a four-fold symmetry then extend and modify it as a half model. The steps to constructing the model are described as follows: the central part of the quarter model is shown in Figure 10 having a wall thickness of 6 mm. The front xz cross-section of the plate was split into 8 small sections each of width 5 mm. The first two sections are linear but have an inclination of 2.5° with the horizontal. This was done to make the depth non-uniform. The next two sections are circular arcs of radius 89 mm and angular widths of 8° and 7.5°. Fifth and sixth sections are again linear, while the last two sections are circular arcs each of radius 98 mm and angular width 9°. Another similar row of 8 sections is stacked at the back of the front row to increase the width of the plate to 10 mm as shown in Figure 10.

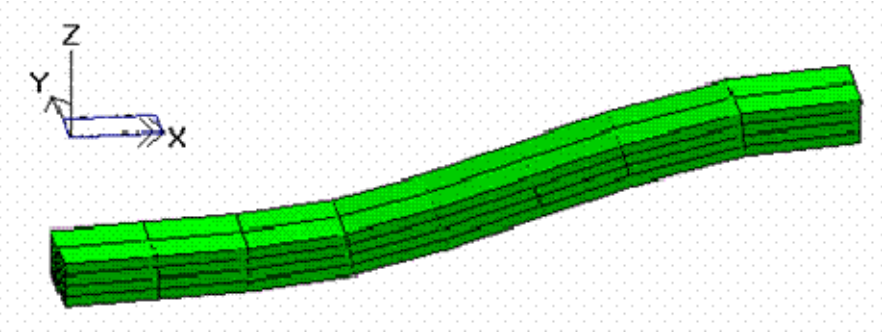

Figure 10: Central part of the quarter model of backhoe dent.

The second row was extended into circular arcs, but ended up producing arcs of different radii and thus a dent of non-uniform width as shown in Figure11. This incorrect geometry was obviously caused by the inclined components of the second row. A number of attempts were made to fix this problem. New models were drawn after changing the size and shape of the elements and extending them in arcs of different radii but without much success. Some of these elements overlapped neighboring elements, leading to an insolvable model.

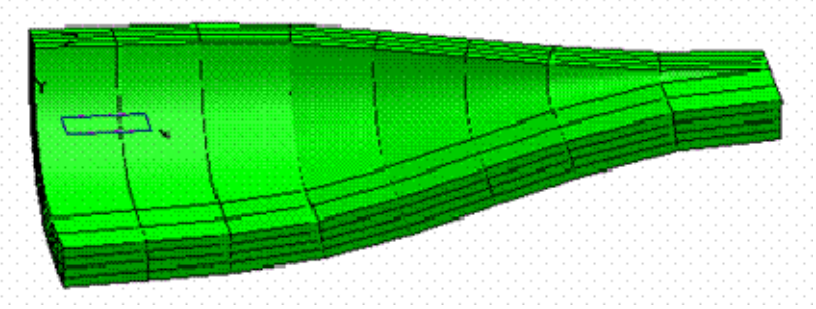

Figure 11: Addition of curved sidewall to the base produced dent of non-uniform width.

Thus we determined that a simplified approach was necessary for modeling complex geometry. A decision was made to prepare a more simplified, symmetrical dent model, and subsequently add asymmetry to the model to see how significantly it affects the MFL result. The symmetrical dent model we constructed is described below in section 5.3.2.

5.3.2 The "Progressive Asymmetry" approach to producing Dent models in MagNet

The topside view of the "starting point" symmetrical half-model dent is shown in Figure 12. The model has overall plate dimensions of 176mm x 108mm x 8mm and magnet dimensions each of 24mm x 108 x 8mm. The topside cross-section of the half dent is rectangular with dimensions 128mm x 16mm with the maximum depth of 16mm. The model consists of about 360 elements. The minimum mesh size used in the gouged region is 2mm. Field Normal boundary conditions were used on the outer surfaces (parallel to yz plane) of the magnets. The H_x field in the plate was about 30,000 A/m just outside the dented region and about 22,000 A/m in the base region inside the dent.

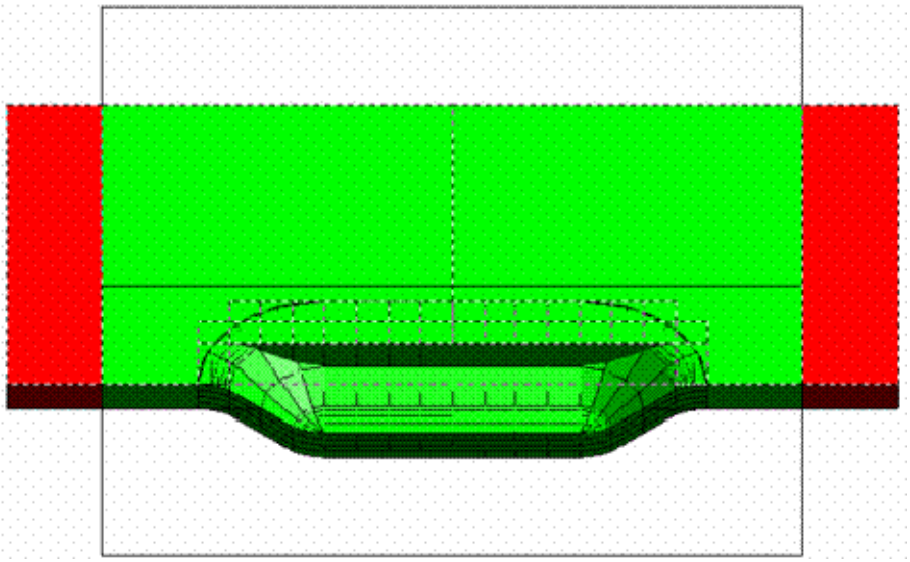

Figure 12: Half model of the backhoe dent.

To introduce asymmetry into the dent, the 'Distort Vertices' option available in the software was used to introduce non-uniform thickness. Although this produced the required geometry, meshing was unsuccessful using this method, apparently because of neighboring element overlap. Success was finally achieved through resizing the sections of the top layer to make a stepladder with a step size of 0.25mm, thus producing a model of variable base thickness and pit depth. The underside geometry was left unchanged and is similar to the symmetric case described in the previous report.

The topside of the asymmetric half model is shown in Fig. 13. The thickness of the base plate near the left side of the dent is 6mm, which is 2mm less than the thickness near the right side.

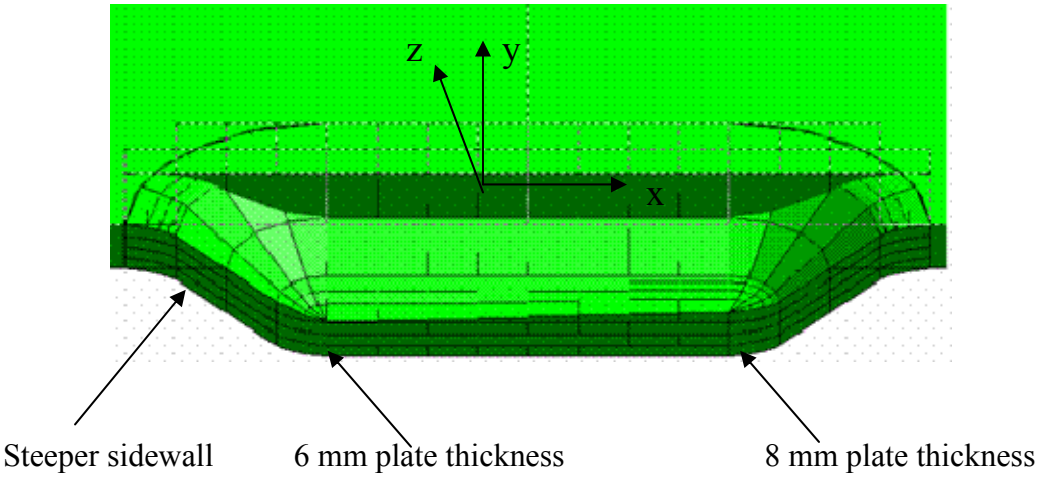

Figure 13: Half section of the plain backhoe dent with gradually changing base thickness as well as depth and having different sidewall slopes near the depressions on the two sides.

Obviously the left half of the half-dent is not a mirror image of the right half. However the model still has a uniform width throughout, which allows the use of two-fold symmetry instead of four-fold. The xz plane is the plane of symmetry in this model. The patterns obtained from this half model can be mirrored in the xz plane to simulate the full MFL pattern. The half model consists of about 360 elements. The minimum mesh size used in the dented region is 2mm. The H_x field inside the plate was about 30,000 A/m just outside the dented region and about 22,000 A/m in the base region underneath the dent.

5.3.3 Topside MFL axial and radial component signals

The topside MFL axial component pattern is shown in Fig. 14. The full pattern was obtained by mirroring the pattern obtained from the half model. The corresponding axial pattern for the symmetric dent case is shown in Fig. 15. The patterns look similar except for the central negative flux leakage region, where the asymmetrical dent is missing the internal negative peaks on the left hand side. These missing peaks correspond to the deeper end of the dent.

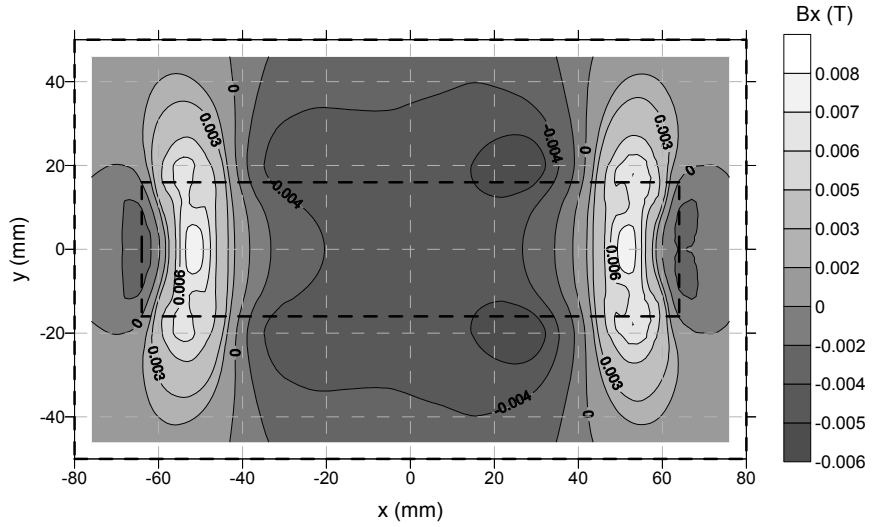

Figure 14: Asymmetrical dent: Topside axial flux density pattern in the direction of the applied field (positive x-axis) for the asymmetric dent of non-uniform depth and base thickness. The broken line rectangle indicates the topside cross-section of the dent.

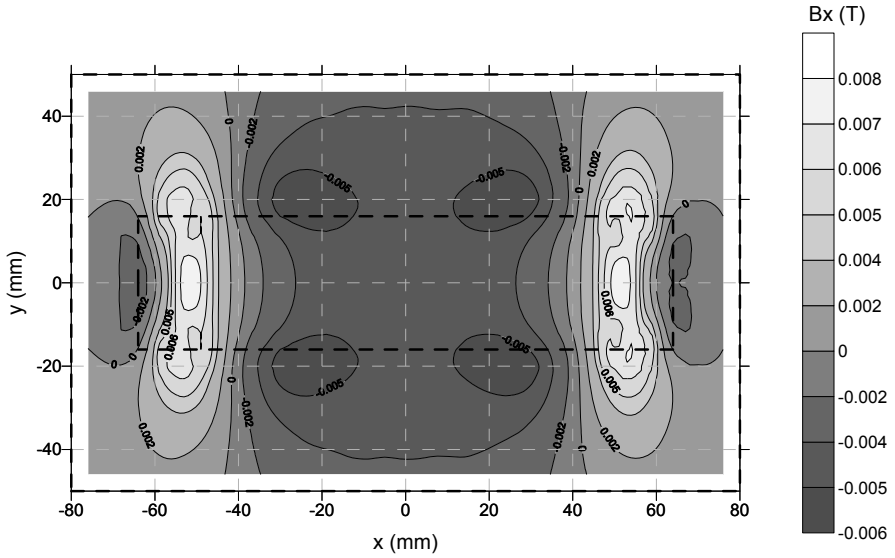

Figure 15: Topside axial flux density pattern in the direction of the applied field (positive x-axis) for the corresponding symmetric dent. The broken line rectangle is the topside cross-section of the dent.

The radial pattern for the asymmetric case (Fig. 16) looks essentially similar to that of the symmetric case (Fig. 17). This shows that the level of depth asymmetry used for this model is not sufficient to change the nature of radial flux pattern.

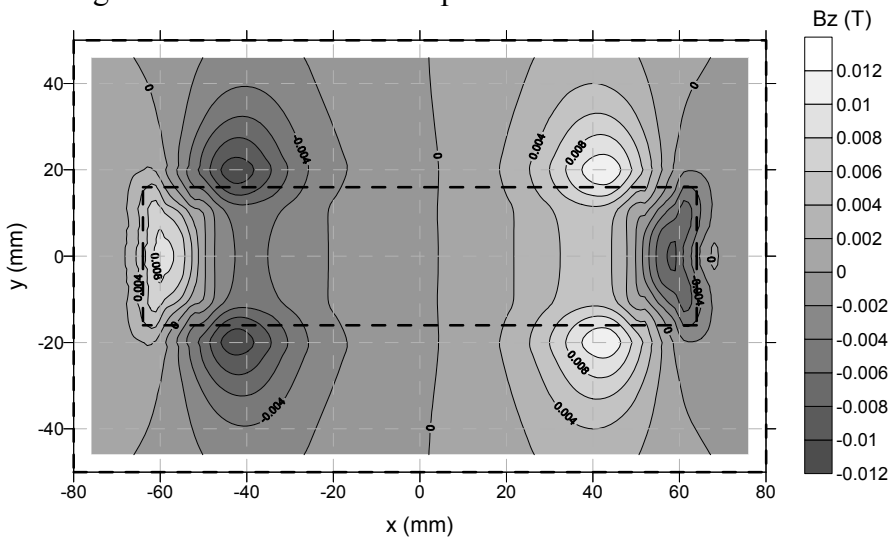

Figure 16: Asymmetrical dent - Topside radial flux density pattern for the asymmetric dent of non-uniform depth and base thickness. Broken line rectangle indicates the topside cross-section of the dent.

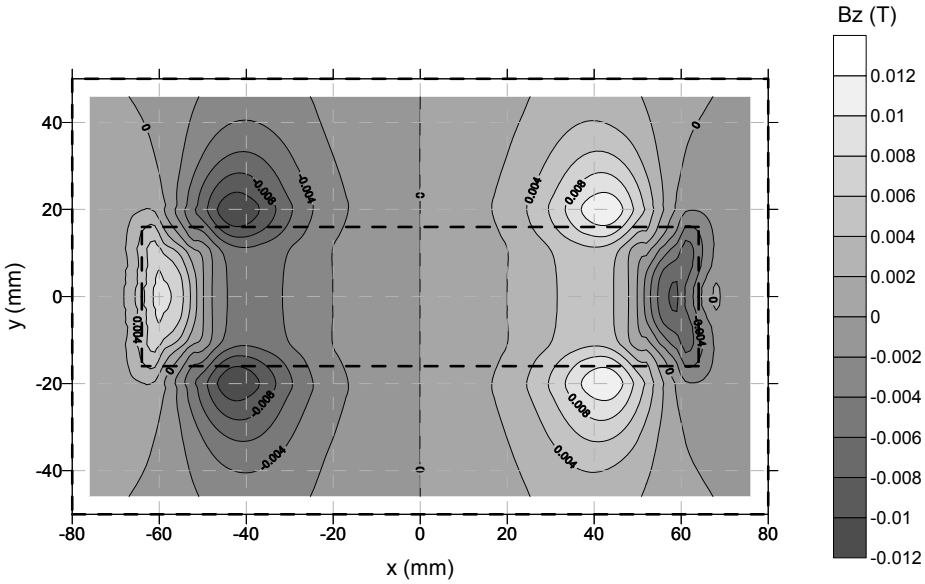

Figure 17: Symmetrical dent: Topside radial flux density pattern for the corresponding symmetric dent case. Broken line rectangle indicates the topside cross-section of the dent.

5.3.4 Underside MFL axial and radial component signals

The underside MFL axial component pattern for the asymmetric dent is shown in Fig.18. The corresponding pattern for the symmetric dent is shown in Fig. 19. Like the topside pattern, the underside axial pattern for the asymmetric case is similar to that for the symmetric case except in the central region where the negative peak region on the left side has become narrower, apparently because of additional positive flux contribution caused by base thinning. The radial flux pattern for the asymmetric case (Fig. 20) is essentially identical to that of the symmetric case (Fig. 21).

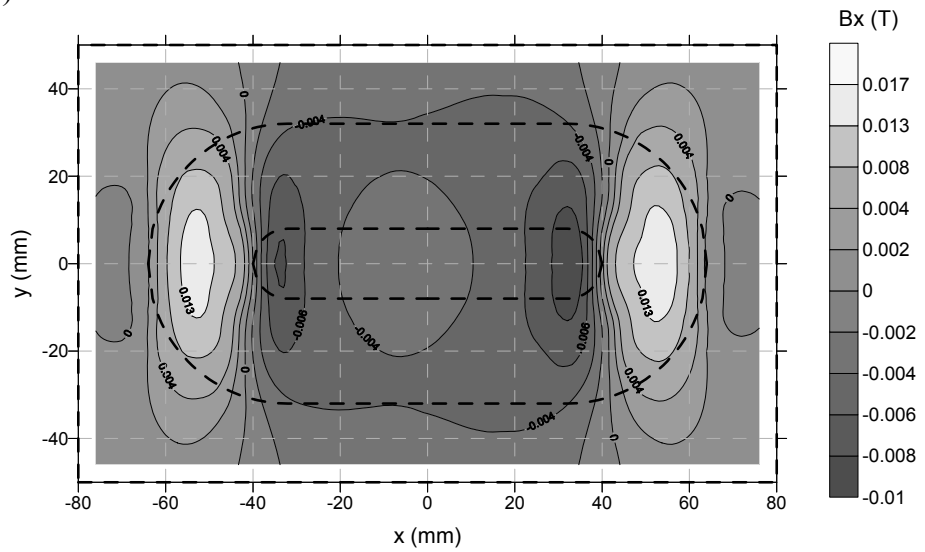

Figure 18: Underside axial flux density pattern in the direction of the applied field for the asymmetrical dent. Broken lines indicate the position and shape of the dented region. The dent wall lies between the inner and the outer elongated tracks.

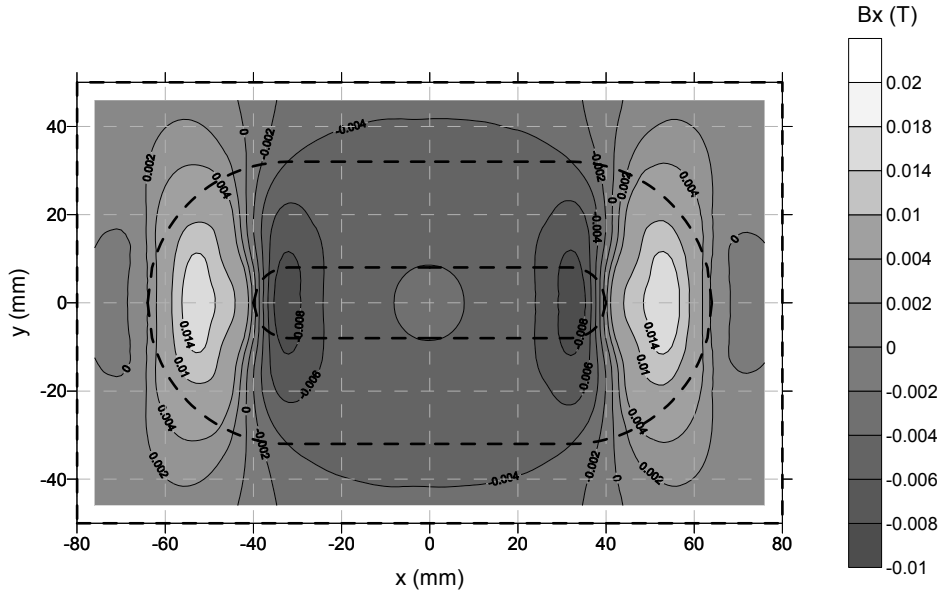

Figure 19: Symmetrical dent: Underside axial flux density pattern for the corresponding symmetric dent case.

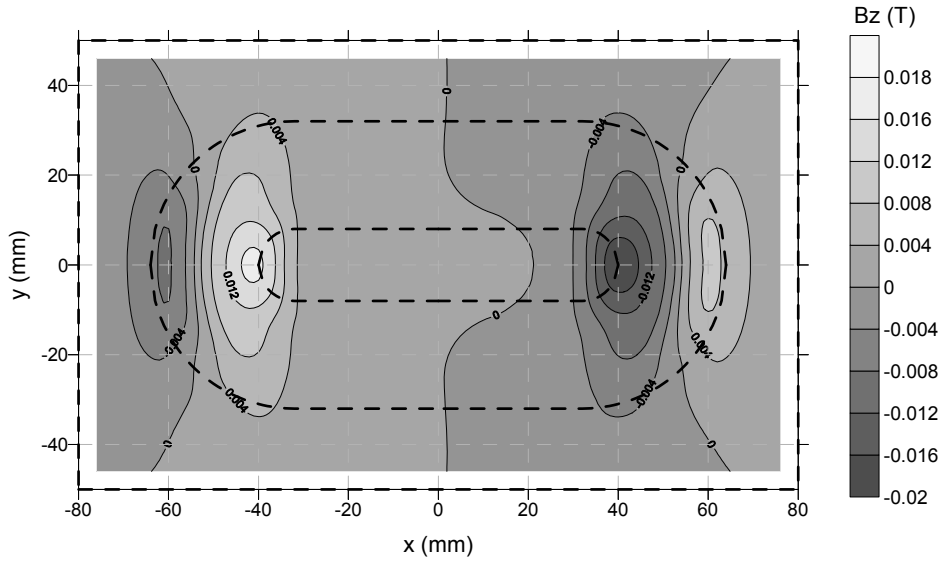

Figure 20: Asymmetrical dent: Underside radial flux density pattern for the asymmetric dent of non-uniform base thickness. Broken lines indicate the position and shape of the dented region. The dent wall lies between the inner and the outer elongated tracks.

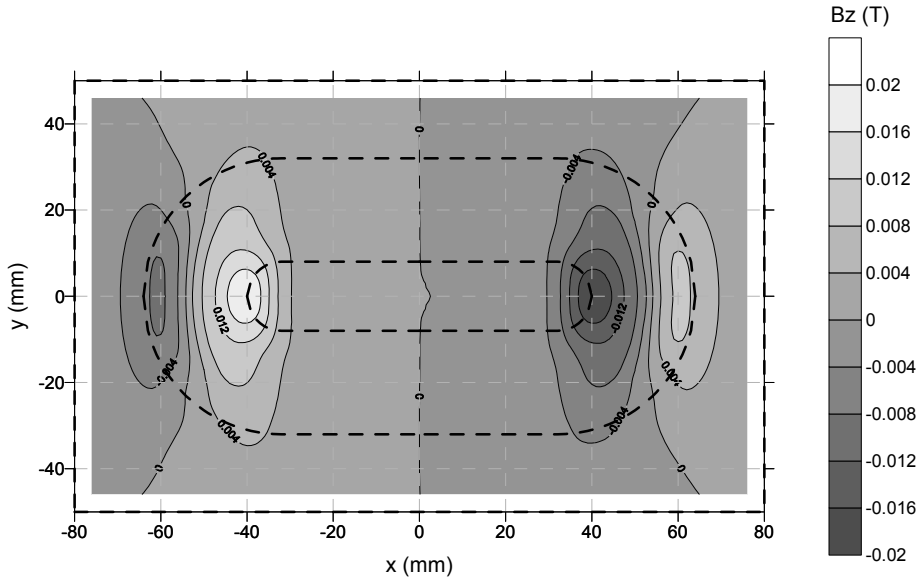

Figure 21: Symmetrical dent: Underside radial flux density pattern for the corresponding symmetric dent case.

5.3.5 Conclusion from asymmetrical dent model study

Although in general the MFL radial component appears to be the most distinctive for dent identification, this work indicates that the radial component is relatively insensitive to dent asymmetry, which is more clearly seen in the MFL axial component signals.

5.3.6 The Laser Scan Import method for creating dent models in MagNet

Ideally, the magnetic modeling process could be simplified significantly if one could directly import topographical data files of dents directly into MagNet. These topographical files could be produced using design software such as AutoCad or by laser scanning of actual mechanical damage defects. At present, however no such capability exists; rather models must be created and modified within the MagNet software itself. Because of the obvious time-saving advantages of importing existing laser scans or AutoCad files, we invested considerable time and effort in attempting to create interface software to enable such importing. The following outlines our (moderately successful) efforts to incorporate laser scan data (obtained from dents and gouges at Gaz de France) into the MagNet modeling software.

Laser scan data was obtained from Gaz de France containing surface coordinates for each sample that had been studied. This information was critical to being able to produce realistic models of the dents, but no simple method existed to convert a surface map into a three-dimensional model in the MagNet modeling software. The software does not have the ability to import AutoCAD files. Although making a 3D model in AutoCAD was certainly possible, the imported files would lose their depth component when brought into MagNet (only 2D drawings were permitted). Hence another approach was required.

A program was written in C++ to read the laser scan data files and produce a list of commands in a script, readable by MagNet, which would automate the creation of the model. After several attempts using different functions in MagNet, an efficient and rather simple algorithm was discovered, and is detailed below.

There are, however, some difficulties that arise during this procedure. Most problematic is the fact that the model is very taxing on computer resources, especially RAM. The full resolution of the laser scans (1 mm) could not be used because the computers could not handle it. In most cases, the resolution is reduced to 2 mm before attempting to make the model, and in some cases where the physical size of the sample was larger than average, a 3 mm resolution was required. This generally results in about 3000 to 4000 data points being used from the laser scans, where each step in the model creation process represents the surface of the sample between four adjacent points. Note that the total number of points used is only one quarter of the number in the original laser scan files, or one ninth in the case where the resolution has been reduced to 3 mm. Even with this loss in data, the toll on computer power is large, and basic functions take significant time to accomplish, especially when the visual model needs to be redrawn on the screen. On a related note, the script file that runs in MagNet to build the model takes so long to complete that it is necessary to have it run over night.

The laser scans received from Gaz de France were obtained only for one side of each sample – typically the outside surface. To create the 3-D model the wall thickness was assumed to be uniform, thus the ‘inside’ of the pipe model has the same shape as the outside laser-scanned surface (in reality this is not the case). Furthermore, modeling of welds and gouges is not possible with the current procedure, due to the inherent depth changes present in those features. If laser scans of both sample surfaces were available, they could be used to create a more realistic model, but lining up the two scans properly is expected to be problematic.

Detailed description of the program

Three separate programs were written to create a MagNet model from a topological laser map. These are discussed separately below.

1. The goal of the first program is to correct any sort of tilt the data may have, so that the axes of the sample align naturally with MagNet's Cartesian coordinate system. For this discussion, tilt can be defined as the angle between the axial direction of the pipe sample and the horizontal direction of the laser scanner's coordinate system. There are several reasons for first stage, including the fact that MagNet has functions to display or output magnetic field components, but only components along its global axes, and that the procedure for building the model is greatly simplified by this alignment. The tilt correction is accomplished by finding the sample's slope, averaged over each row of data. The new x-axis is then defined to lie parallel to this line, and all data points are converted to the new coordinate system. Floating-point numbers give MagNet some difficulty, so additionally the data needed to be interpolated to find the height at integer values of x and y. The tilting program also reduces the resolution of the data to the desired size, to alleviate memory problems later. Figure 22 shows the result of the "tilt correction program" – on the left is the original data, and on the right is the corrected data where both sides of the plot are at the same height.

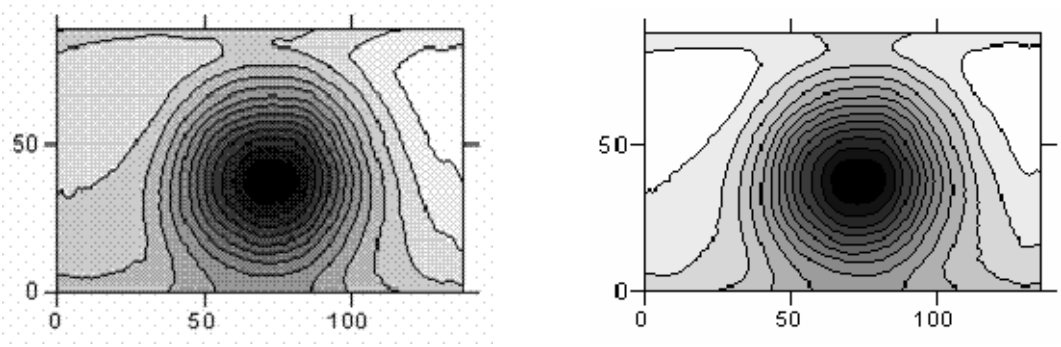

Figure 22: On the left is the original laser map of sample P42[2]. The result of the tilting program can be seen on the right, where both ends are at the same height, in comparison to the first image.

2. The second program reads the tilted output data and creates a MagNet script file that constructs the model. The final version of this program, or the script it makes, is very simple in its operation, and is illustrated schematically in Figure 23. A grid of boxes is created in MagNet such that the (x, y) positions of the vertices coincide with those of each data point in the laser scans, and the boxes are initialized with arbitrary thickness (frame 1 in figure 23). Then a MagNet function is used to adjust the vertices at the top of the boxes so that their z coordinates match the ones listed in the data file (frames 2 and 3), and the vertices at the bottom of the boxes are moved accordingly to give the desired

[2] see Table 3, page 35 for description

thickness to the sample (frame 4). Magnets are then attached at the ends of the sample by sweeping the end faces 30 mm in the axial direction (frame 5). In reality, however, the method is slightly different, for the sake of efficiency. The vertices for each box are adjusted immediately after that box is created, and this new component is then combined with all the previous ones into one component, to reduce system resources. Magnet sections are created after the first and last boxes in each row are made, and combined with previous magnet sections in the same way.

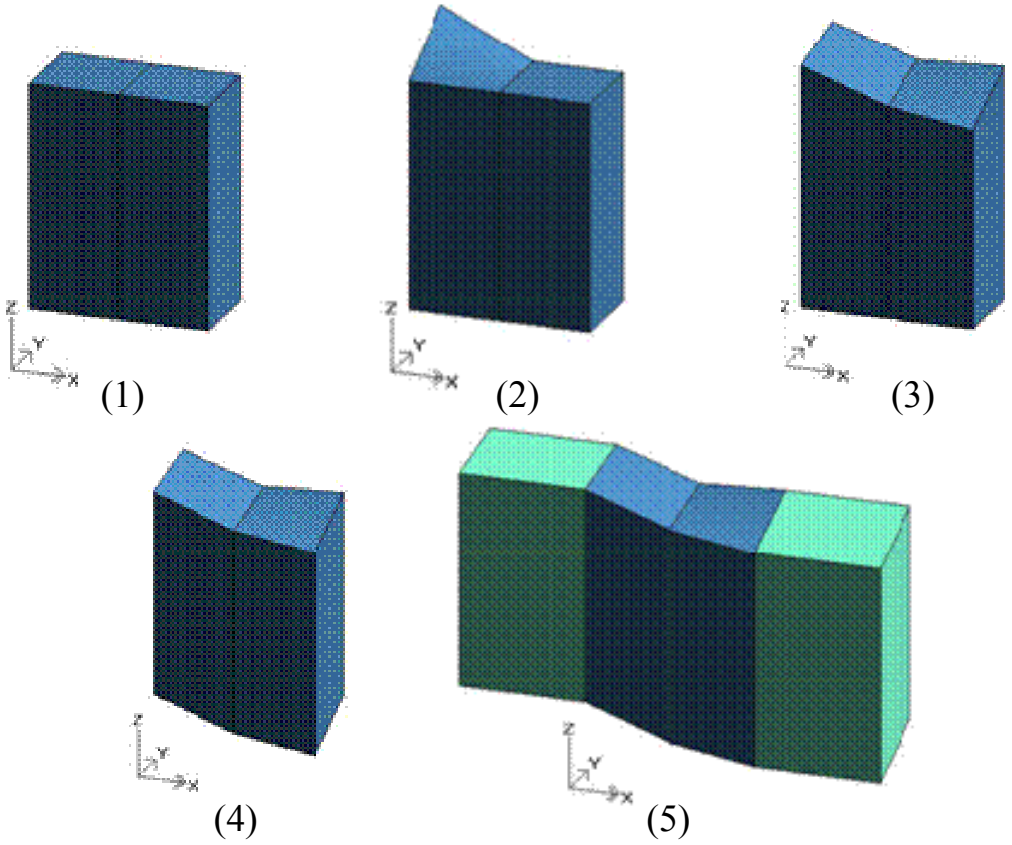

Figure 23: A sequence of simplified events (frames) that occur during Step 2 of the model-building process.

3. The third program produces another script file, whose purpose is to probe the magnetic field data after the model has been solved in MagNet. It works off of a second output file from the tilting program, where the data is corrected for tilt but not reduced in resolution. Effectively, a grid with this resolution is laid over the model, but some distance from its surface (1 mm is generally used), and MagNet is queried for the B field components at each grid point. The information is delivered directly to a spreadsheet to be analyzed and plotted. Both surfaces of the model can be done at once, but currently any sample with a weld or gouge is not well represented on the bottom (inner) side. This is due to the way the models are made with a fixed thickness, and hence a bump from a weld on the top side yields a trough on the other side. A fourth program will be needed to incorporate gouges and welds properly. This will be the next task on the modeling front, and although welds have a fairly simple solution, gouges will require much more effort.

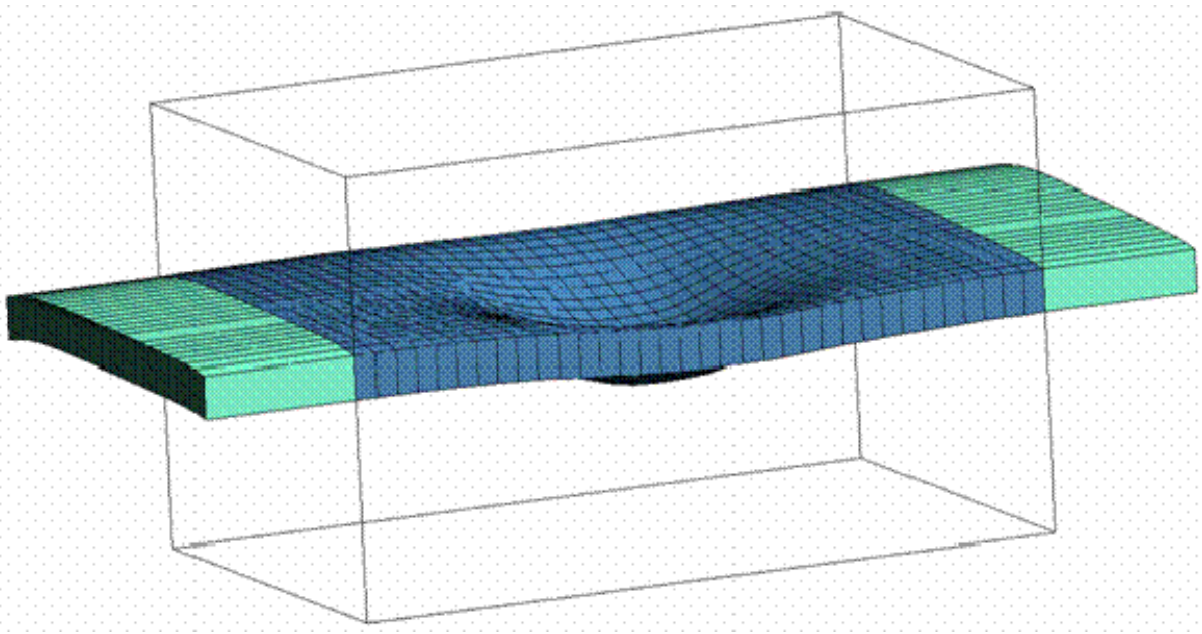

Figure 24: The full model for sample P42.

Results

Due to complications involving the detail of some of the models and the computing time required to build even an unsuccessful model, only one of Gaz de France's samples has been modeled accurately using this procedure. The sample is P42, a plain dent. Figure 24 shows the model created in MagNet from the outer surface laser scan data according to the steps described above.

The MFL results from this model are shown in Figure 25. Figure 25 (left) shows the modeled MFL_{radial} component result extracted from the outer surface of the pipe, looks quite recognizable in terms of the geometrical peaks visible (see Figure 3 for modeling results using the "standard" techniques). Similarly, the axial scan figure (right), is also not unlike that seen for a circular dent. Again, note that these are for the outer surface, and hence, the comparison with other results in this paper is not entirely valid, due to their measurements being from the inner surface. Of course, the field near the inside surface can be obtained from these models, but the contour plots depict little more than noise. The reason for this may be that the sample was not saturated – a problem that can be corrected relatively easily in the future by adjusting the strength of the magnets used during the modeling procedure.

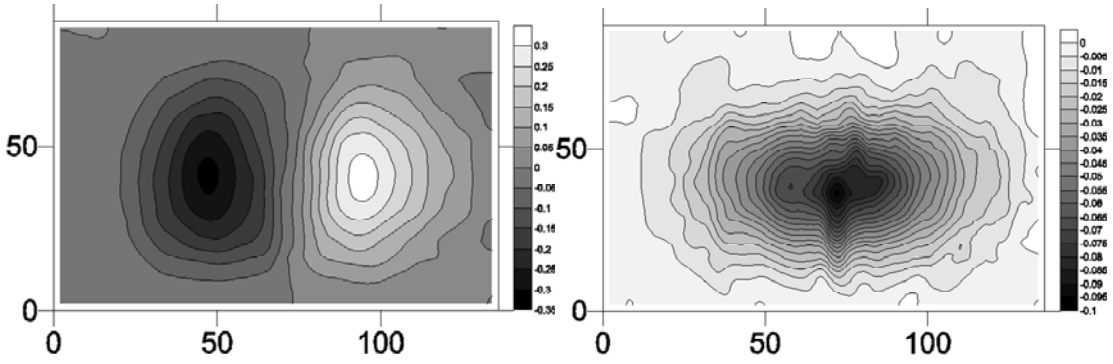

Figure 25: Top-side MFL results for sample P42. The radial component is on the left, and the axial signal is on the right. Horizontal and vertical axes represent x and y co-ordinates in mm respectively. These plots were produced using the same procedure that was used on the raw data from Gaz de France.

5.4 Gaz de France Dented Samples – Modeling and Experimental MFL Results

5.4.1 General description of samples and testing procedure

Approximately 14 dented samples were made available to us at the Gaz de France laboratories in St. Denis, France. These samples were in the form of coupons, a typical example of which is shown in Figure 26.

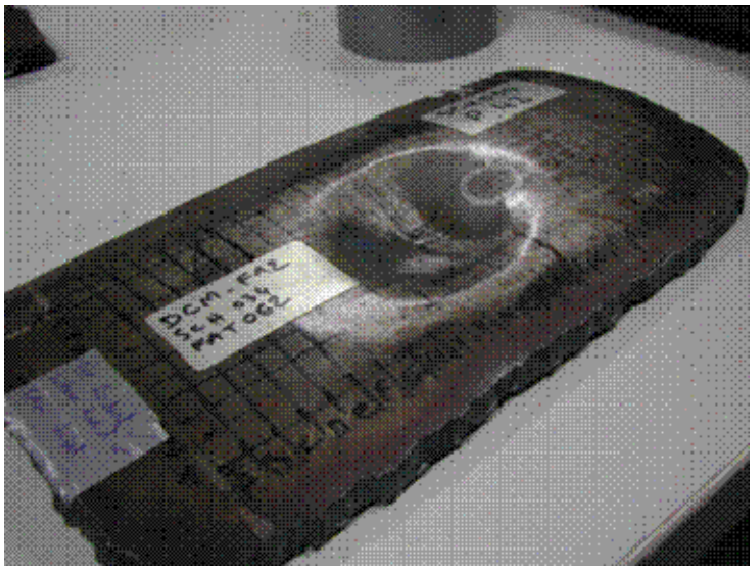

Figure 26: A typical example of a Gaz de France sample coupon containing a dent. This particular sample, which contained a circular dent of about 9cm diameter, was labeled P42. The sample was 17cm wide and 30cm long.

These coupons are the final result of an extensive dent production process in the laboratory facilities of Gaz de France. The steps in this process are as follows:

1. Endcaps are welded onto an intact pipeline section of approximately 30m in length. This pipeline section can be of any diameter from 16" to 36".

2. The pipeline section is pressurized to a typical line operating pressure.

3. The section is placed in a large pit, and then dented using the PAR (Pipeline Aggression Rig). The PAR is essentially a large laboratory backhoe, which can be adjusted to create an infinite variety of dents and gouges in a pipe wall.

4. The now-dented pipe is removed from the PAR pit and moved to a second pit, where it is typically pressurized to failure. In many cases the dent changes shape (pops out) during this pressurization process. Failure usually occurs in the dent vicinity.

5. After failure the coupon containing the dent is cut from the pipe using a torch, after which the coupon and included dent undergoes further testing.

The sample coupon dimensions varied considerably depending on the size of the defect. Unfortunately not all were suitable for MFL measurements; some of the coupons were too small to mount the MFL magnets (since the coupons were not cut with the intention of later making MFL measurements). Ultimately a total of 7 dent samples were of large enough dimensions for MFL measurements, however one of these was not measured due to the fact that a very large weld bead prevented the MFL magnet from sitting flush with the pipe wall surface.

Figure 27 shows a coupon undergoing MFL testing. The MFL magnet is mounted on the outside of the sample, which is lying with the inner wall facing upward. The Hall probe for MFL measurements is mounted on the end of a scanning arm which scans over the inner surface of the coupon. The DC magnet system mounted on the outer surface of the pipe saturates the pipe wall to a level of ~1.8T, similar to that in a typical MFL inspection operation. The Hall probe can be oriented to measure either the radial, axial or circumferential component of the MFL field at the pipe surface.

Once the MFL plot had been obtained, background subtraction was necessary. The procedure for this was to create a straight line defined by the endpoints of a single row, or a single column. This line was subtracted from the data points and the resulting data was smoothed by taking an average value of all points in a 5x5 grid square centered on the point of interest.

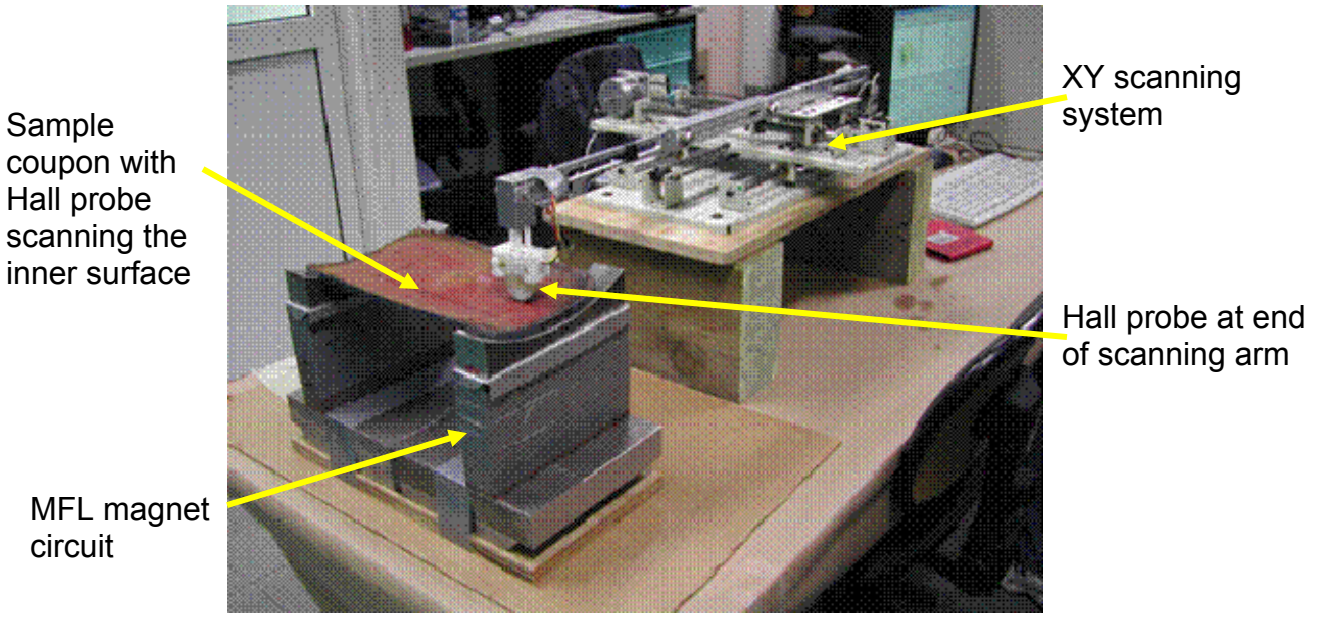

Figure 27: Photograph of the experimental MFL rig with a sample coupon being tested.

As mentioned above, a total of 6 dented sample coupons were tested. Table 3 contains a summary of each of these samples with a brief description. The full set of data (photos, MFL measurements, and laser scans) for each sample is contained in Appendix 1.

Table 3: Summary of all tested dent samples

Sample No.	Defect Type	Defect Description
P1	Axial Elongated Dent Dent Length ~ 14 cm, Width ~ 5 cm	Plain axial elongated dent. The pipe was wound with a clockspring over the top of this dent before pressurizing to failure. Failure was via a small circumferential crack located at one end of the dent.
P35	Circular Dent + Circumferential Weld Dent Diameter ~ 13 cm	Plain circular dent containing a circumferential girth weld. The weld is quite rough and is cracked at the inside surface where it was likely pressure tested.
P38	Circular Dent + Axial Weld Dent Diameter ~ 8 cm	Plain circular dent with a very clean (no weld bead) axial weld running through the middle. The weld is ground and looks like it failed during a pressure testing procedure.
P42	Circular Dent Dent Diameter ~ 9 cm	Plain circular dent – no weld nearby. No failure evident
P43	Axial Elongated Dent + Diagonal Weld Length ~ 14 cm, Width ~ 10 cm	Plain axial dent located on the top of a spiral weld that cuts it approximately diagonally. Pressurizing resulted in a slight 'double bump' effect with the bumps centered on the deepest indenter marks at the end. There are some small axial cracks at these ends of the dent coming from the deepest indenter marks.
P56	Axial dent with partial rerounding Total Length ~ 19 cm, Width ~ 8 cm	Plain axial dent – no weld nearby, and no cracking apparent. Pressurizing has resulted in a significant 'double bump' effect with bumps centered on the indenter corners. A very small gouge is also apparent at the centre, but no failure cracks are evident.

Although the results from these samples will be discussed in the following section, a few general characteristics of the Gaz de France sample dents are worth noting. Included in the sample set are three circular dents ranging in size from 8 – 13cm diameter (P35, P38, P42). One of these, shown earlier in Figure 26, has not been pressure tested and is from a region away from any welds. The other two circular dents have welds running through them – one a girth weld and the other an axial weld. Both of these weld+dent samples have been pressure tested and exhibit cracks in the weld vicinity.

Also in the sample set are three axially elongated dents (P1, P43, P56), with lengths between 14-19 cm and widths 5-10 cm. One of these (P43) contains a spiral weld, and is shown in Figure 28. The other two elongated dents are weld-free. All three of the elongated dents have undergone pressure testing, during which failure occurred through cracking in the dent region. Figure 28 illustrates an interesting feature of the elongated dent samples. At the base of these dents the indenter marks can clearly be seen, particularly at the locations corresponding to the indenter corners. Upon pressurizing, the dent re-rounds, but not uniformly – specifically the dent center re-rounds much more than the indenter corner regions. As seen in Figure 28, this leads to a dent geometry which resembles two adjacent circular dents, rather than one long axial dent. For convenience this has been termed the 'double bump' effect. Both axially elongated dents P43 and P56 exhibited these double bumps, however this effect was non-existent in sample P1. In P1 the sample had been wound with a clockspring prior to pressurizing, which may have contributed to the deformation conditions during pressurization.

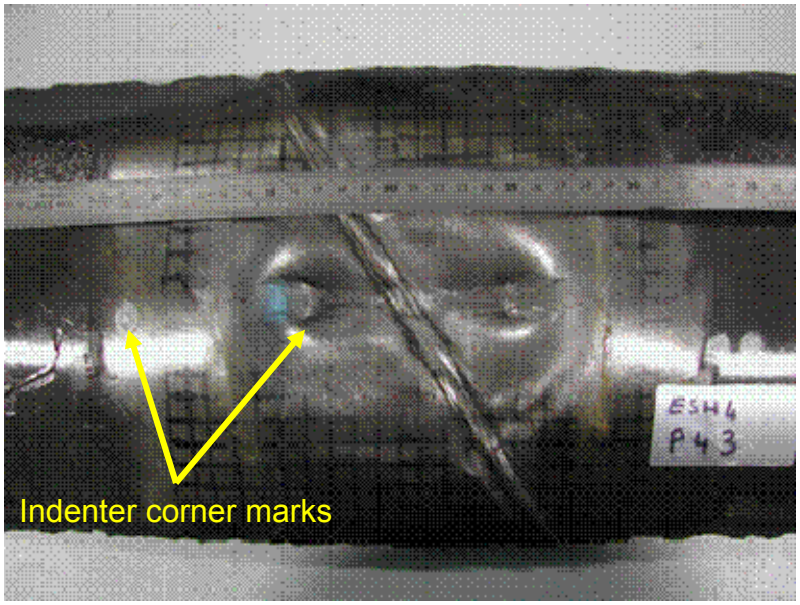

Figure 28: Gaz de France sample P43 containing a axially-elongated dent with a spiral weld (top view of outer pipe surface). Dent length is about 14cm. The indenter corner marks are clearly seen. These indenter marks lie at the base of two 'double bumps'.

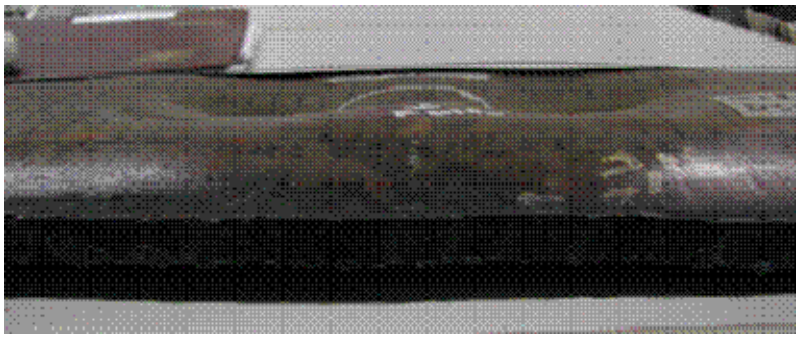

Figure 29: Side view of axially-elongated dent P56, showing the 'double bump' effect that occurs when pressurizing to failure. As in sample P43, the base of each 'bump' corresponded to the indenter corners.

5.4.2 MFL modeling of the Gaz de France samples

Section 5.3 outlined three different methods for creating the pipe geometries in MagNet necessary to correctly predict MFL signals. Of these, the second method, outlined in Section 5.3.2, proved to be the most consistently useful method. In this section, models for large circular dents with welds, and large axially-elongated dents, will be shown.

It is important to note that our earlier MFL modeling work of laboratory dent samples included residual stress, as well as geometry contributions to the MFL signal (see summary in Section 2). The residual stress state was readily deduced for these laboratory dents since the stress history was simple and well documented. Unfortunately, this was not the case for the Gaz de France dents, since the stress history was complex and extremely difficult to model. As noted earlier, the stress history for most of the Gaz de France dents was as follows: 1) dent introduction under pressure, followed by 2) non-uniform grinding of the dent, followed by 3) pressure testing of the pipe to dent failure, followed by 4) removing the coupon containing the dent. As noted in section 5.2 (the section dealing with stress modeling around dents) stress models were created to predict the residual stress pattern after step 1 (dent introduction under pressure) but not after steps 2, 3 and 4. Since the residual stress distributions were unknown for these sample coupons, the stress contributions to the MFL signals were not modeled. This will be discussed in the next sections.

The method outlined in section 5.3.2 was used to produce two basic models for comparison with the Gaz de France sample results – one of these was a circular dent containing a weld (circumferential or axial) and the other was an elongated dent. Example results are presented below for each of these; they will be shown again for comparison with the MFL measurements for the Gaz de France samples in section 5.4.3.

5.4.2.1 Circular dent with a girth weld – modeling results

The dent modeled in this particular case is shown in Figure 30. The dent itself is ~9cm in diameter, and thus similar in geometry and size to circular dents P38 and P42. The weld is circumferential, with a width of 8mm. For magnetic modeling purposes the weld was assumed to have the same magnetic properties as the pipe wall.

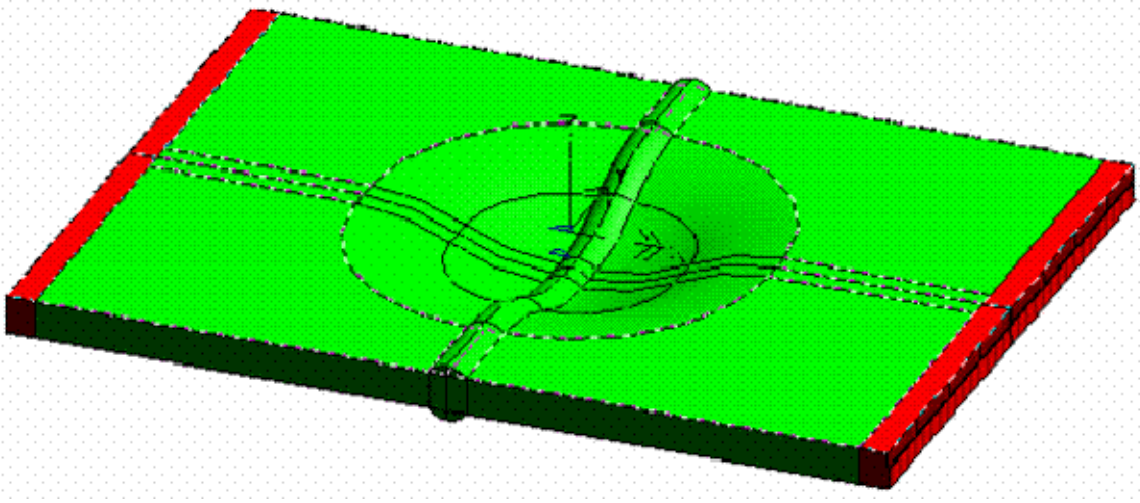

(a)

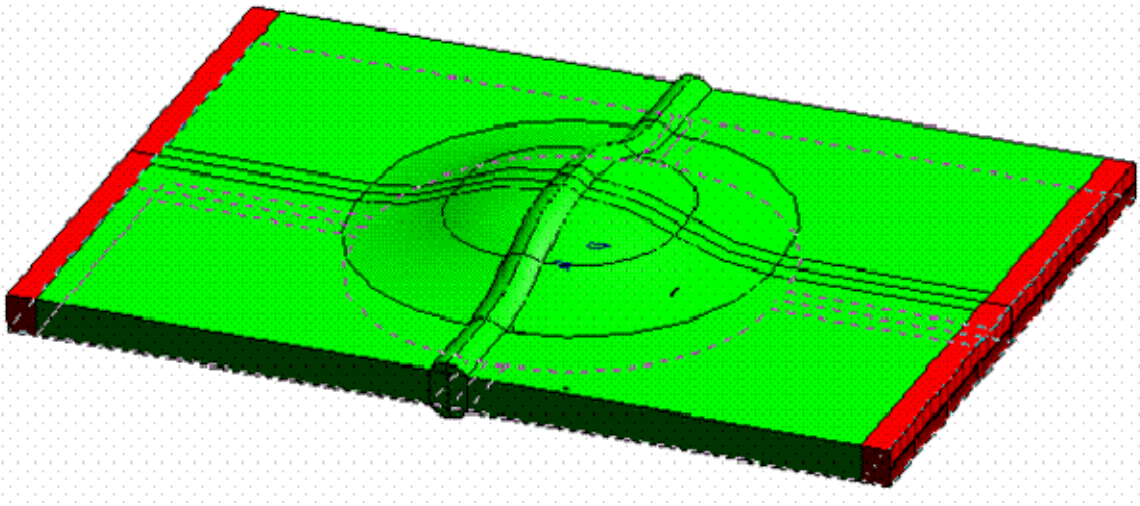

(b)

Figure 30: Circular dent with circumferential weld (a) topside, and (b) underside.

Figures 31 and 32 show typical MFL modeling results for the circular dent + circumferential weld. Results are for the inside pipe wall. Figure 31 shows the MFL_{axial} component results, Figure 32 the MFL_{radial} component results. The top diagram in Figure 31 shows a profile of the MFL signal taken along an axial cut through the center of the dent. The middle diagram shows a contour plot over the top of the dent, and the bottom a surface plot of

the same. The dent perimeter and weld line is indicated by the dotted line in the middle plot. In general the model results are similar to those found before for smaller circular dents (for example Figures 2 and 3 – without the stress effects included).

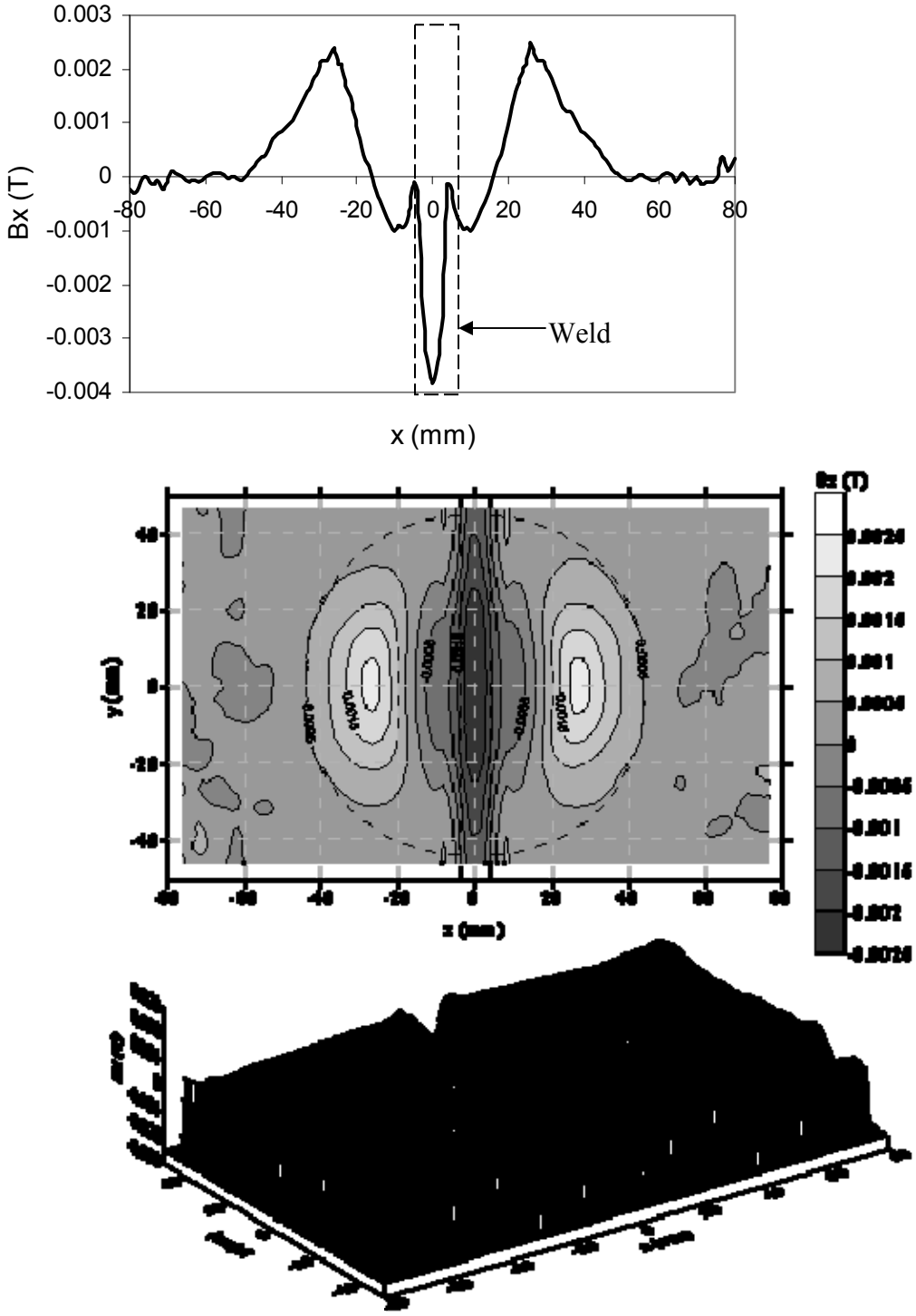

Figure 31: MFL_{axial} component results for the 9cm diameter circular dent model with a girth weld. The top diagram shows the MFL_{axial} result along the axial centerline of the sample. The middle diagram is a contour plot over the dent region, with weld and dent perimeter shown as dotted lines. The lower diagram is a surface MFL_{axial} plot over the same region.

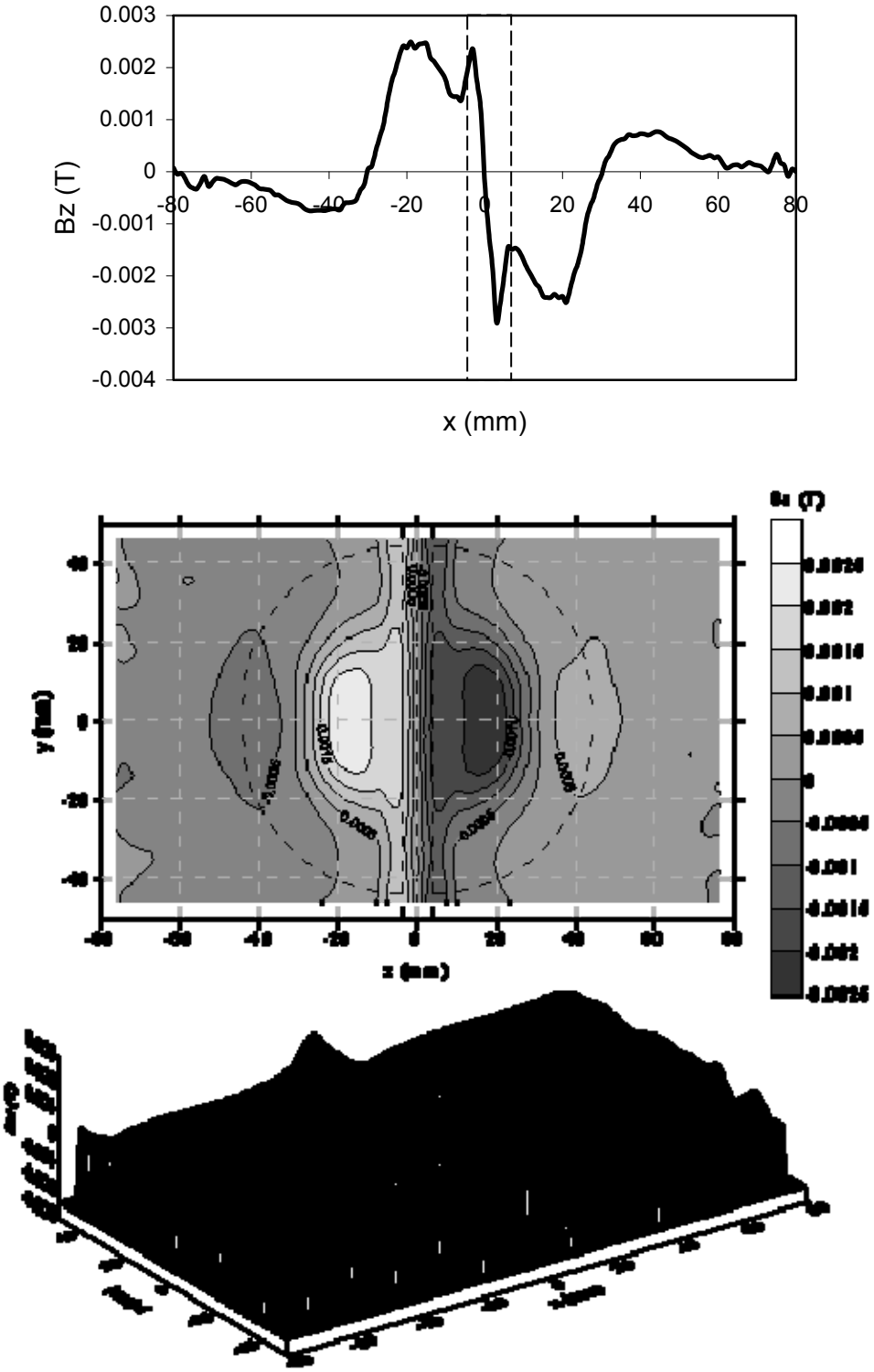

Figure 32: MFL_{radial} component results for the 9cm diameter circular dent model with a girth weld. The top diagram shows the MFL_{radial} result along the axial centerline of the sample. The middle diagram is a contour plot over the dent region, with weld and dent perimeter shown as dotted lines. The lower diagram is a surface MFL_{radial} plot over the same region.

5.4.2.2 Axially-elongated dent in pipe section – modeling results

The axially-elongated dent modeled using MagNet is shown in Figure 33. The dent is 14.4 cm long, 4.8 cm wide, and is similar to axial dent P1 (the dent without the 'double bump'. No weld is modeled in this case.

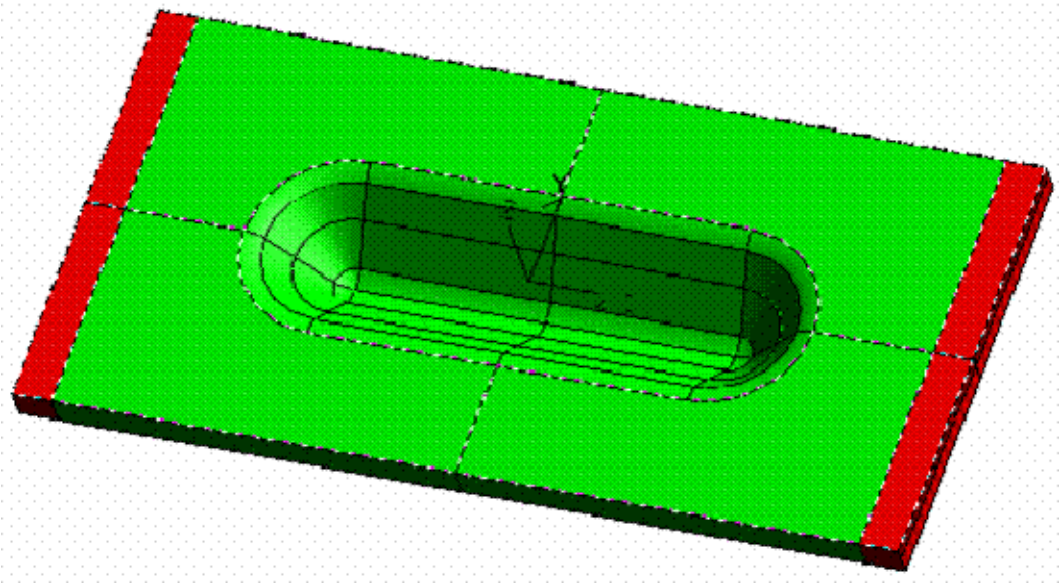

(a)

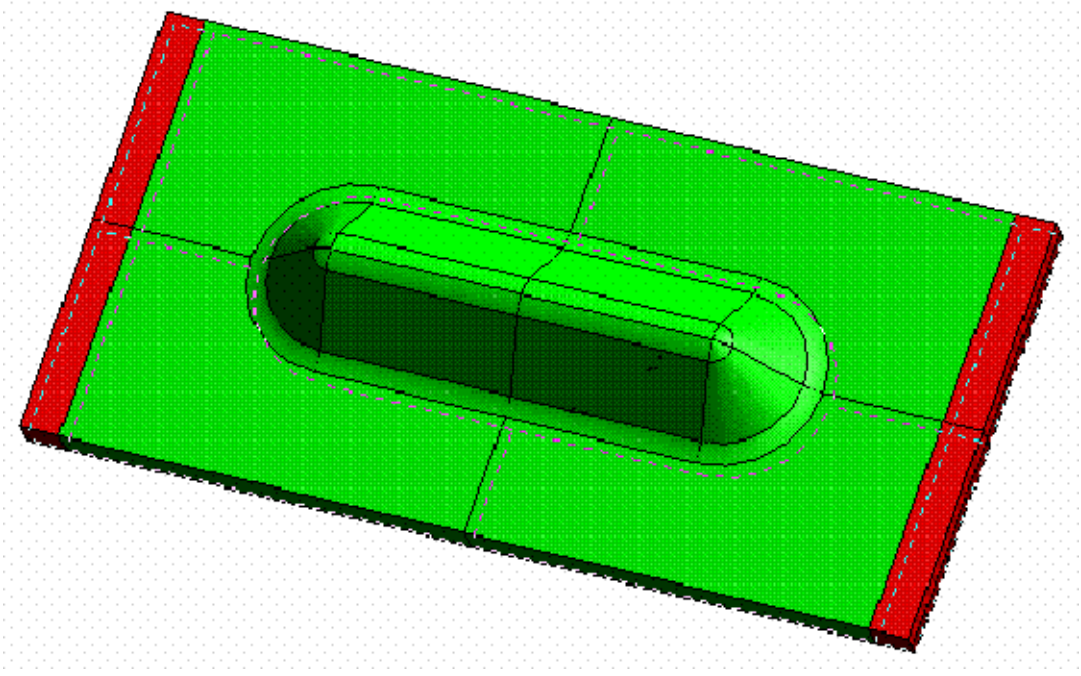

(b)

Figure 33: MagNet model of an axially-elongated dent of the type P1, (a) topside and (b) underside (inside pipe wall).

Figures 34 and 35 show typical MFL modeling results for the axially-elongated dent. Results are for the inside pipe wall. Figure 34 shows the MFL_{axial} component results, Figure 35 the MFL_{radial} component results. The top diagram in Figure 34 shows a profile of the MFL signal taken along an axial cut through the centre of the dent, the middle diagram shows a contour plot over the top of the dent, and the bottom a surface plot of the same. The dent perimeter and weld line is indicated by the dotted line in the middle plot. In general the model results are similar to those found before for smaller axially-oriented dents (for example Figures 4 – geometry only case).

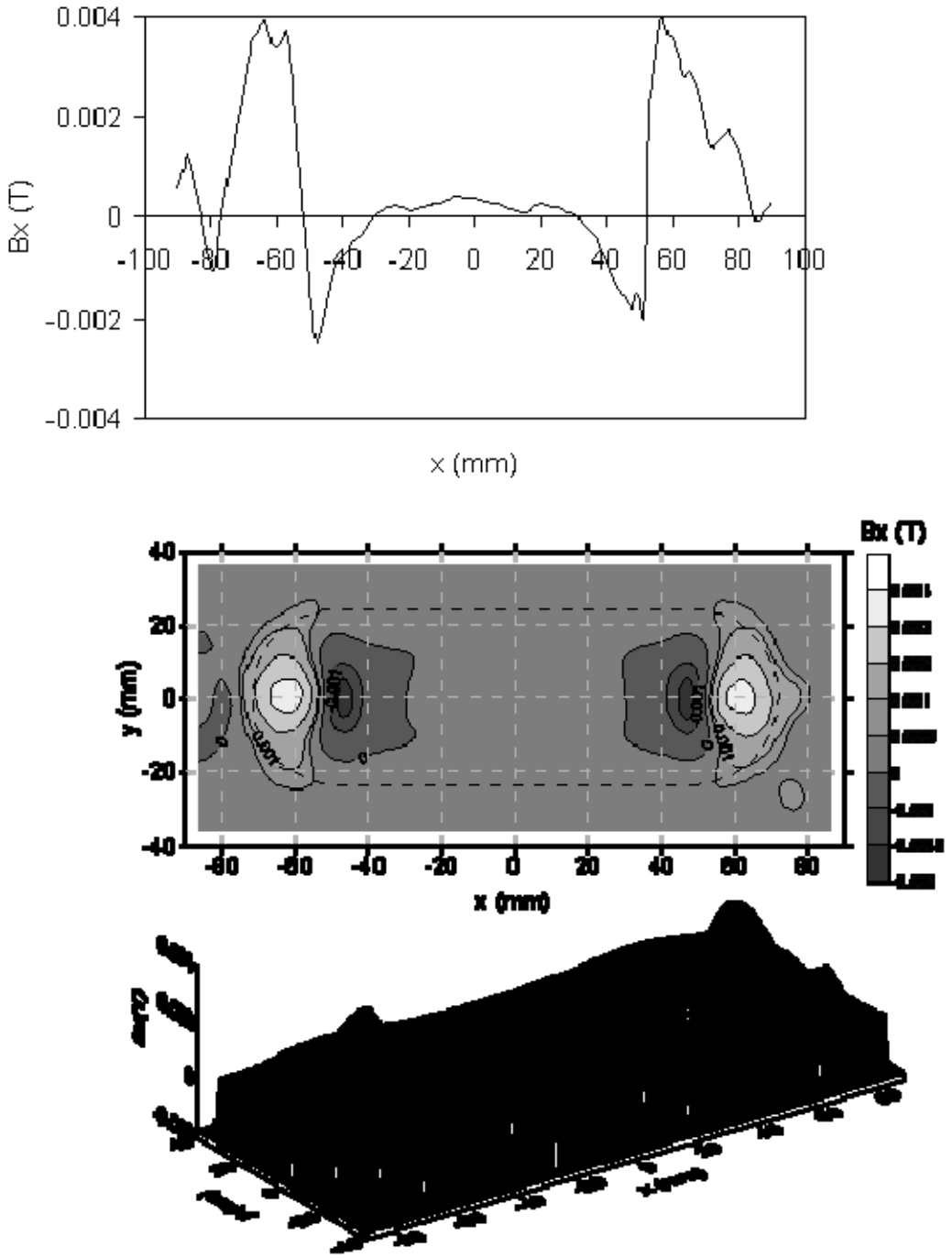

Figure 34: MFL_{axial} component results for the axially-elongated dent model (no weld is present). The top diagram shows the MFL_{axial} result along the axial centerline of the sample. The middle diagram is a contour plot over the dent region, with the dent perimeter shown as a dotted line. The lower diagram is a surface MFL_{axial} plot over the same region.

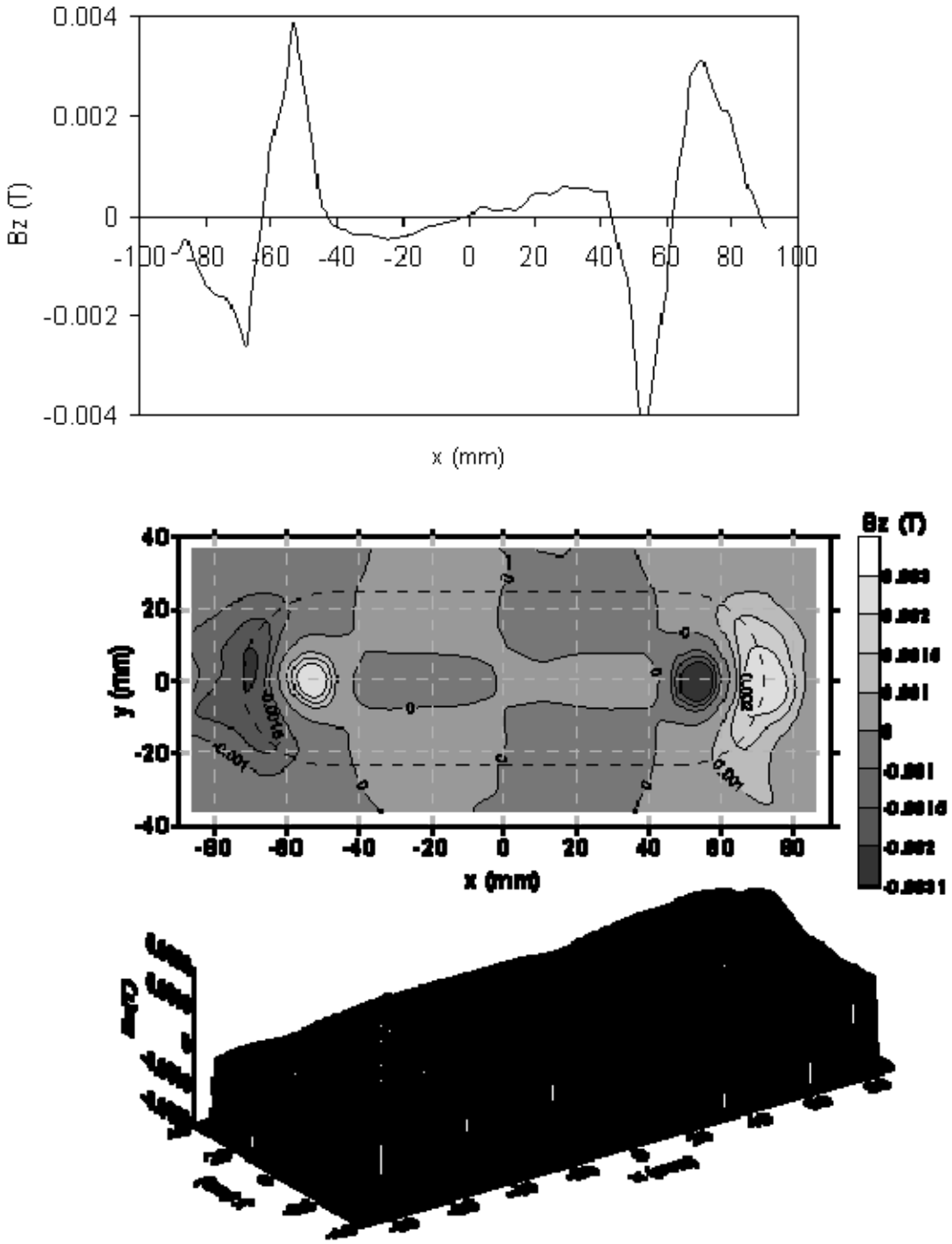

Figure 35: MFL_{radial} component results for the axially-elongated dent model. The top diagram shows the MFL_{radial} result along the axial centerline of the sample. The middle diagram is a contour plot over the dent region, with weld and dent perimeter shown as dotted lines. The lower diagram is a surface MFL_{radial} plot over the same region.

Results and Discussion of MFL measurements on Gaz de France sample dents

Appendix 1 contains the results of all Gaz de France dent samples tested in the current study. In addition to photographs, MFL_{axial} component scans, and MFL_{radial} component scans, Gaz de France also provided laser scan data for each sample. These are also included in Appendix 1. The discussion below summarizes the results observed for each sample. Circular dents are considered first as a group, followed by the axially-elongated dents.

Circular dents

MFL measurements were made on the inside surface of all three circular dent samples. Figure 36 shows the inside surface photos of all three circular dents, Figure 37 shows the MFL_{axial} component plots, and Figure 38 the MFL_{radial} component plots. For comparison, Figure 38 shows the MFL_{axial} modeling result, and Figure 32 the MFL_{radial} modeling result. On the experimentally-measured plots the approximate dent perimeter location is indicated with a dashed line, and the MFL peaks that arise from the geometry of the dent rim (as deduced from the MFL models results of Fig 31 and 32) are indicated with a dent rim (DR) annotation.

MFL results for all three circular dents (Fig 37 and 38) exhibit the same basic features as the modeling results in Figure 31 and 32 (i.e. the DR indications). Note that the models include the basic circular dent + girth weld geometry, but ***without any residual stress contributions*** to the MFL signal. Additional peaks are often present in the measured MFL results, these are discussed below.

P42: Circular dent, 9 cm diameter, no weld: This is a relatively simple dent, with no welds or unusual features present. As such both the axial (Fig 37) and radial (Fig 38) MFL signals match the modeling results (Fig 31 and 32) very well, as the DR annotation indicates. There may be some very small peak features at the defect centre –these may be associated with grinding at the base of the dent on the outside surface.

P35: Circular dent, girth weld: This dent has a girth weld running through it. The DR peaks are clearly identifiable here, both in the MFL_{axial} (Fig 37) and MFL_{radial} (Fig 38) plots. Examination of the MFL modeling results in Fig 31 and 32 indicates that a circumferential weld line should have a smooth MFL 'ridge' associated with it. However, this particular sample has had the weld bead ground off at the base of the dent as seen in Figure 36. This accounts for the fact that the MFL weld signal in Figs 37 and 38 is not a smooth ridge but rather distinct peaks. There are also few random peaks in the dent centre which are likely associated with stresses from the grinding process.

P38: Circular dent, axial weld: This dent has an axial weld running though it, however it is worth noting that the weld bead has been removed on both the inner and outer pipe surface. As a result little or no MFL indication is expected and none is seen. The MFL plots in Fig 37 and 38 indicate the usual dent rim (DR) indication, but also another set of peaks in the dent centre. Close inspection of the dent at the inner surface indicated the presence of a surface-breaking defect, which appeared to be corrosion but could have been a deeper crack. No

grinding was apparent at this inner surface, although there were numerous areas on the upper surface which may have contributed the MFL signals at the inner wall.

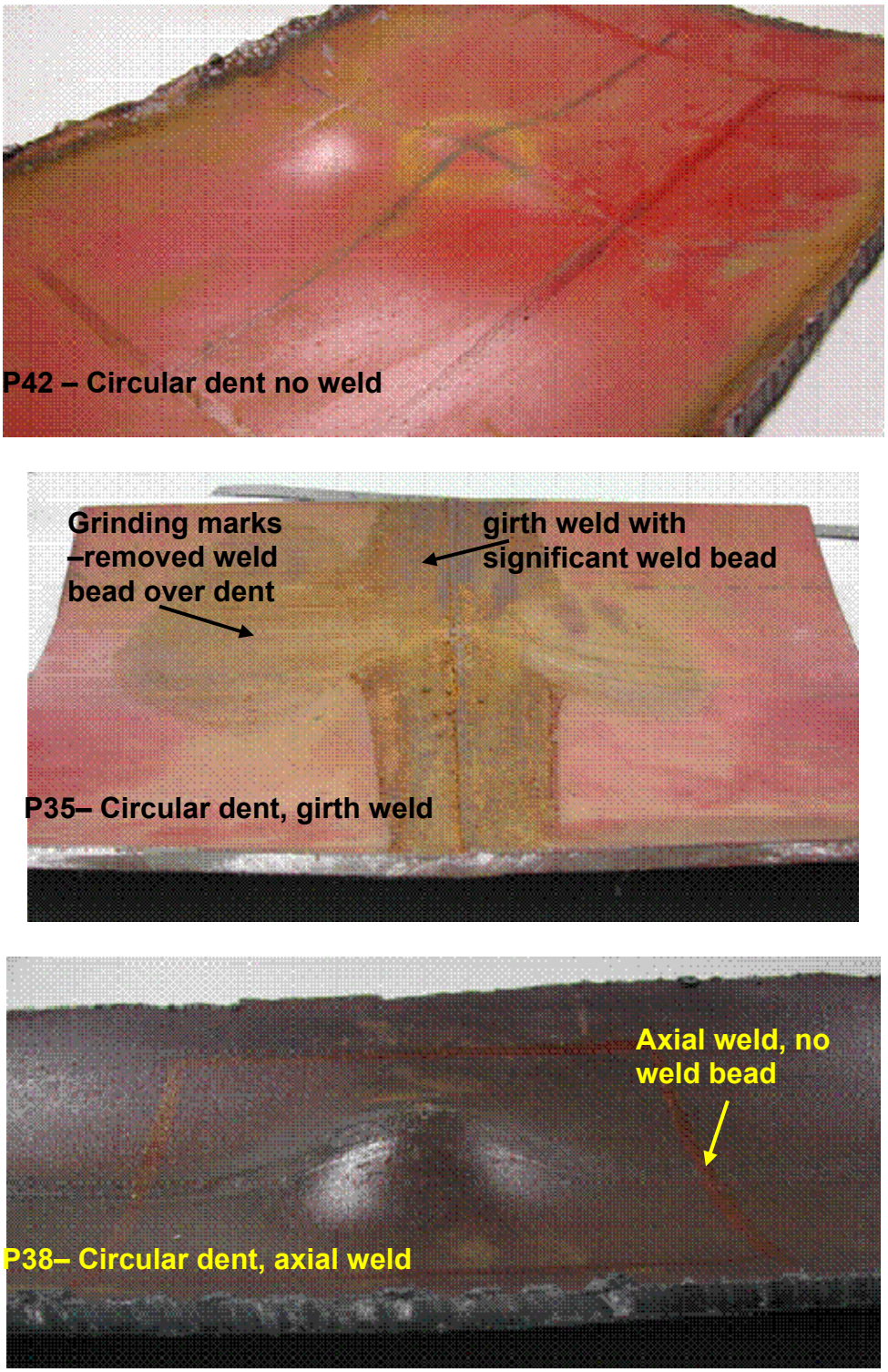

Figure 36: Inside surface photos of all three coupons containing circular dents. Samples are labeled accordingly.

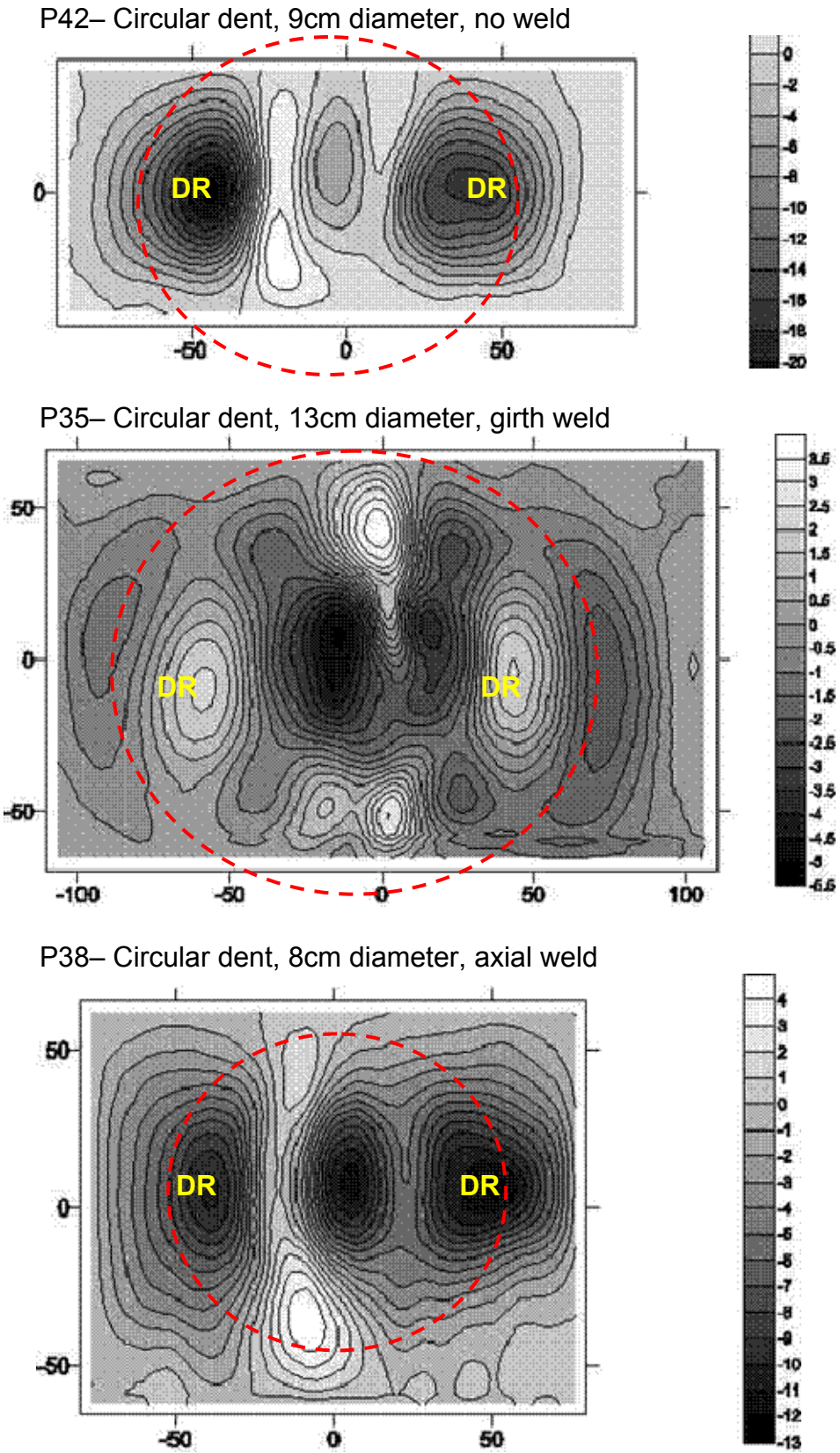

Figure 37: MFL_{axial} component signals for Gaz de France circular dents. Note that the polarity of the peaks (negative or positive) is arbitrary.

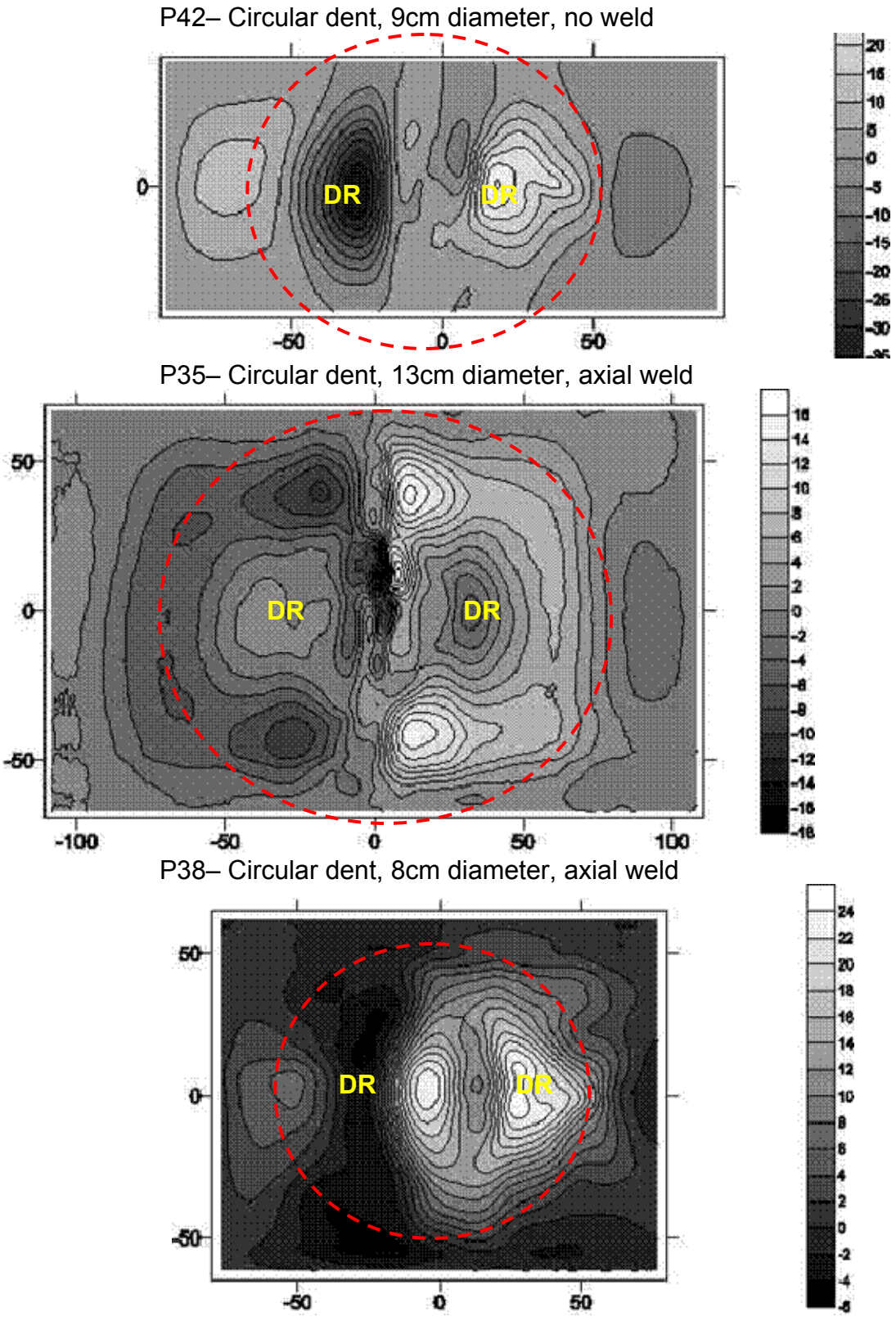

Figure 38: MFL_{radial} component signals for Gaz de France circular dents. Note that the polarity of the peaks (negative or positive) is arbitrary.

Axially-Elongated Dents

MFL measurements were made on the inside surface of all three axially-elongated dent samples. Figure 39 shows the inside surface photos of all three circular dents, Figure 40 shows the MFL_{axial} component plots, and Figure 41 the MFL_{radial} component plots. For comparison, Figure 34 shows the MFL_{axial} modeling result, and Figure 35 the MFL_{radial} modeling result. On Figures 40 and 41 the approximate dent perimeter location is indicated with a red dashed line, and the MFL peaks that arise from the geometry of the dent rim (as deduced from the MFL models results of Fig 34 and 35) are indicated with a DR annotation.

The MFL results for all three axially-elongated dents (Fig 40 and 41) in general exhibit the same basic dent-induced features as the modeling results in Figure 34 and 35 (i.e. the DR indications). Note that the models include the basic axially-elongated dent geometry, but ***without any residual stress contributions*** to the MFL signal. Additional peaks are often present in the measured MFL results, these are discussed below.

P1: Axially Elongated Dent, significant crack evident at dent end: Although geometrically this is a relatively simple dent, it is likely to have a rather complex stress history, given the fact that it was wound with a clockspring and did not 're-round' during over pressurization. As seen in both the MFL_{axial} (Fig 40) and MFL_{radial} (Fig 41) plots, the dominant feature here is the circumferential crack at the end of the defect. Apart from this crack, the MFL_{axial} (Fig 40) plot indicates that the expected dent rim (DR) geometry peaks are present. The crack signal on the MFL_{radial} signal plot is so large that unless one re-scales, the remainder of the peaks cannot be seen (these plots are in Appendix 1). Figure 41 shows the re-scaled version of the uncracked end of the dent. There are a number of peaks here, and the expected dent rim (DR) peak is actually split in two. The outside surface was ground; in addition strain gauges are present at the base of the dent. All of these, in addition to an expected complex stress field, may result in the smaller peaks seen in the P1 MFL_{radial} signal in Figure 41.

P43: Axially elongated dent over a spiral weld: The MFL signals for this dent are very clean and symmetrical, with dent rim (DR) features clearly visible in both the MFL_{axial} (Fig 40) and MFL_{radial} (Fig 41) plots. In addition the spiral weld (which has a significant weld bead) is also clearly indicated in both MFL_{axial} and MFL_{radial} components. Interestingly, extra symmetrical peaks appear at both 'sides' of the dent signals – in Figure 40 these are the 4 white peaks, in Figure 41 alternate light and dark peaks in the same location. These MFL_{axial} and corresponding MFL_{radial} peaks are consistent with a 'dent-type' feature at the sides of the defect. When one examines the 'side view' of the outside surface of this dent – shown in Figure 42 - it is possible to understand the origin of these peaks. Interestingly, at the ends, this dent has convex bumps which extend beyond the outer diameter of the pipe. These must form during pressurization as a type of 'rerounding' process, and are responsible for the peaks marked DR on Figures 40 and 41 for dent P43. The other, opposite polarity peaks at the dent sides are due to the more normal concave dent. The reason why there are two peaks on each side, rather than one, is the dent centre has 'rerounded' to a small degree (but not a lot because of the presence of the spiral weld). Given the unusual geometry, all peaks appear to be accounted for geometrically, with none likely to be stress-related.

P56: Axially elongated dent with partial re-rounding: This dent has much more significant re-rounding than the other two axially elongated dents – in fact it has the appearance of two adjacent circular dents as seen in Figure 39. The MFL_{axial} (Figure 40) plot appears as one would expect for two adjacent axial dents – with two sets of similar polarity peaks side by side. It should be noted that due to the large size of the dent the step size of the scanning probe was necessarily large, thus the closely adjacent peaks are not clearly resolvable. The MFL_{radial} (Figure 41) plots also indicate peaks associated with adjacent circular dents. There may also be some stress indications present in this result, although it is difficult to determine because of problems with the scan – the geometry changes were so significant in this case that the probe would occasionally become temporarily halted during the scanning process.

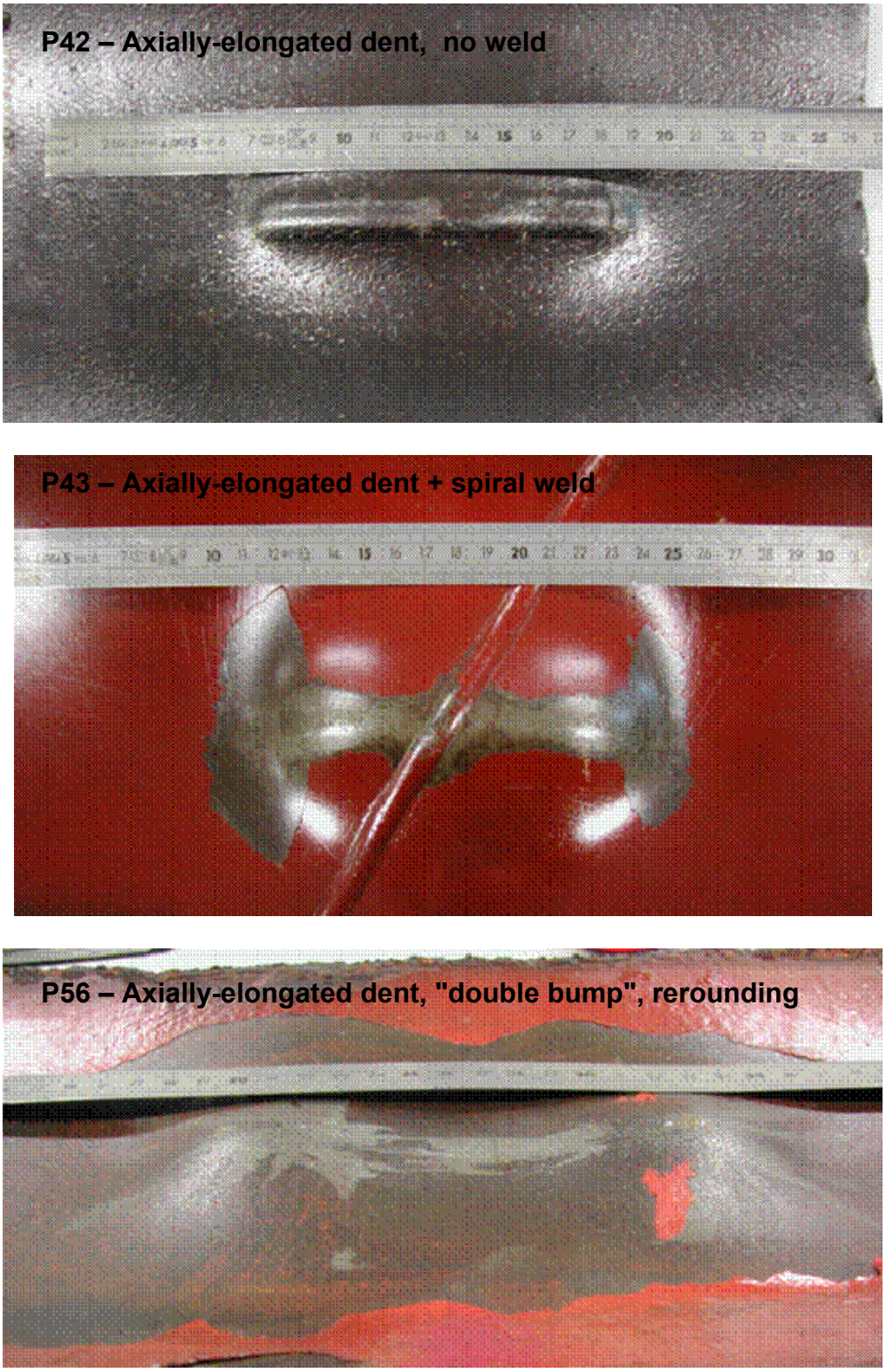

Figure 39: Inside surface photos of all three coupons containing axially-elongated dents. Samples are labeled accordingly.

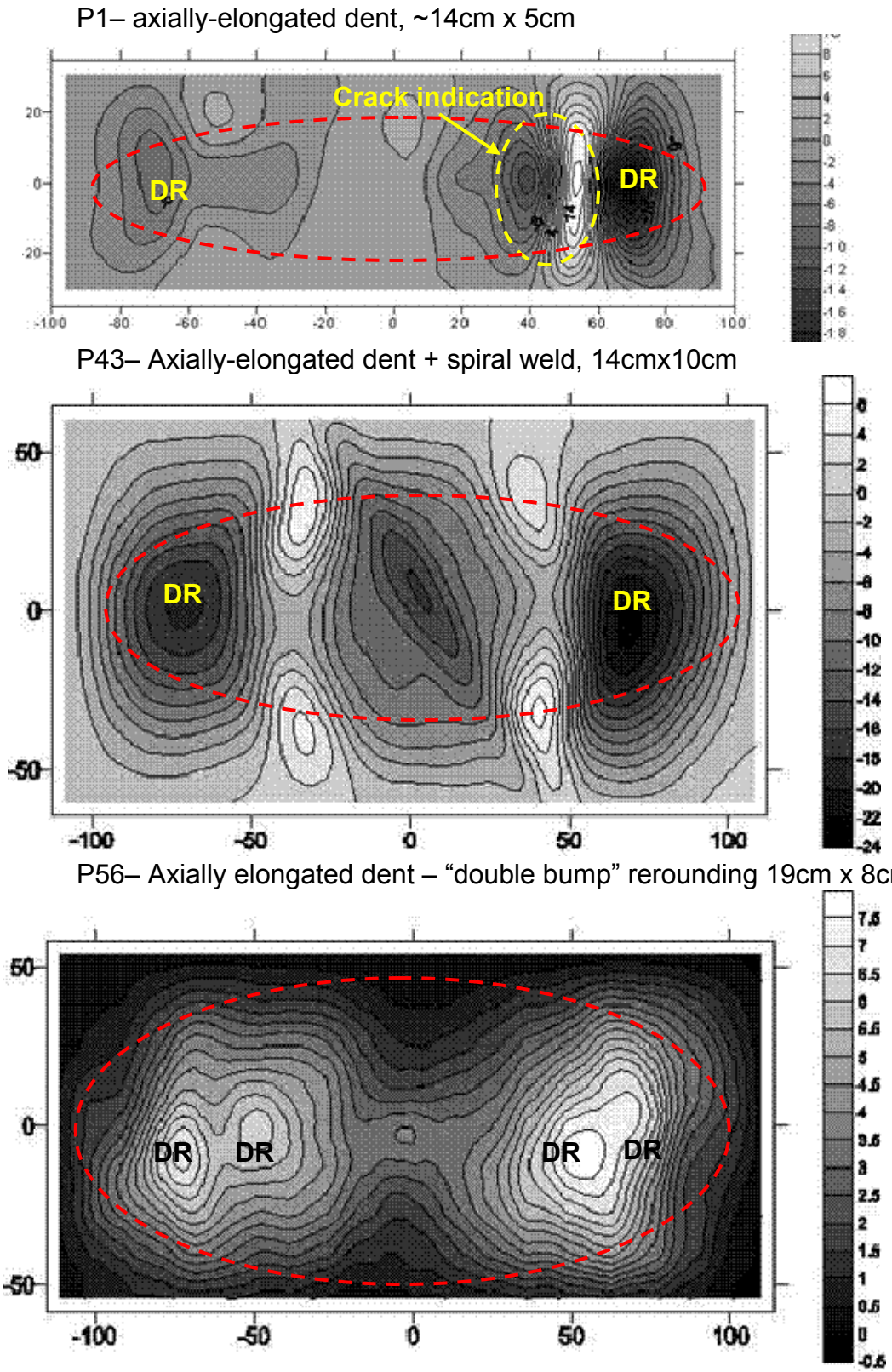

Figure 40: MFL_{axial} component signals for Gaz de France axially-elongated dents. Note that the polarity of the peaks (negative or positive) is arbitrary.

P1– axially-elongated dent, ~14cm x 5cm

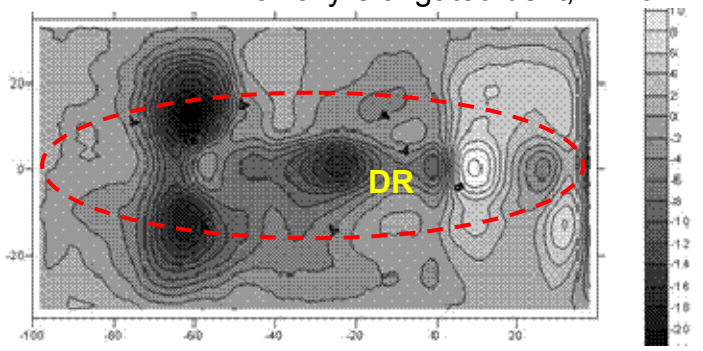

P43– Axially-elongated dent + spiral weld, 14cmx10cm

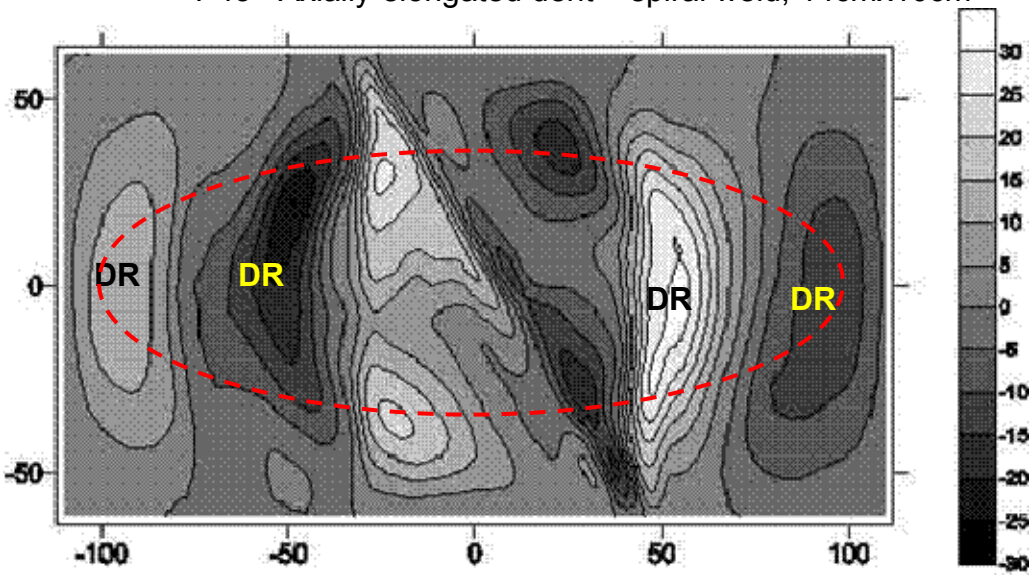

P56– Axially elongated dent – “double bump” rerounding 19cm x 8cm

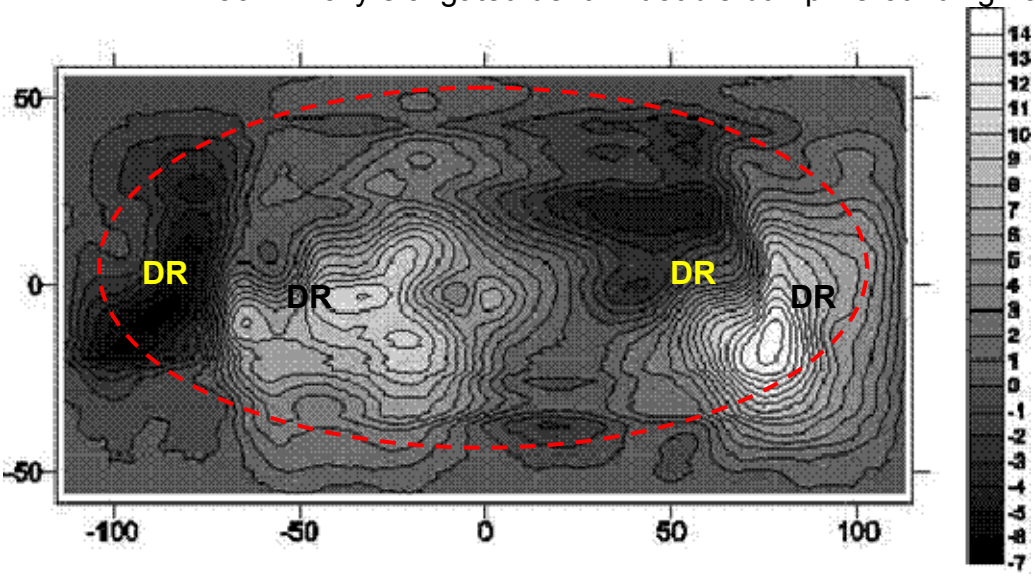

Figure 41: MFL_{radial} component signals for Gaz de France axially-elongated dents. Note that the polarity of the peaks (negative or positive) is arbitrary.

Figure 42: Side view of sample P43 – showing the interesting geometry that leads to the MFL signals in Figures 40 and 41.

5.5 Gaz de France Gouged Sample – Modeling and Experimental MFL Results (preliminary)

A detailed examination of MFL signals from gouges is expected to come in Phase III of this study (next year). However, at this point some preliminary work on gouges was conducted to determine some of the issues that will need to be addressed in the future study. The preliminary study involved magnetically modeling a gouge as a simple surface-metal-loss defect, with no geometry change at the inside wall. The result from this simple model was compared with the results from MFL measurements on a gouge sample at the Gaz de France facilities. This work is discussed in detail below.

5.5.1 MFL modeling of a simple "metal-loss" gouge in a pipe wall

A simple geometrical model was constructed, with the gouge region having the same magnetic properties as the surrounding steel material. The simple geometrical model dimensions were based approximately on the dimensions of the P22 gouged sample measured at Gaz de France. Figure 43 shows the simple gouge used in this study. As seen here, the preliminary model assumes that the gouge is a relatively simple metal-loss type defect, with straight walls and a flat bottom, and having sharp corners and edges. It is located at the top surface of a 12mm thick pipe wall. The gouge has a length of 160mm, width of 16mm, and a uniform depth of 5mm.

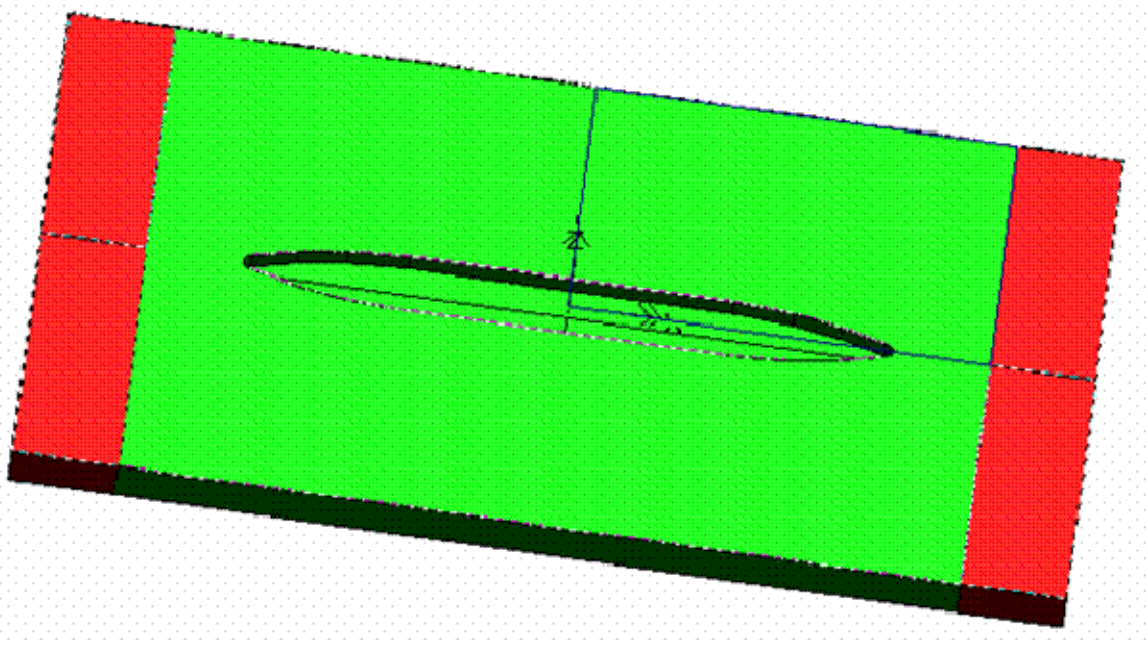

Figure 43: Magnetic finite element model of a simplified gouge. Gouge has a length of 160mm, width of 16mm, and a uniform depth of 5mm. The pipe wall is assumed to be 12mm thick.

Figures 44 - 47 shows the modeled MFL signals from the above gouge geometry. Shown are both the topside results (radial and axial) as well as the underside results (radial and axial). Note that the underside results correspond to the more realistic case of an internal pipeline inspection, but the topside results are also included for completeness.

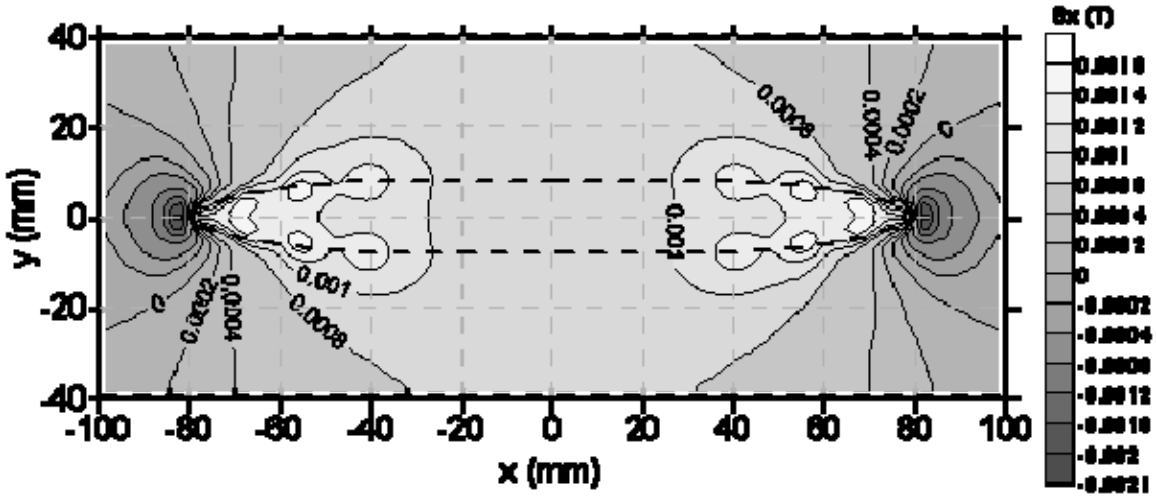

Figure 44: Topside MFL axial component.

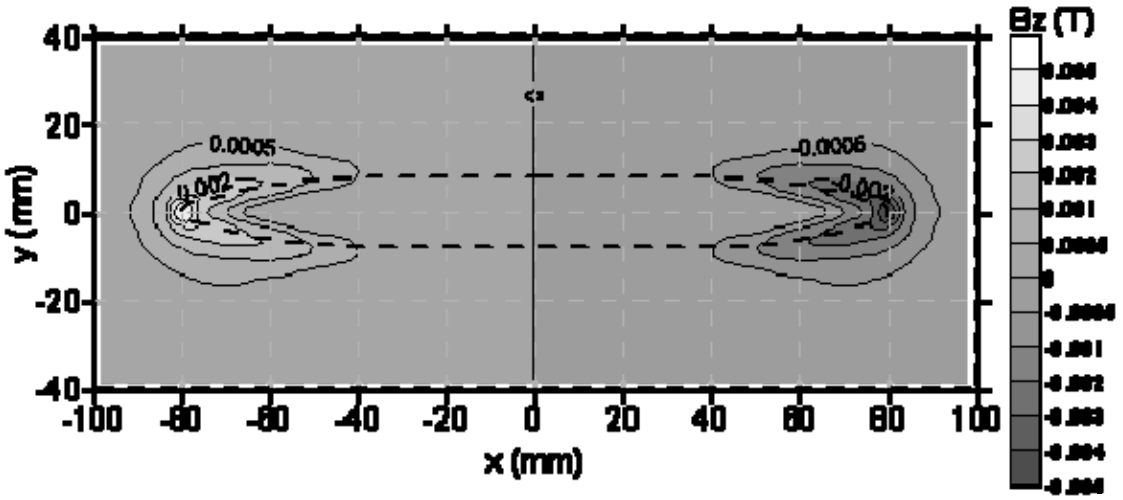

Figure 45: Topside MFL radial component.

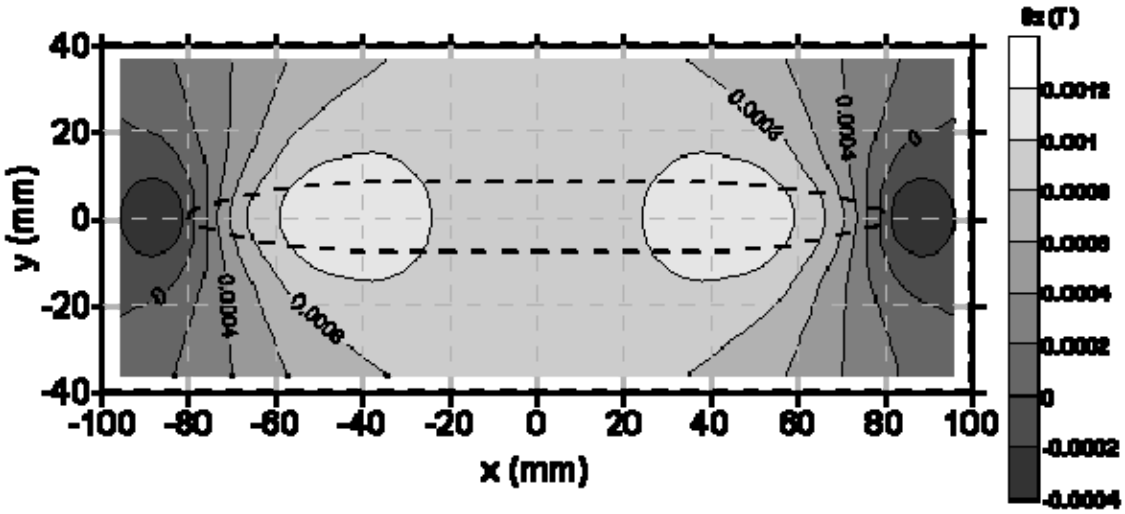

Figure 46: Underside MFL axial component.

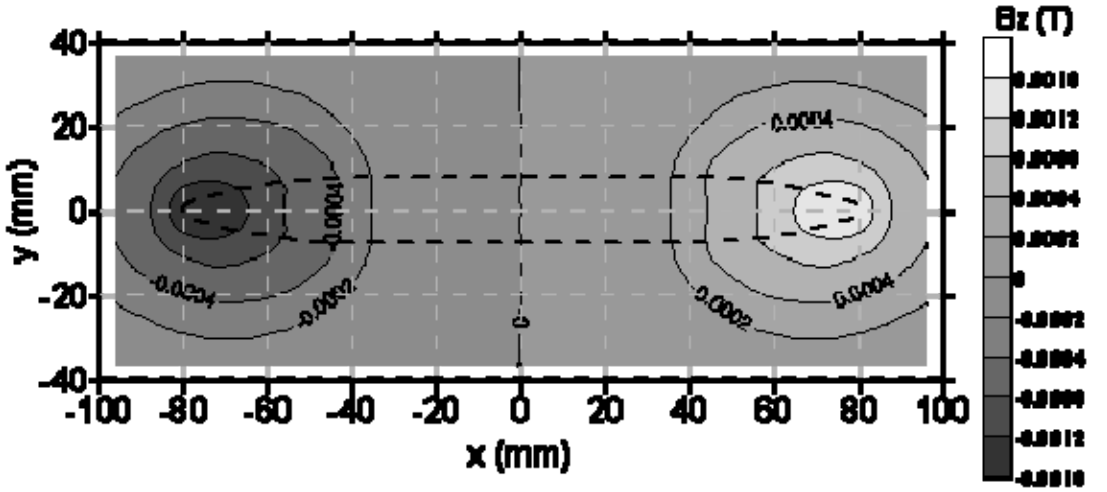

Figure 47: Underside MFL radial component.

5.5.2 Experimental results of MFL gouge measurements on Gaz de France samples

MFL measurements were made on the inside surface of the gouged sample labeled P22. This was a gouge of significant length and severity but with essentially no geometry change on inner pipe wall. The results of this study are shown in Appendix II.

Figure 48 shows the outside pipe surface containing the gouge, which is approximately 17cm long. The inside surface is not shown here since it was essentially free of any features or geometry changes (see Appendix II).

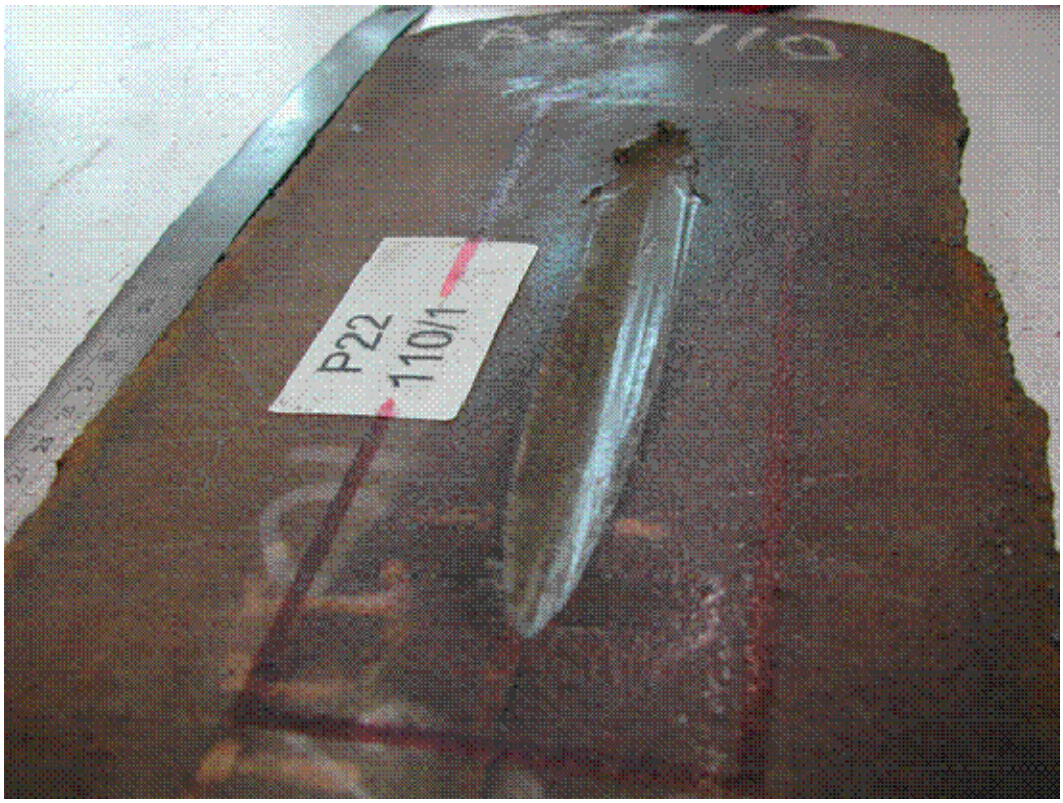

Figure 48: End-on photo of the outside surface of the gouged pipe coupon. There were no features or geometry changes at the inside wall of this coupon.

Figure 49 shows the experimental MFL_{axial} component plots, and Figure 50 the MFL_{radial} component plots for this gouge, measured from the inside surface. On both figures is shown the approximate gouge perimeter location indicated with a red dashed line.

Perhaps the most obvious difference between the measured MFL signals from this gouge and the earlier dents is the relative size of the MFL signals. Dented samples produce MFL signals up to levels as high as 50G peak to peak. The MFL signals from this gouged sample, however, are typically less than about 5G peak to peak.

In comparing modeled and measured results for gouges, recall that in earlier work on Gaz de France ***dented*** coupons, the measured signals corresponded to the modeled result. In comparing the simple metal-loss-type model gouge results to the corresponding experimental results in Figures 41 and 42, it is clear that this very simple model is not realistic for this case. This suggests that a simple geometry-based model is inappropriate for gouged samples, where the magnetic signal from the heavily deformed metal region is likely to strongly influence the result. Work in the following year (Phase III) is intended to quantify the contribution of the gouge to the magnetic signal in order to facilitate more accurate modeling.

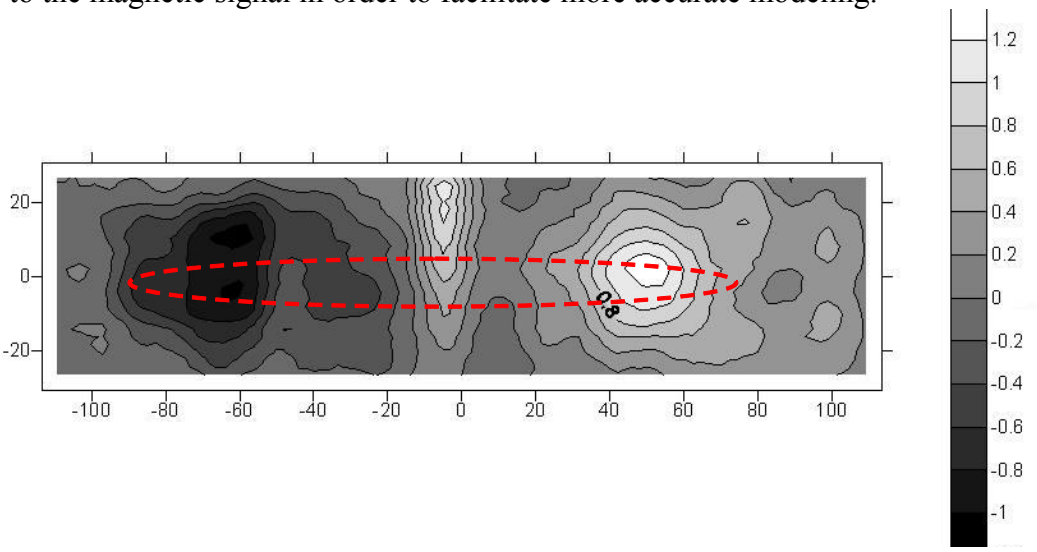

1.

Figure 49: MFL_{axial} component signals for Gaz de France gouge sample, measured from the inside pipe wall surface.

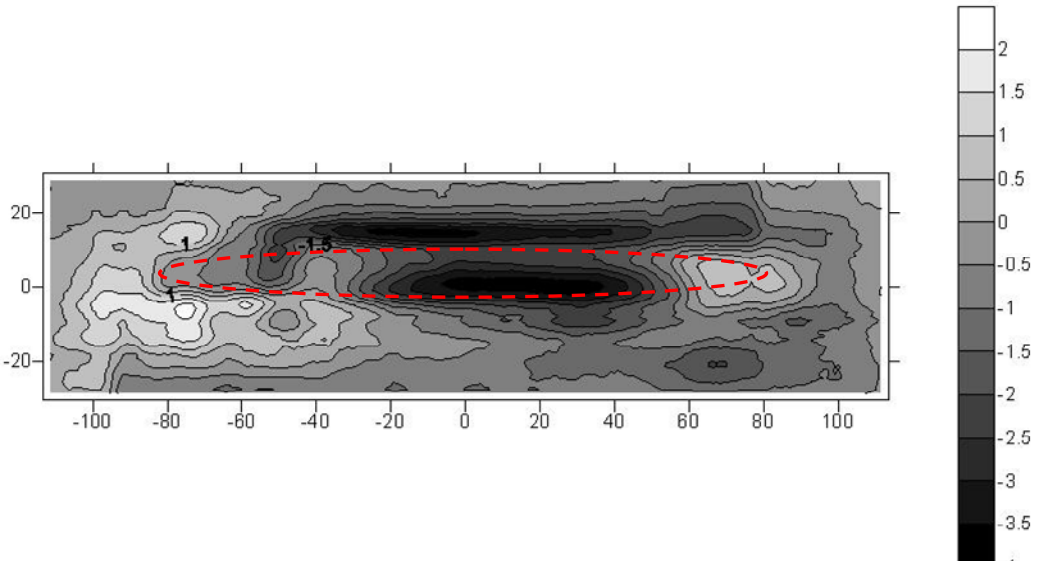

Figure 50: MFL_{radial} component signals for Gaz de France gouge sample, measured from the inside pipe wall surface.

5.6 Web-based template library - further developmental work

As mentioned in the previous year's report, the number of MFL scans associated with this study is very large. In the previous year's work (Phase I) approximately 400 MFL data plots were produced. As such it was decided that a web-accessible "template library" database would be created to allow users ready access to modeled and experimental data for comparison with their own MFL results. Figure 48 show the 'entry window' for the database constructed in Phase 1. The dent Aspect Ratios are given in the left column where 1:1 is the circular dent, 2:1 and 4:1 represent axially-elongated dents and 1:2 and 1:4 represent circumferentially-elongated dents (all studied in Phase I of this project). The three table columns indicate MFL radial, axial and circumferential component signals measured from topside and underside. When the database is online, clicking on a particular link will take the user to a .pdf page containing both unannealed and annealed data plots of increasing dent depths from 3mm to 7mm, resulting in a total of 10 plots for each link.

In the present year (Phase II) another ~40 scans were done, this time on Gaz de France samples. We propose to add these results to the template library in a similar way, with Figure 49 showing the typical entry window for this database. Greater functionality can be added as the project progresses, but it is believed that this database will provide excellent accessibility for interested users to gain easy access to the results of this study.

	Topside|Underside	Topside|Underside	Topside|Underside
Aspect Ratio	**Radial**	**Axial**	**Circumferential**
1:1 large	1:1lgTR||1:1lgUR	1:1lgTA||1:1lgUA	1:1lgTC||1:1lgUC
2:1 normal	2:1TR||2:1UR	2:1TA||2:1UA	2:1TC||2:1UC
4:1 normal	4:1TR||4:1UR	4:1TA||4:1UA	4:1TC||4:1UC
1:2 normal	1:2TR||1:2UR	1:2TA||1:2UA	1:2TC||1:2UC
1:4 normal	1:4TR||1:4UR	1:4TA||1:4UA	1:4TC||1:4UC

Figure 51: Database of MFL results for dented samples - topside and underside.

Database of MFL Results for Dented Samples for Gaz de France
All measurements made on inside surface of all pipe samples

	Inside surface	Inside surface
Sample ID	**Radial**	**Axial**
P1	P1 Radial	P1 Axial
P35	P35 Radial	P35 Axial
P38	P38 Radial	P38 Axial
P42	P42 Radial	P42 Axial
P43	P43 Radial	P43 Axial
P56	P56 Radial	P56 Axial

Figure 52: Database of MFL results for measurements on Gaz de France samples.

6.0 Summary and Conclusions

The overall goal of this phase of the project was to measure and model MFL signals from experimental dents produced using the Gaz de France pipeline aggression rig. Overall this work was successful, since modeling was found to accurately reflect the main features of the measured MFL patterns, except where anomalous stresses were believed to be present. An overall summary of work during the year is presented below.

Upgrade of the existing MFL testing rig at Queen's to improve portability and for accommodation of Gaz de France samples (outlined in section 5.1)

A number of modifications were made to the Queen's laboratory MFL equipment in order to make it portable as well as to allow it to accommodate the range of sample geometries measured at Gaz de France. On the data acquisition side these included replacing the computer monitor, upgrading the software, refurbishing the XY scanner system, and building new carriage mounts for Hall probes for the radial, circumferential and axial component scans. The magnetic circuit was also rebuilt to accommodate the larger samples, and a number of pole piece end sections were produced to fit the different diameter dented pipe samples. The completed magnetic circuit was left in the Gaz de France labs for future measurements.

Structural FEA modeling results from Gaz de France (outlined in section 5.2)

In earlier MFL modeling work we incorporated stresses into our MFL models. This was done by first modeling the stresses using structural FEA, then incorporating the stress results into the MFL models. In the present phase of the study Gaz de France provided us with some structural FEA modeling of dented pipeline samples. However, the accurate structural modeling of dents is exceedingly difficult and time consuming. The Gaz de France modeling was able to predict elastic residual stresses around a dent in a pressurized pipe, immediately following the denting process. The dented coupons we examined, however, were obtained from pipes that, after denting, had (in most cases) subsequently been ground, pressurized to failure (and thereby depressurized) and then cut out of the larger pipe. Therefore the "ideal" FEA-predicted local stresses were unlikely to be representative of the actual stresses around the dents. As a result the subsequent MFL modeling work focused mainly on modeling MFL results generated from the dent geometry, rather than the dent stresses.

Improving and upgrading magnetic FEA modeling techniques to accommodate larger and more realistic samples (outlined in section 5.3)

Our earlier modeling work involved relatively small, symmetrical dents in flat plate samples. This modeling work is complex and time consuming, even for these relatively simple cases. However, 'real' pipeline dents, such as the ones produced at Gaz de France, are much more difficult to model – since they are larger, generally asymmetrical, and located in curved pipe sections rather than flat plate. We therefore spent considerable time and effort in this phase of the project to determine the best way to produce magnetic FEA models that accurately reflected the features of the real dents. Infolytica's MagNet 6.16.3 software was used, for all of the modeling in this work. Three approaches were attempted:

1. A direct 'manual' approach, which involved measuring the main features of the dent and creating the model directly from these. This was very time consuming and ultimately unsuccessful.

2. A progressive asymmetry approach. This involved starting with a symmetric model having the same dimensions as the 'real' dent, and then progressively introducing asymmetry until the overall geometries match closely. This was successful and was the procedure ultimately used. A further conclusion from this study of asymmetry was that, although in general the MFL radial component appears to be the most distinctive for dent identification, this work indicates that the radial component is relatively insensitive to dent asymmetry. Asymmetry was found to me more clearly seen in the MFL axial component signals.

3. The laser scan import method for creating dent models in MagNet. While at Gaz de France we were able to obtain laser scan data for the 'topside' dent geometries for each of the dent we measured. Ideally, one would like to be able to directly import those scans into the MagNet MFL modeling software, and we spent approximately 3 months (of graduate student time) attempting to do this. Ultimately, however, we had to abandon this approach. Although the method is still 'promising' the resolution obtained was much lower than with the progressive asymmetry approach and the model took too long to solve (over 2 days). Work in this area was therefore suspended for now.

Results of modeling and experimental studies of Gaz de France dented samples (outlined in section 5.4)

A total of 6 Gaz de France dented samples were measured using MFL, and these results compared with modeling results. Three of these samples were circular dents, one weld-free and the other two containing welds (one girth and one axial). Both of the circular dent samples with welds were pressurized to failure. The other three samples contained axially-elongated dents. All three of these axially-elongated dents were pressurized to failure, which in most cases caused the centre region to partially re-round; as a result the elongated dents often ended up with geometry similar to two adjacent circular dents.

In comparing the modeled and measured MFL results, the following points were noted:

1) The MFL modeling results for the Gaz de France circular and axially-elongated dents were similar in form to modeled MFL results obtained for smaller dents in the Phase 1 study of the previous year.
2) As noted earlier, MFL modeling in Phase 2 only included geometry effects - stress effects were not incorporated. This was due to the fact that the stress history of the Gaz de France samples was very complex, due to denting, grinding, pressurizing to failure, 'rerounding' and then coupon removal. Accurate stress FEA analysis accounting for all these steps was beyond the scope of this project.
3) For both the circular dents and also the axially-elongated dents, the geometry-induced MFL features predicted by the MFL modeling are all consistent with those seen in the experimental results.

4) In addition to the large, significant geometry peaks predicted by the modeling, smaller, more minor peaks are seen often in the experimental MFL data. These are attributed to residual stresses around the dent (resulting from grinding, over pressurizing, and cracking), although these have not yet been quantified.
5) The weld-bead-induced MFL signal is clearly evident as a ridge across the signal. In some of the dent samples this weld bead has been partially removed during the grinding process, resulting in an MFL signal with sporadic peaks, rather than a continuous ridge. It was interesting to note that, in pipes where the weld bead had been removed (so the weld was flush with the surface) there was little or no MFL weld indication. This suggests that MFL is relatively insensitive to the material/microstructural changes between the weld and parent material.
6) Significant MFL signals often resulted from the cracks which were created during pressurization to failure. However it was not possible to determine if the large MFL signals were from the cracks themselves or the stresses associated with the cracks. An example of this was seen in sample P1, where the crack signal was very significant.
7) As mentioned above, many of the axially-elongated dents had geometries similar to two adjacent circular dents, and this was consistent with the MFL signals.

Preliminary results of modeling and experimental studies of a Gaz de France gouged sample (outlined in section 5.5)

Although the main focus of the Phase 2 study was MFL signals from dents, one measurement was taken from an undented gouge sample produced using the Gaz de France pipeline aggression rig. This preliminary measurement was conducted largely to determine whether gouges behave in a similar way to dents (whose signals have very significant geometry-induced MFL features). The gouge chosen for study was one which resembled a simple metal-loss defect – a surface depression in a pipe with no geometry change on the inside pipe wall. Despite the fact that the gouge appears visually similar to a metal-loss defect, modeling indicated that the MFL result is not consistent with a typical metal-loss signal. This indicates that further work needs to be done if MFL gouge signals are to be accurately characterized.

Web-based template library (outlined in section 5.6)

The results of the Gaz de France work were added to the template library.

7.0 Issues, Problems, and Challenges

Overall Phase II of the project has gone very well, with the experimental MFL data from dented Gaz de France samples correlating well with the modeled results. However, a number of issues have come to light this year which will be addressed in the proposed Phase III of the work. These are outlined below.

1) Although it has been very useful to examine the Gaz de France samples, the stress history is very different than that of an in-service pipe. It is also very complex and currently impossible to model accurately. Therefore, although the geometry-induced

MFL modeling results matched the experimental results very well, it was not possible to do any more than speculate regarding the stress-induced MFL patterns results. What is needed is to be able to produce dents in pipe sections where the stress patterns around dents is much better understood. This is proposed for Phase III of the study.

2) One aspect that continues to challenge us is the creation of defect models in the MagNet software. Unfortunately this software is not designed to import CAD drawings or laser scan data. The importing of laser scan data, in particular, would make the modeling much more straightforward. We attempted to do this in the current year but only had limited success. This may be an area that we may want to work on in future.
3) It is clear that dent and metal loss-modeling will not provide accurate predictions for modeling of MFL signals from gouges. The modeling of gouges will be a main focus of our future work.

8.0 Plans for Future Activity

As mentioned earlier, this was the second year of a study that is intended to extend over 4 years. This year the experimental work involved MFL measurements on 'real' dents and gouges produced by Gaz de France using their Pipeline Aggression Rig (PAR). While these PAR dents and gouges have proved extremely useful, the number of samples and their variety is limited due to the cost of producing the samples. In addition the stress history of the samples is generally complex and as a result the local stresses around the dents and gouges are unknown. It is now clear that in order to examine fully the large range of MFL effects from mechanical damage, a combination of laboratory-produced samples AND Gaz de France-produced samples is desirable. With this in mind, future project tasks are as follows:

- Develop an 'analogue' experimental laboratory dent/gouge introduction apparatus. This apparatus would be able to produce a wide range of mechanical damage geometries in steel samples, with MFL signals from selected samples being verified through comparison with similar samples produced using the Gaz de France Pipe Aggression Rig.
- Conduct magnetic measurements on gouges to determine the appropriate magnetic parameters to use for heavily cold-worked material, and magnetically model gouges using these parameters
- Extend the work on gouges to look at the effects of varying lengths/widths/depths.
- Examine MFL signals from "off axis" dents and gouges – i.e. those that have their long axis lying between the pipe circumferential and axial directions.
- Conduct a sensitivity analysis of MFL signals to specific dent and gouge geometry parameters – for example how sensitive is the MFL signal to changes in gouge sidewall/endwall slope, compared to sensitivity to depth or length changes?
- Conduct a similar sensitivity analysis of MFL signals to stress variations – for example is the MFL signal more sensitive to variations in dent rim stresses or dent base stresses?
- Modeling of the changes in MFL signals as a function of how the MFL sensors 'ride' over the top of dented regions under typical MFL inspection conditions.

9.0 References

[1] D.L. Atherton. (Oct. 1986) "Effect of line pressure on the performance of magnetic inspection tools for pipelines", Oil and Gas J., V84, No.43, 86-89.

[2] Gas Research Institute contract #5093-260-2605 "3D details of Defect-Induced MFL and Stress in Pipelines", Annual Reports 1998-2002.

[3] Gas Technology Institute contract # PR-GRI-8682 "3D Details of Defect-Induced MFL and Stress in Pipelines (Detection of Mechanical Damage using Magnetic Flux Leakage)", Annual Report 2004

[4] L. Clapham, V. Babbar and J. Byrne "Detection of Mechanical Damage using the Magnetic Flux leakage Technique", 2004 International Pipeline Conference, Oct 2004, Calgary, Alberta.

[5] Vijay Babbar, James Byrne and Lynann Clapham, "Mechanical Damage Detection using Magnetic Flux Leakage tools: Modeling the Effect of Dent Geometry and Stresses", Non-destructive Testing and Evaluation (NDT&E) International, 2005, V38, 471-477.

[6] L. Clapham, A. Rubinshteyn and V. Babbar, "Understanding Magnetic Flux Leakage Signals from Pipeline Dents" 2006 International Pipeline Conference Sept 2006, Calgary, Alberta.

[7] L. Clapham, V. Babbar and J. Bryne, "Mechanical Damage and Magnetic Flux Leakage", 16th annual World Conference on Non-destructive Testing, Montreal, August 2004.

[8] C.-G. Stefanita, D. L. Atherton and L. Clapham, "Plastic versus elastic deformation effects on magnetic Barkhausen noise in steel," Acta Mater., vol. 48, pp. 3545-3551, 2000.

[9] Infolytica Corp., P.O. Box 1144, 300 Leo Pariseau, Suite 2222, Montreal, Quebec H2W 2P4.

APPENDIX 1

Table 3: Summary of all tested dent samples

Sample No.	Defect Type	Defect Description
P1	Axial Elongated Dent Dent Length ~ 14 cm, Width ~ 5 cm	Plain axial elongated dent. The pipe was wound with a clockspring over the top of this dent before pressurizing to failure. Failure was via a small circumferential crack located at one end of the dent.
P35	Circular Dent + Circumferential Weld Dent Diameter ~ 13 cm	Plain circular dent containing a circumferential girth weld. The weld is quite rough and is cracked at the inside surface where it was likely pressure tested.
P38	Circular Dent + Axial Weld Dent Diameter ~ 8 cm	Plain circular dent with a very clean (no weld bead) axial weld running through the middle. The weld is ground and looks like it failed during a pressure testing procedure.
P42	Circular Dent Dent Diameter ~ 9 cm	Plain circular dent – no weld nearby. No failure evident
P43	Axial Elongated Dent + Diagonal Weld Length ~ 14 cm, Width ~ 10 cm	Plain axial dent located on the top of a spiral weld that cuts it approximately diagonally. Pressurizing resulted in a slight 'double bump' effect with the bumps centered on the deepest indenter marks at the end. There are some small axial cracks at these ends of the dent coming from the deepest indenter marks.
P56	Axial dent with partial rerounding Total Length ~ 19 cm, Width ~ 8 cm	Plain axial dent – no weld nearby, and no cracking apparent. Pressurizing has resulted in a significant 'double bump' effect with bumps centered on the indenter corners. A very small gouge is also apparent at the centre, but no failure cracks are evident.

Sample P1:

Identifying marks:
P1
Clockspring 1999

Description:

Sample size: 18cm x 28 cm.
Plain axial dent of size ~14 cm long and 5cm wide. Strain gauges seen mounted at outside wall in centre of dent. A circumferential crack is located at one end of dent – this extends through to the other side.

This was a test sample that a plain dent was made in – no gouge. It was then ground on nearly all the dent surface (outside). After that it was wound with a clockspring, and then pressure tested. It failed via the circumferential crack seen at the end of the dent.

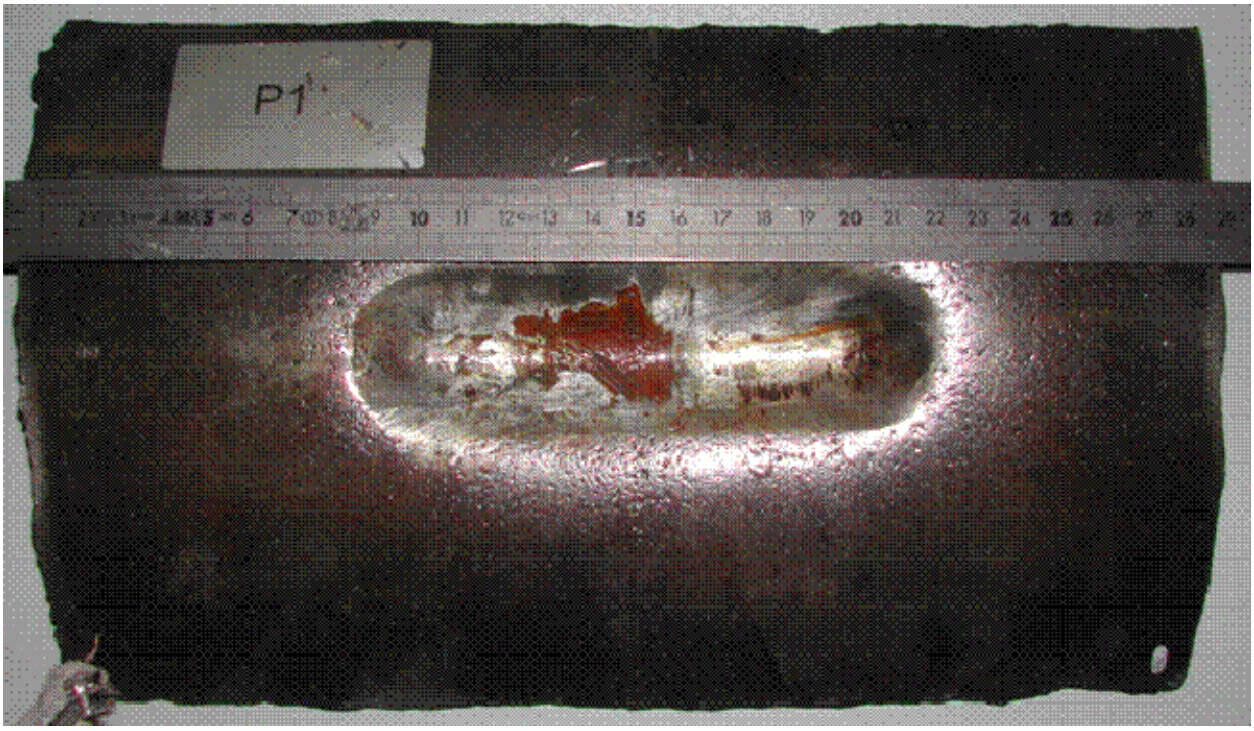

(a)

(b)

Figure P1:1: Outer pipe wall – a) top view and b) end-on view of P1 elongated dent.

(a)

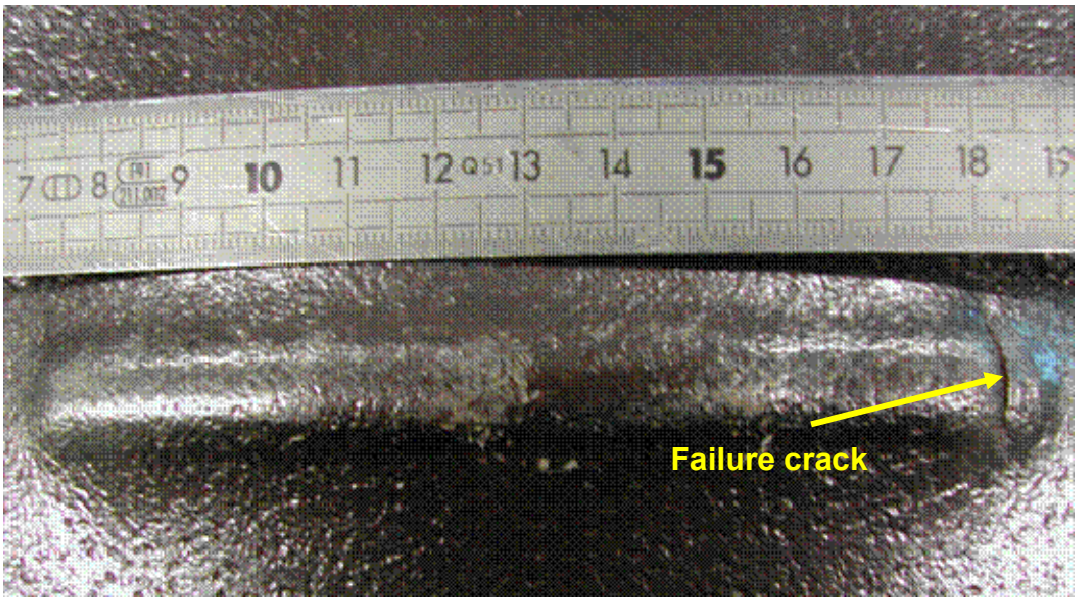

(b)

Figure P1:2: Inner pipe wall – a) overall plan view and b) close-up view of dent.

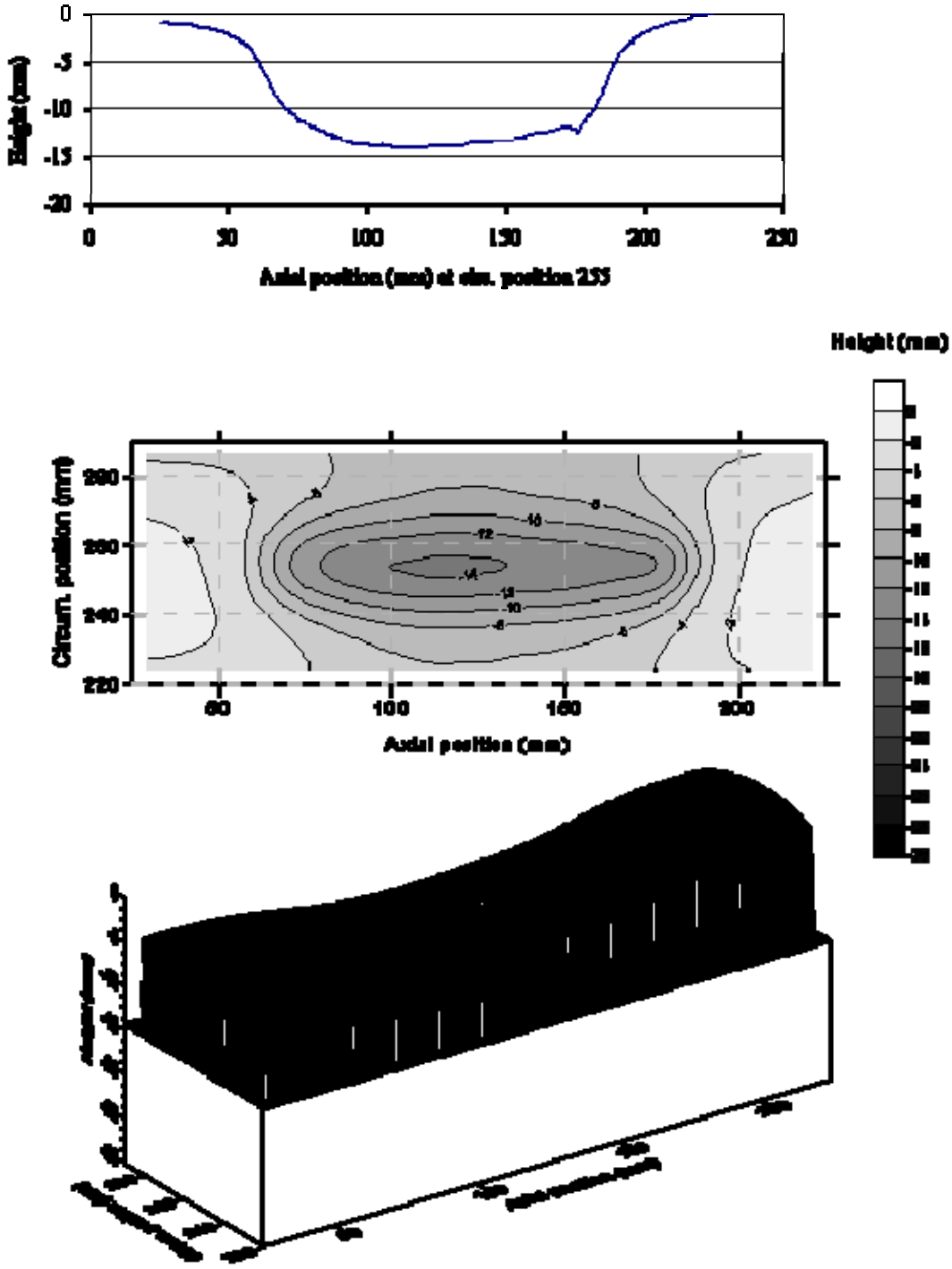

Figure P1:3: Laser geometry scan plots of Sample P1. Line scan through mid-width axial line (top), contour plot (middle), and 3D surface plot (bottom). All laser scans taken from the top surface of the sample.

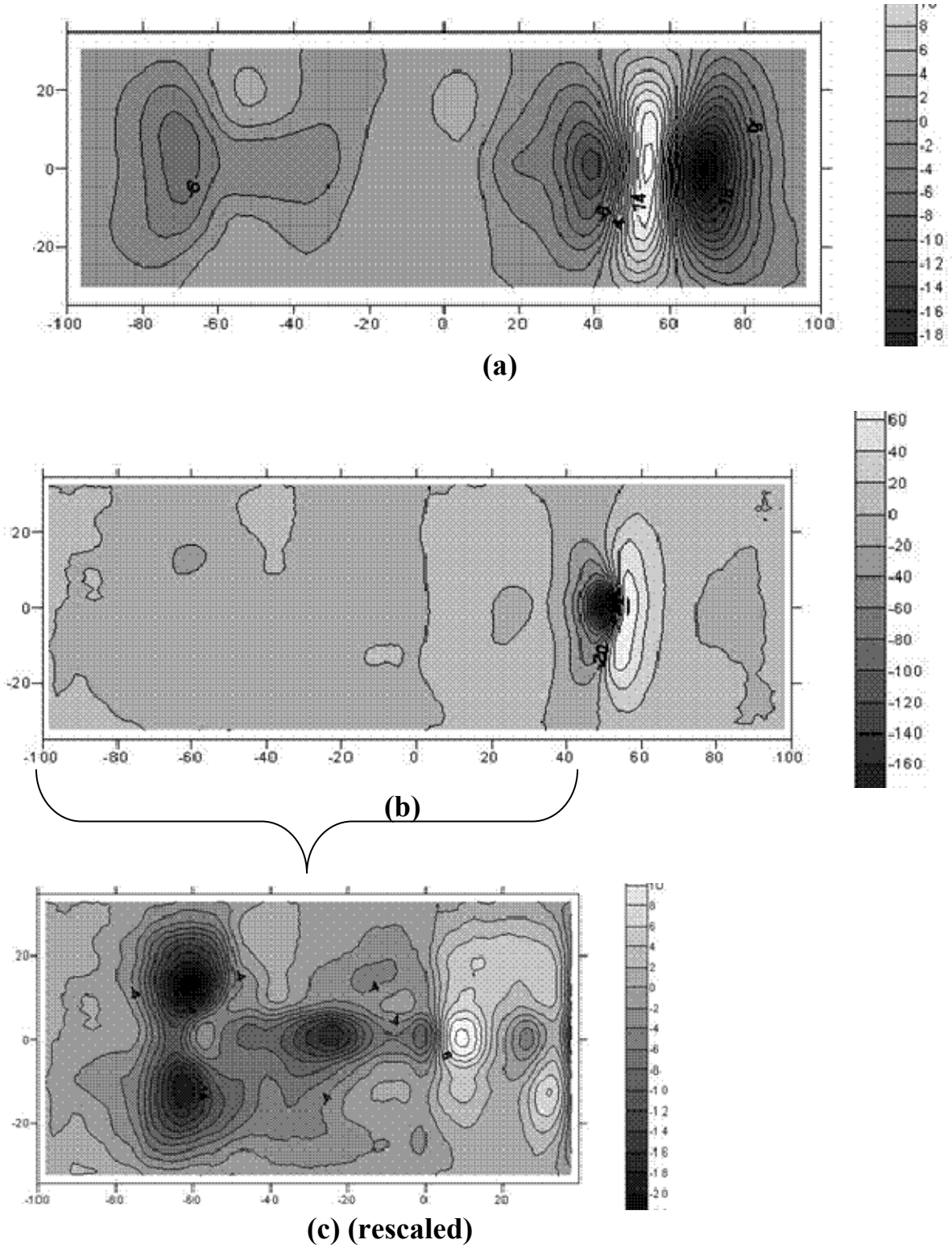

Figure P1:4: MFL (measured) results for Sample P1. a) axial, b) radial and c) radial, rescaled in region away from the circumferential crack, which dominates the MFL signal.

Sample P35#2

Identifying marks:
P35 ESC2 two sets of strain gauges on the top, and a grid marking – along with some numbers – 370 along the axial direction.

Description:

Sample size: 30cm x 37cm
Plain circular dent of size ~13 cm diameter - located on the top of a girth weld. It has been ground also – particularly at the top of the girth weld itself.

This was a test sample – plain dented and then ground across the dent outside. The weld is quite rough and at the inside surface the weld has cracked where it was likely pressure tested.

(a)

(b)

Figure P35:1: Outer pipe wall – a) top view and b) end-on view of P35 circular dent with girth weld.

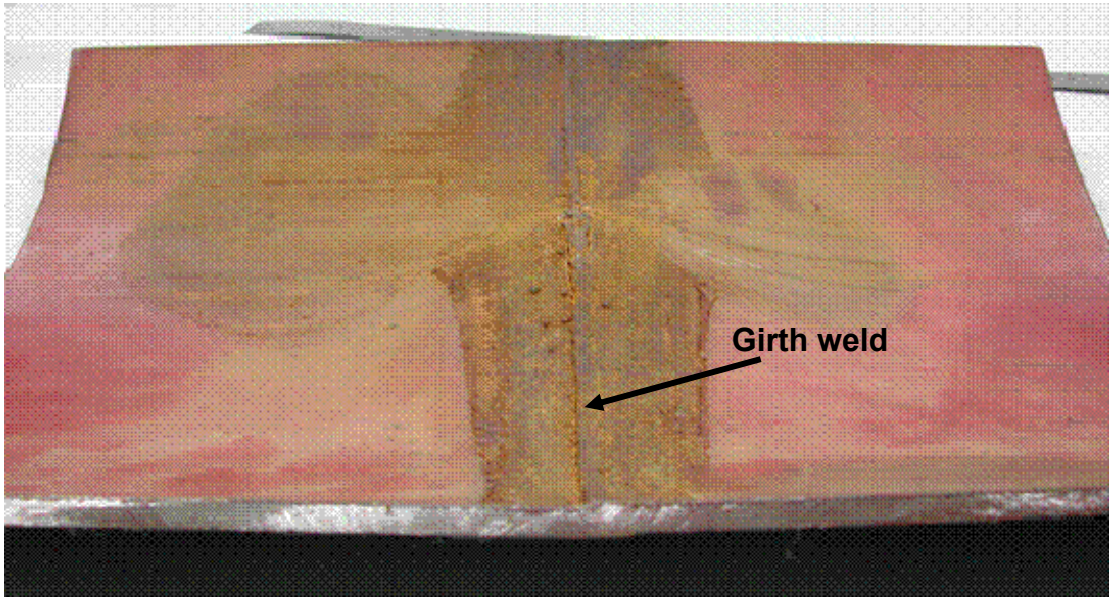

(a)

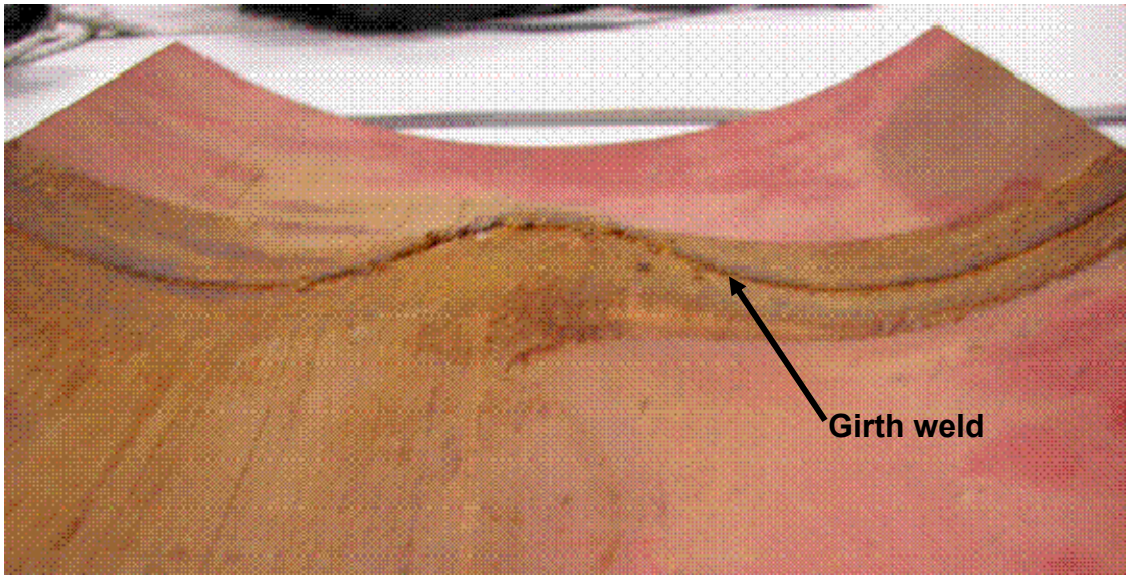

(b)

Figure P35:2: Inner pipe wall – a) view from the side b) end on view.

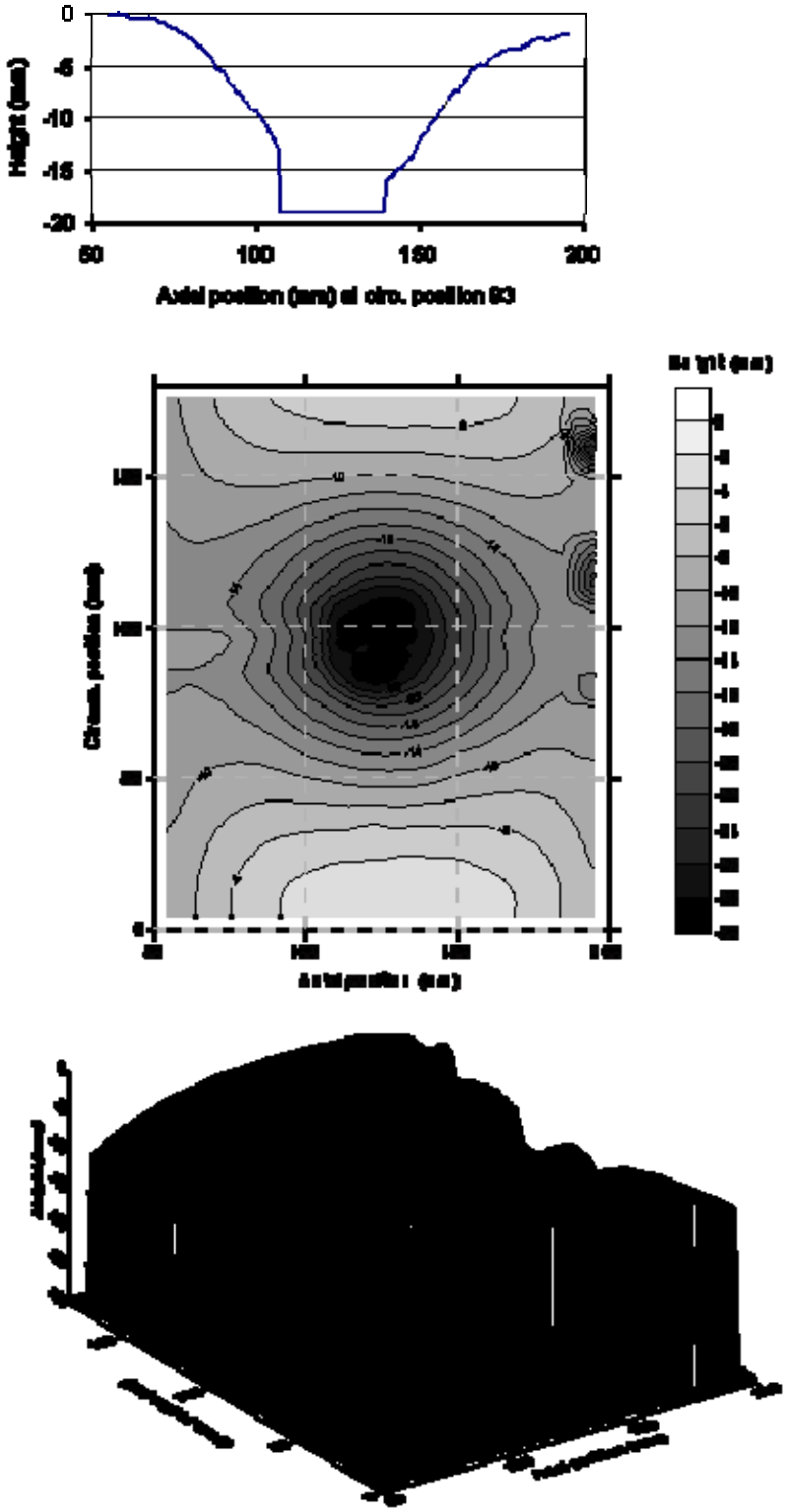

Figure P35:3: Laser geometry scan plots of Sample P35. Line scan through mid-width axial line (top), contour plot (middle), and 3D surface plot (bottom). All laser scans taken from the top surface of the sample.

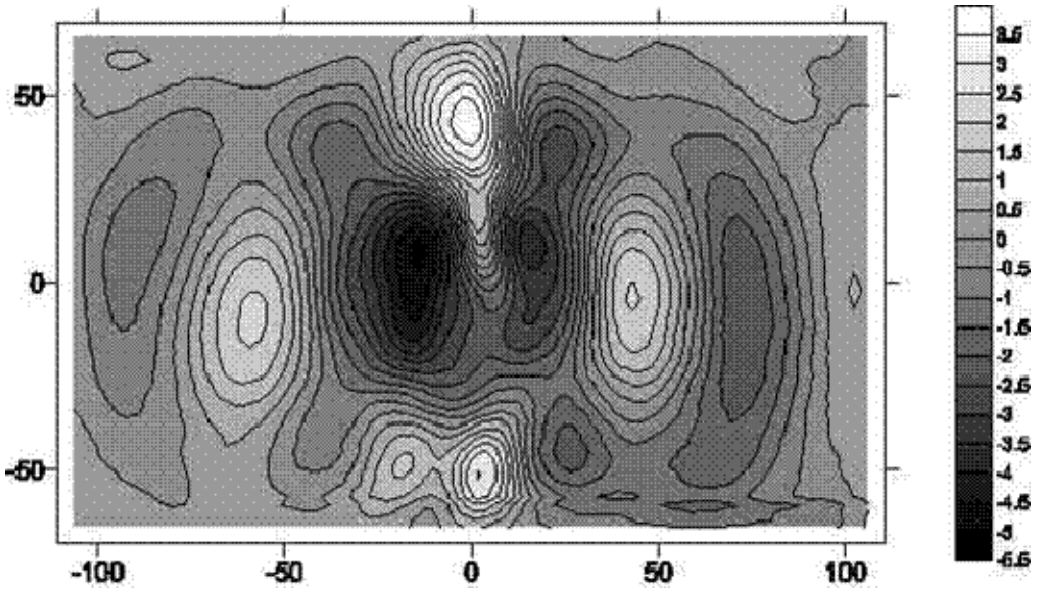

a)

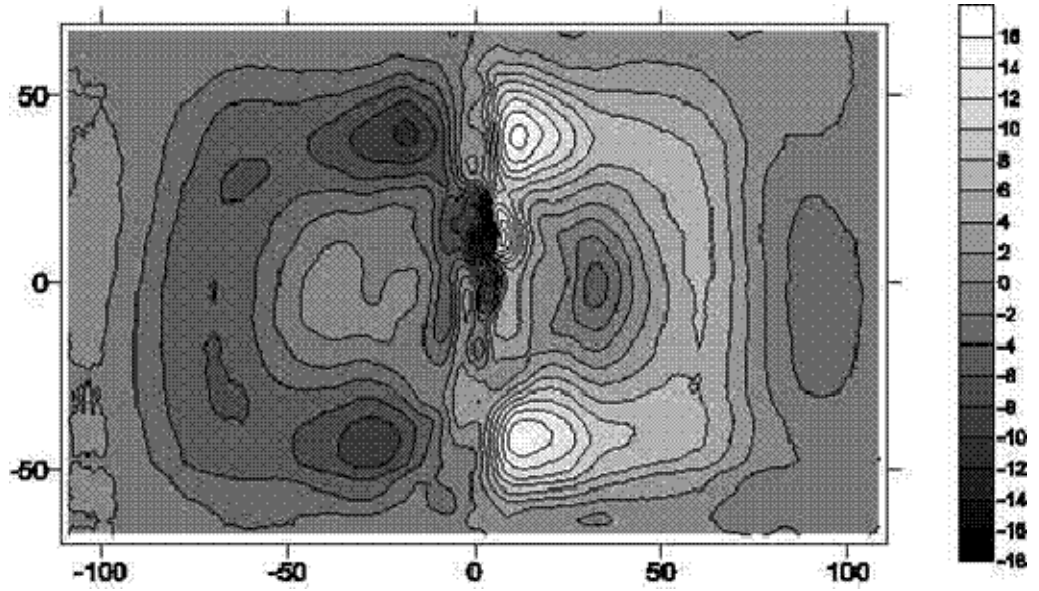

b)

Figure P35:4: MFL (measured) results for Sample P35. a) axial and b) radial.

Sample P38

Identifying marks:
P38 ESI2 various markings on the outside as seen

Description:

Sample size: 18.5cm x 38.5cm
Plain circular dent of size ~8 cm diameter – it has a very clean axial weld running through the middle of it – the weld is almost not noticeable from the outside (no scarf at all). This has been ground also and then looks like it failed during a pressure testing procedure.

There are strain gauges located in the dent rim region in two locations. The red region indicates the approximate scan region.

(a)

(b)

Figure P38:1: Outer pipe wall – a) top view and b) end-on view of P38 circular dent. This coupon has an axial weld running through the centre of the defect, although it is difficult to see from the outside surface.

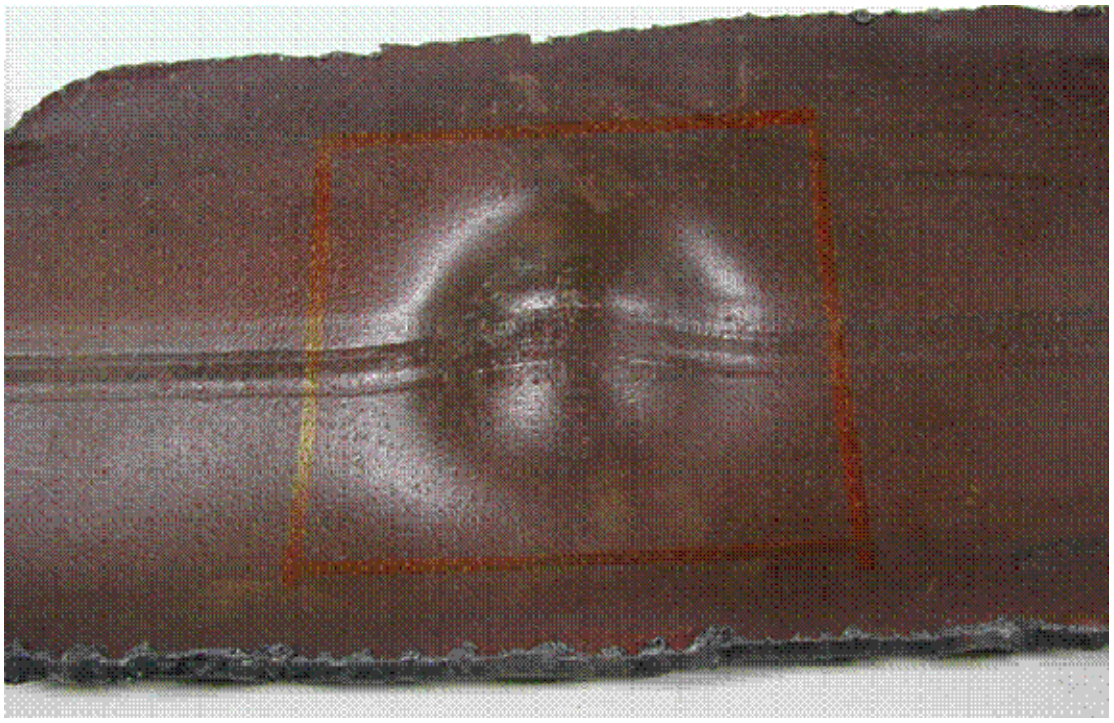

(a)

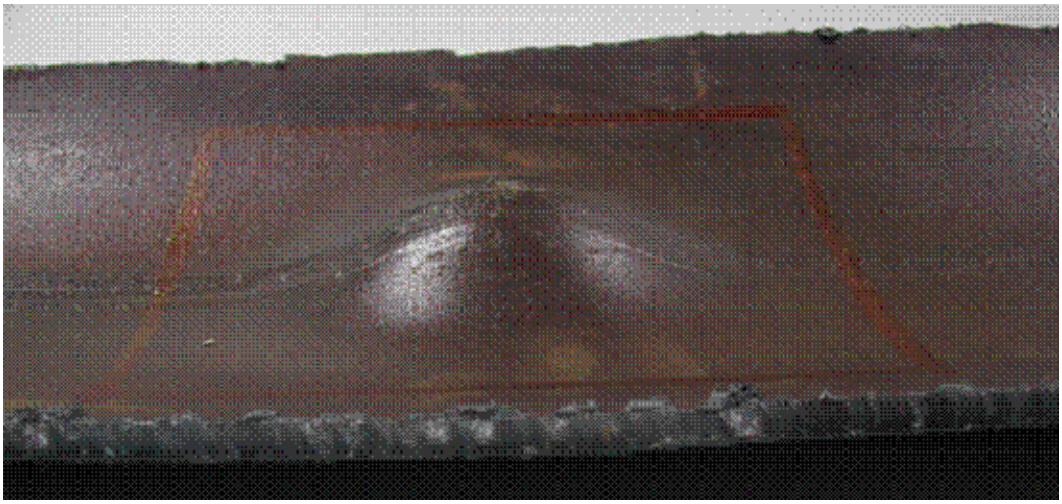

(b)

Figure P38:2: Inner pipe wall – a) plan view and b) side-on view of P38 circular dent. Although the axial weld was difficult to see on the outer surface (Figure P38:1) it is clearly visible in these two photos.

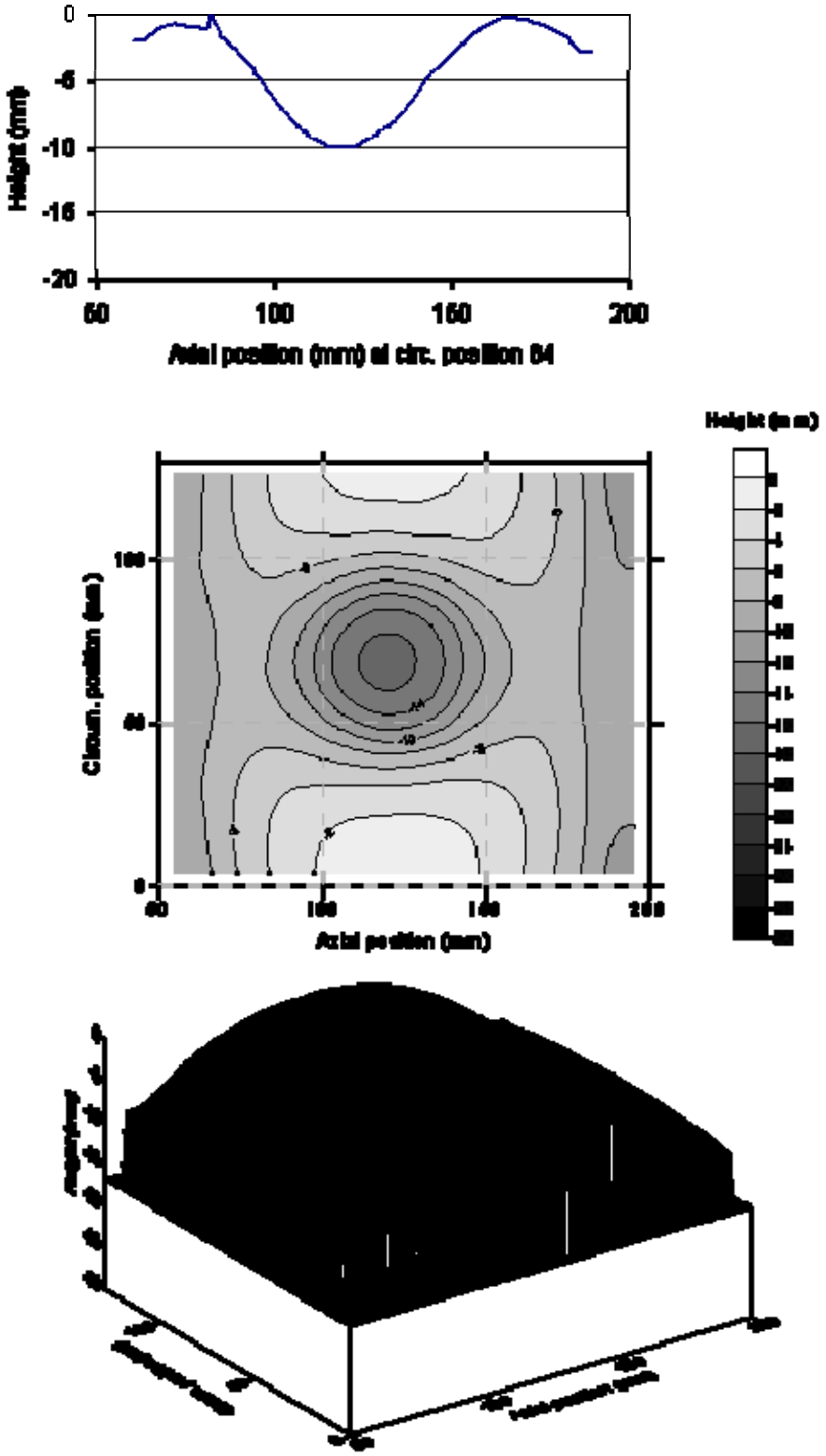

Figure P38:3: Laser geometry scan plots of Sample P38. Line scan through mid-width axial line (top), contour plot (middle), and 3D surface plot (bottom). All laser scans taken from the top surface of the sample.

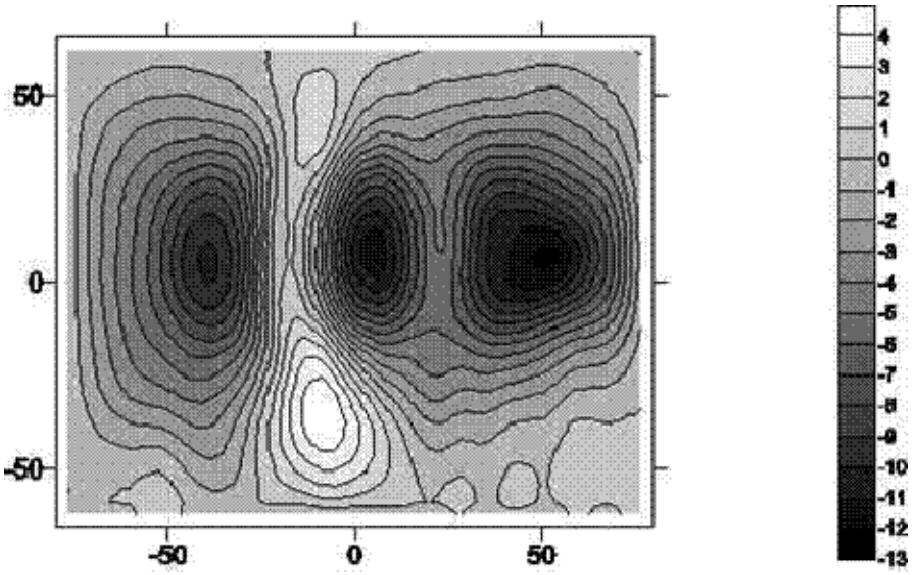

a)

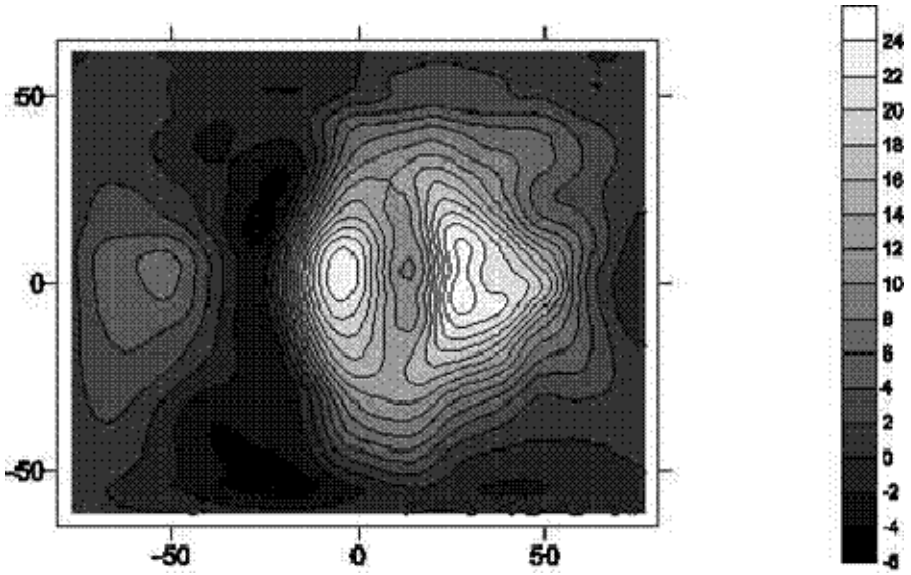

b)

Figure P38:4. MFL (measured) results for Sample P38. a) axial and b) radial.

Sample P42

Identifying marks:
P42 SCH O34

Description:

Sample size: 17cm x 30 cm
This is a circular plain dent – no gouge and no weld nearby. The dent diameter is about 9 cm, some grinding marks evident.

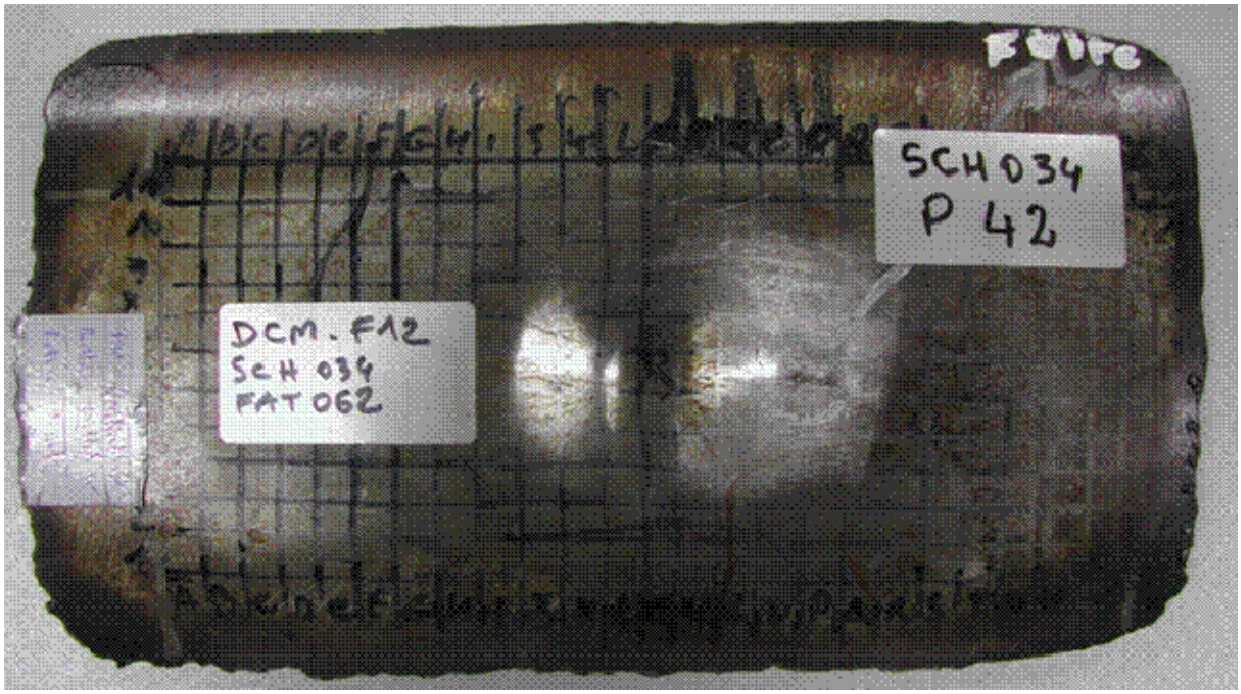

(a)

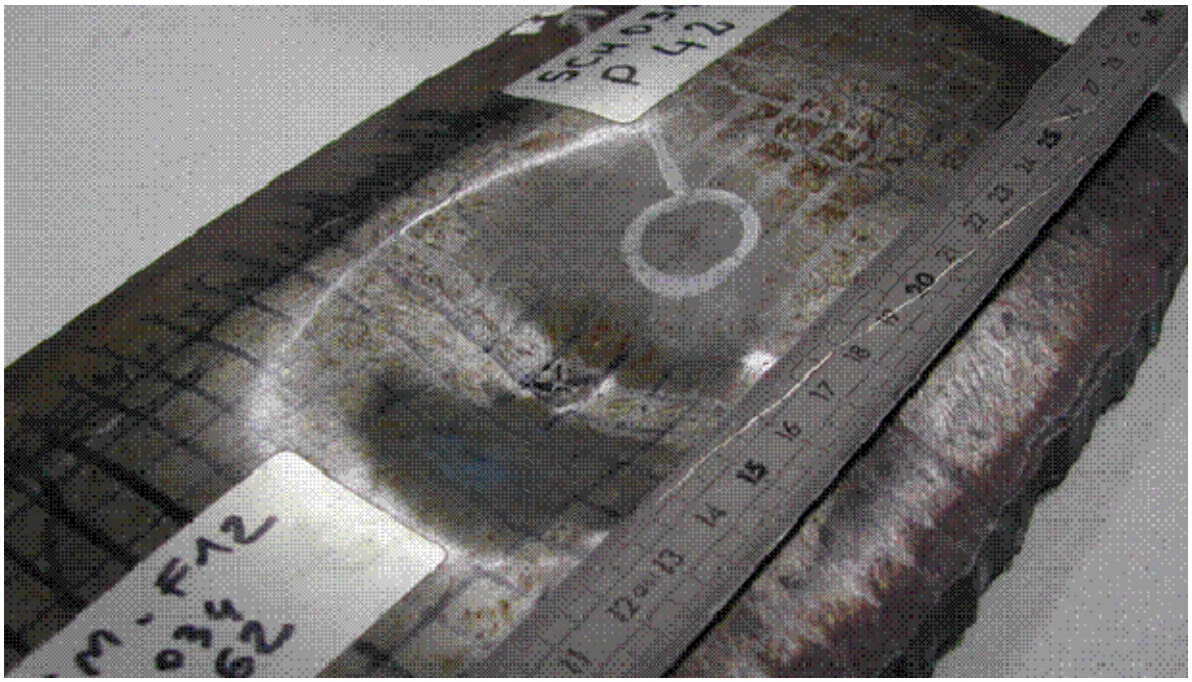

(b)

Figure P42:1: Outer pipe wall – a) top view and b) oblique view of P42 circular dent. This coupon has no welds.

a)

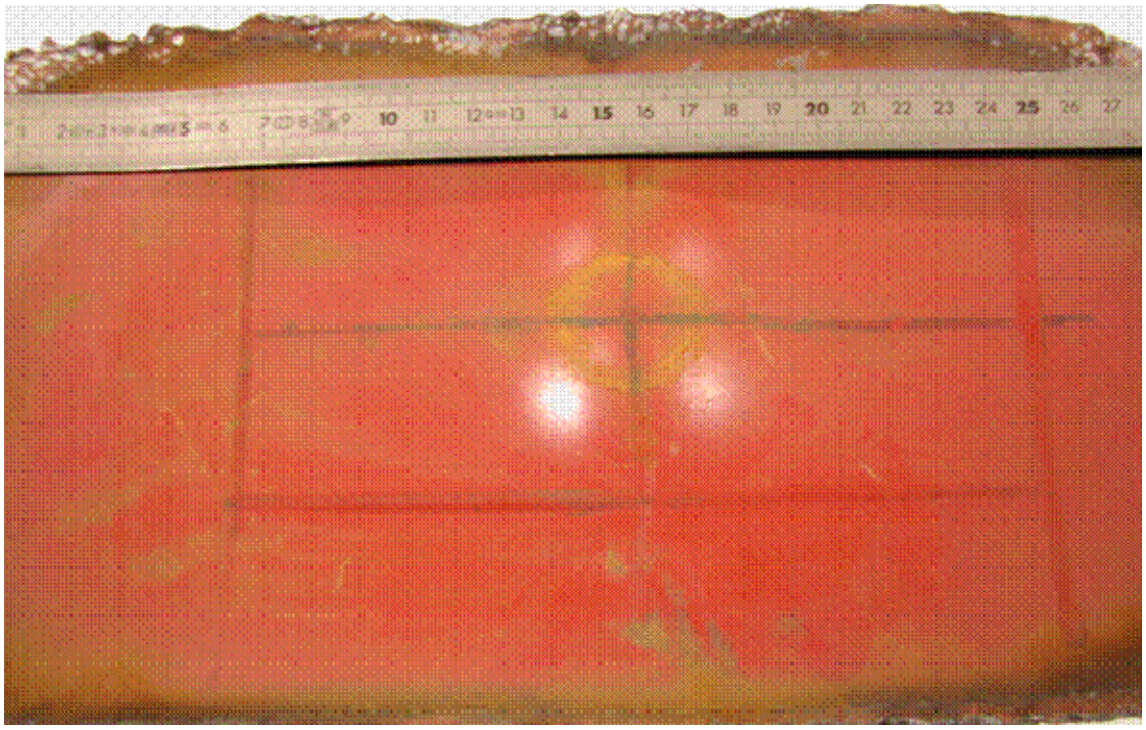

(a)

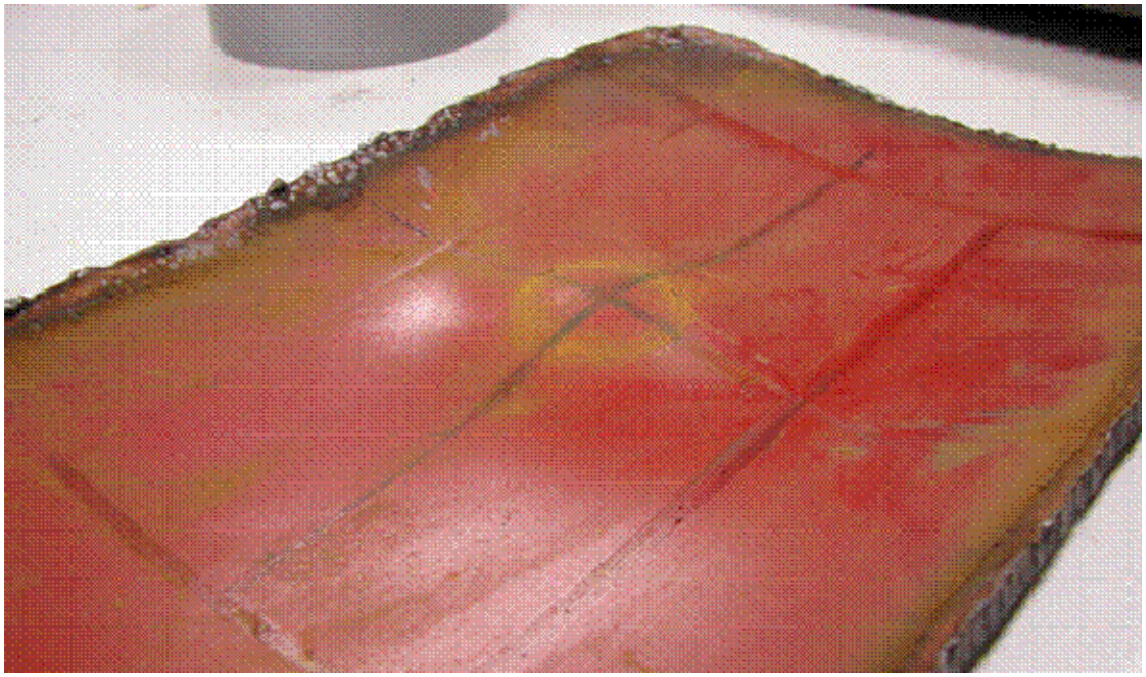

(b)

Figure P42:2: Inner pipe wall – a) top view and b) oblique view of P42 circular dent. This coupon has no welds.

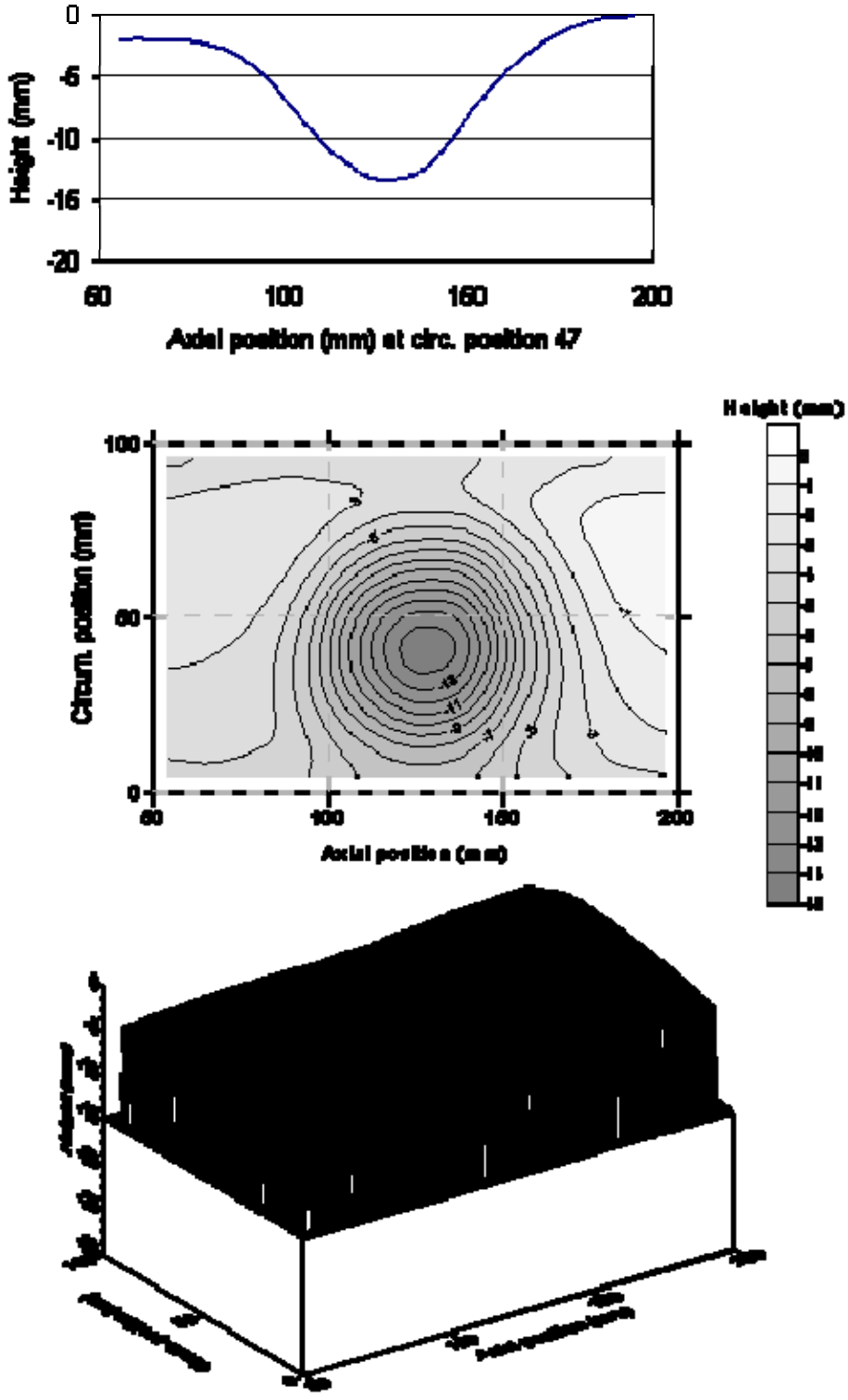

Figure P42:3: Laser geometry scan plots of Sample P42. Line scan through mid-width axial line (top), contour plot (middle), and 3D surface plot (bottom). All laser scans taken from the top surface of the sample.

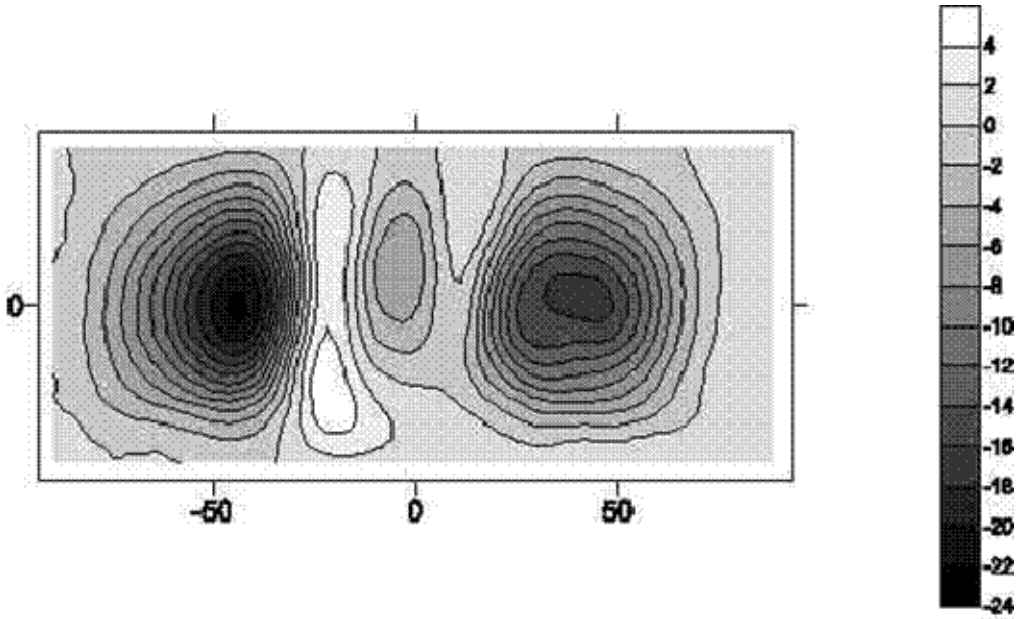

a)

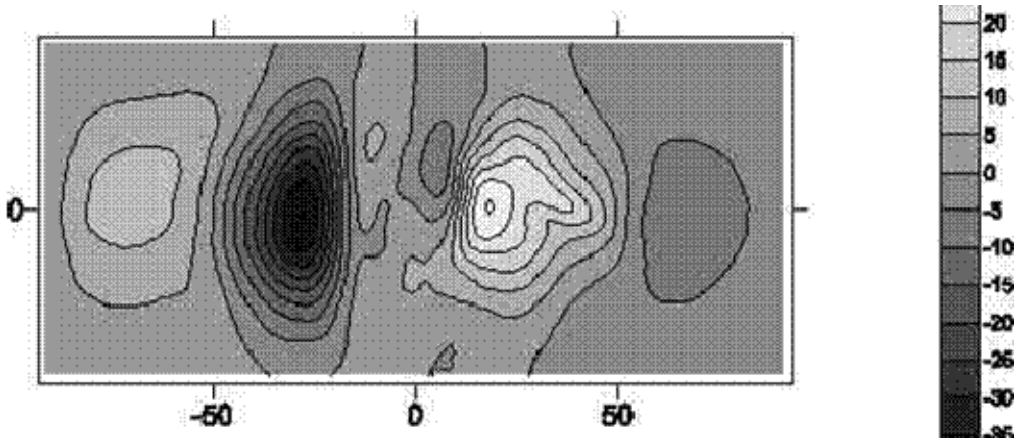

b)

Figure P42:4: MFL (measured) results for Sample P42. a) axial and b) radial.

Sample P43

Identifying marks:
P43 ESH4

Description:

Sample size: 22cm x 44 cm
Plain axial dent of size ~14 cm long and 10cm wide – located on the top of a spiral weld which cuts it approximately diagonally.

This was a test sample – plain dented and then ground across the dent outside. It has quite large ridges at the end on the outer surface. There are some small axial cracks at the end of the dent coming from the deepest indenter marks.

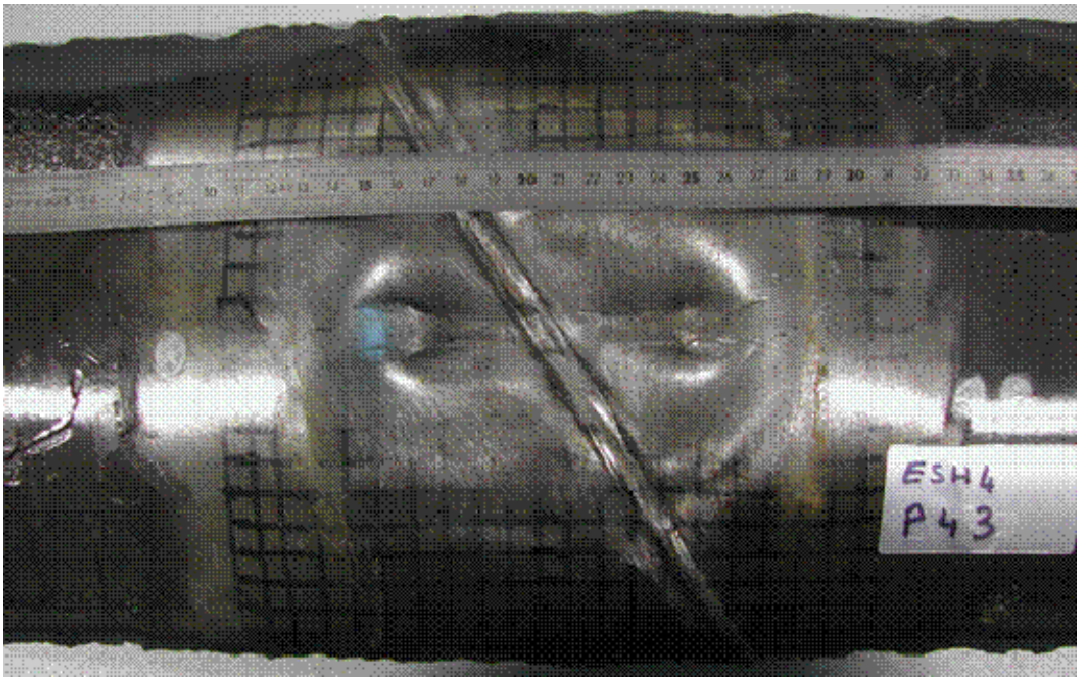

(a)

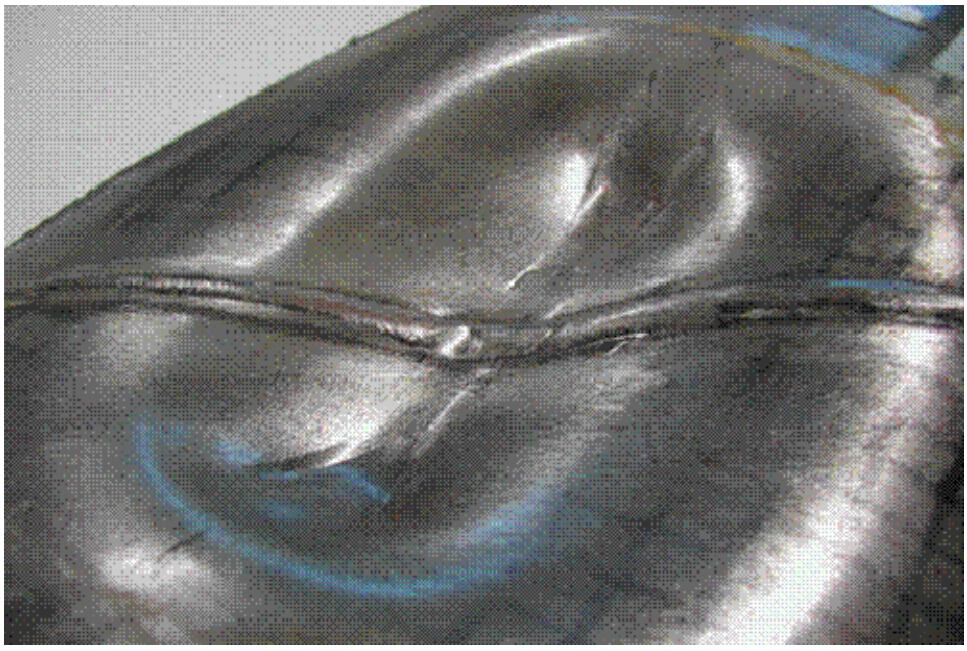

(b)

Figure P43:1: Outer pipe wall – a) top view and b) oblique view of P43 elongated dent over the top of a spiral weld. Indenter corner marks are clearly seen.

(a)

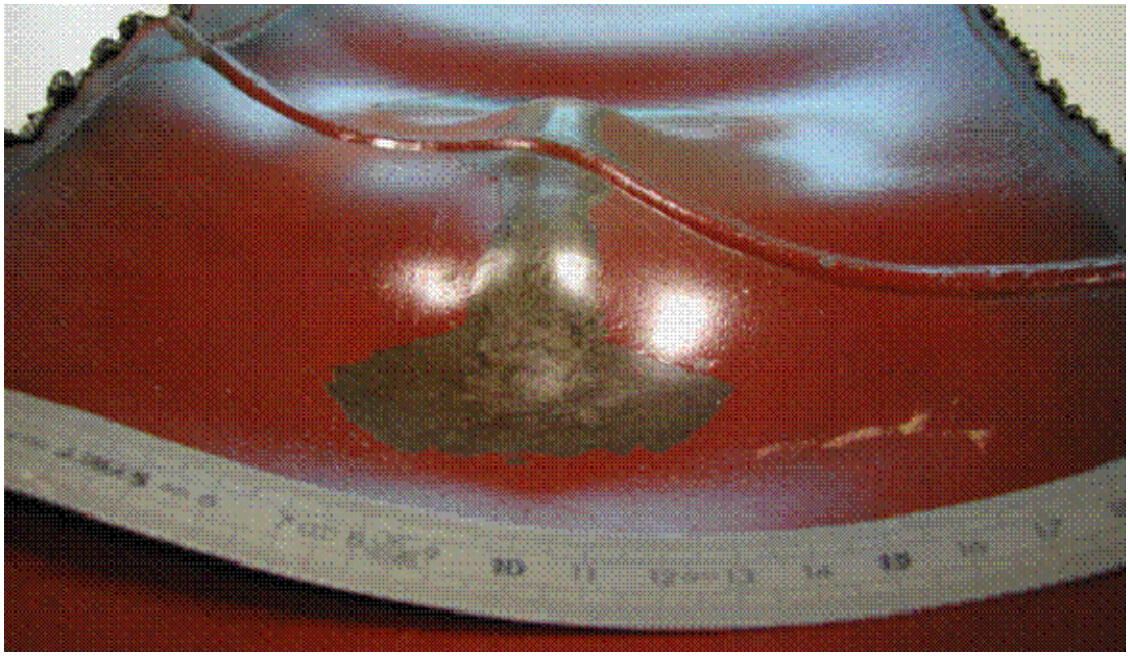

(b)

Figure P43:2: Inner pipe wall – a) top view and b) end-on view of P43 elongated dent over the top of a spiral weld. No grinding marks are evident on this surface.

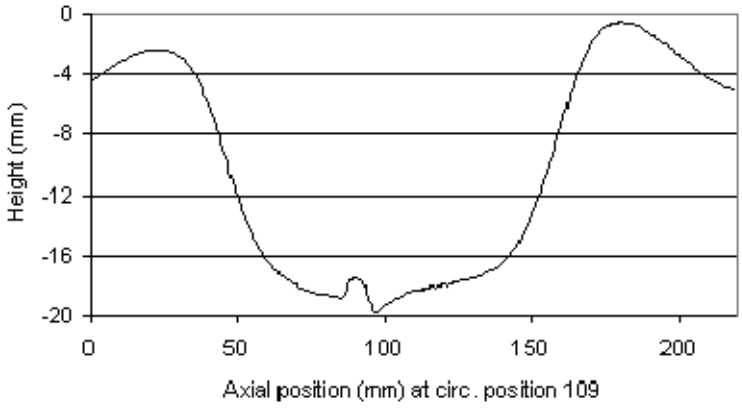

….

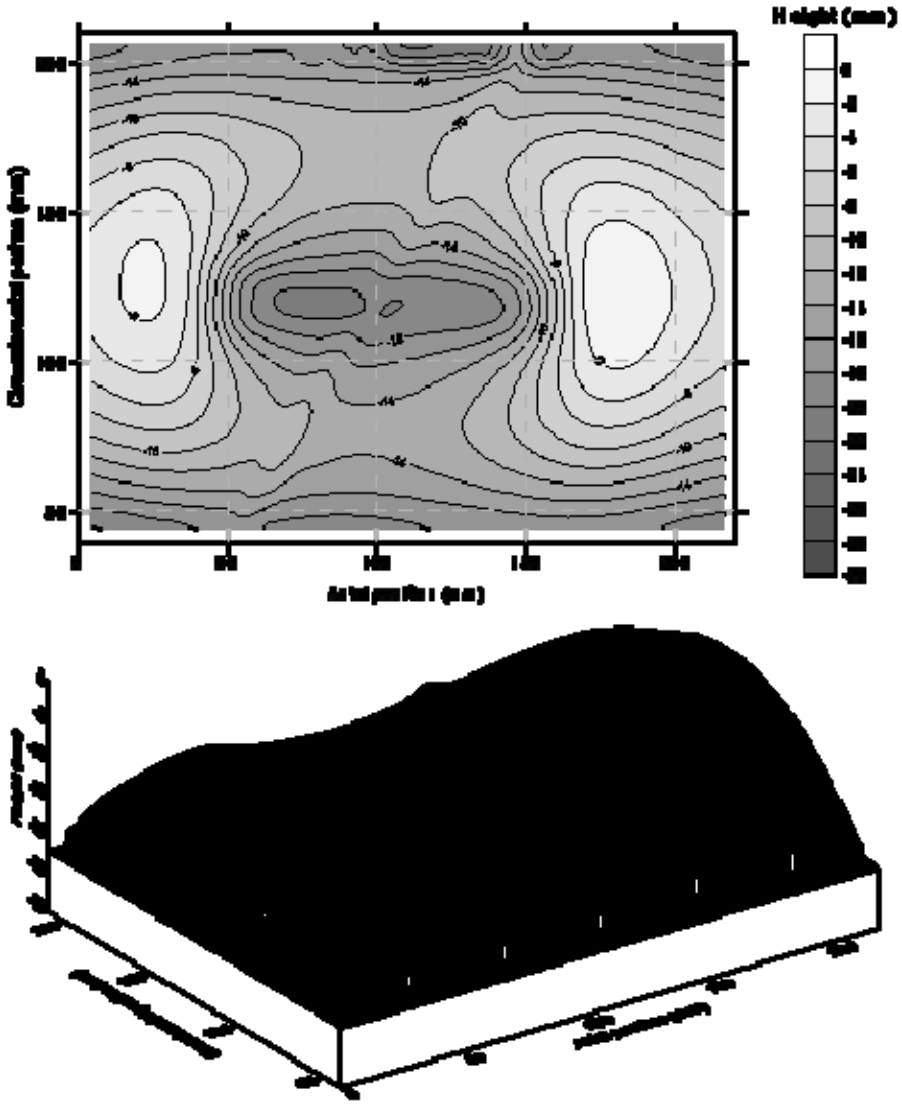

Figure P43:3: Laser geometry scan plots of Sample P43. Line scan through mid-width axial line (top), contour plot (middle), and 3D surface plot (bottom).

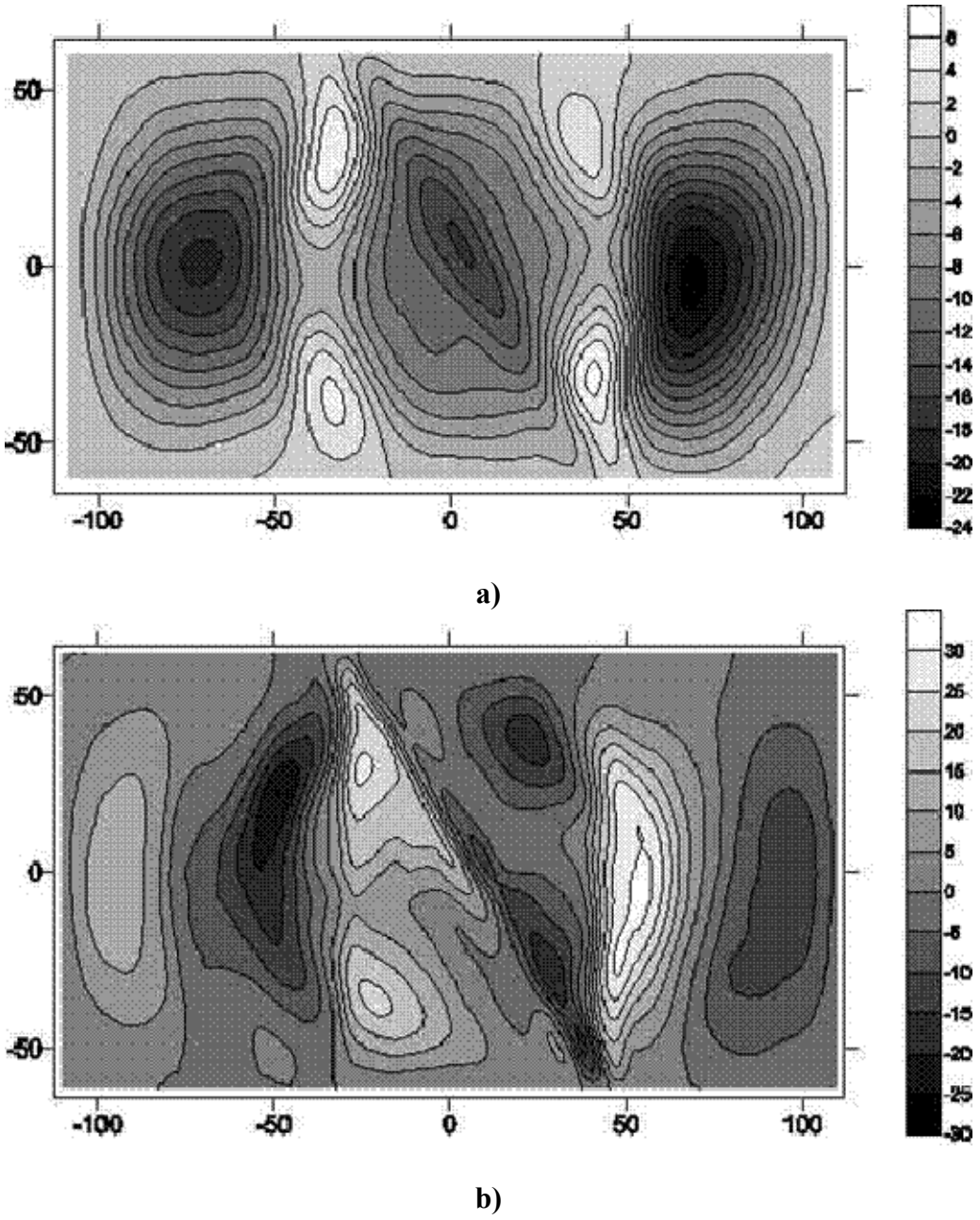

Figure P42:4. MFL (measured) results for Sample P43. a) axial and b) radial.

Sample P56

Identifying marks:
P56 DCMF15 also has markings C18

Description:

Sample size: 23cm x 49 cm
This is an elongated dent of total size ~19 cm long and 8cm wide. Upon pressure testing the centre region re-rounded but the ends of the dent (corresponding to the indenter corners) did not reround as much as the middle. This created a feature which looks like 2 axially adjacent plain axial dents. No other features except some 'humps" at the ends and a bit of a gouge at the centre. No cracking apparent.

a)

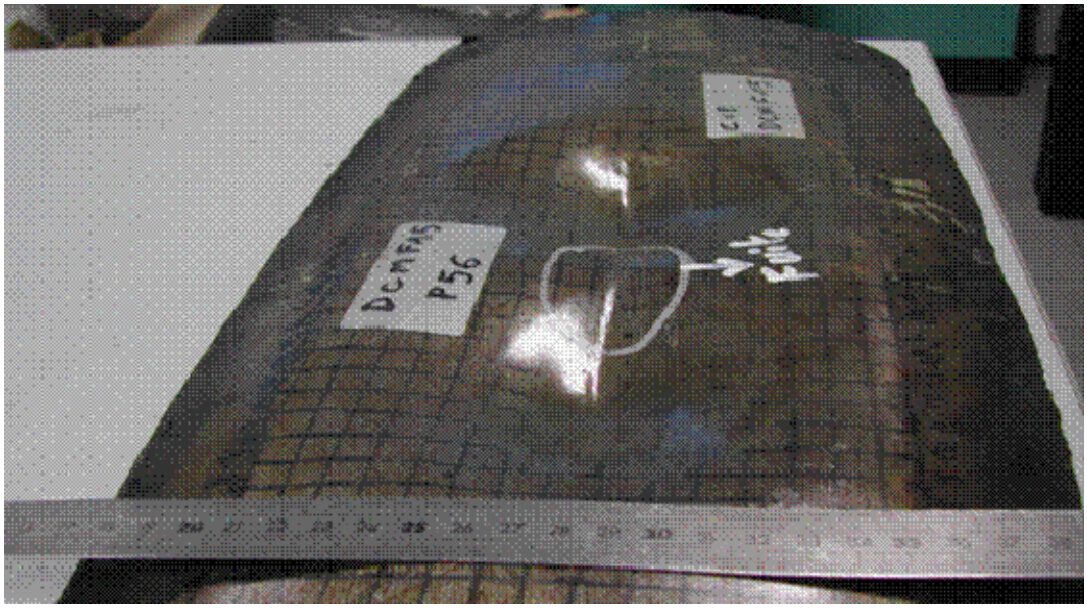

b)

Figure P56:1: Outer pipe wall – a) top view and b) end on view of P56 elongated dent which has partially re-rounded.

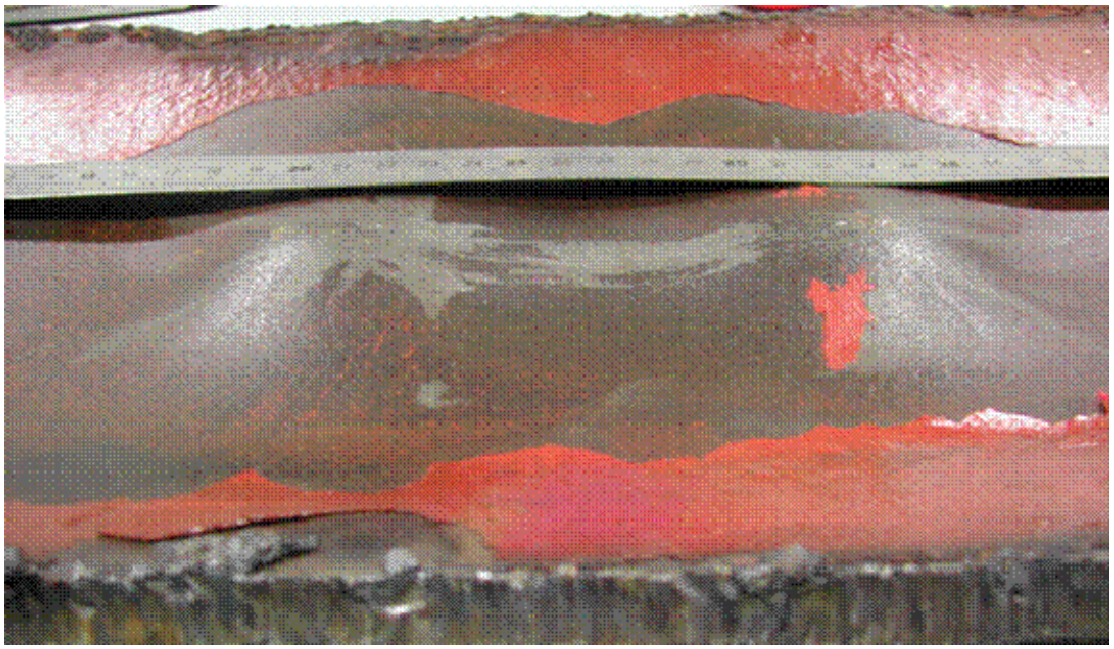

(a)

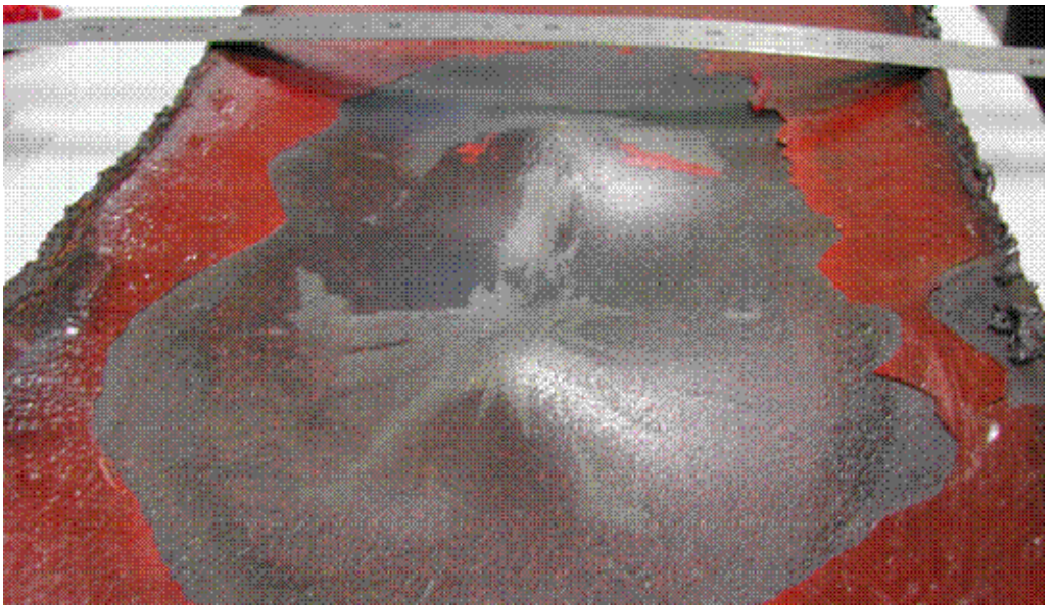

(b)

Figure P56:2: Inner pipe wall – a) side view and b) end on view of P56 elongated dent which has partially re-rounded.

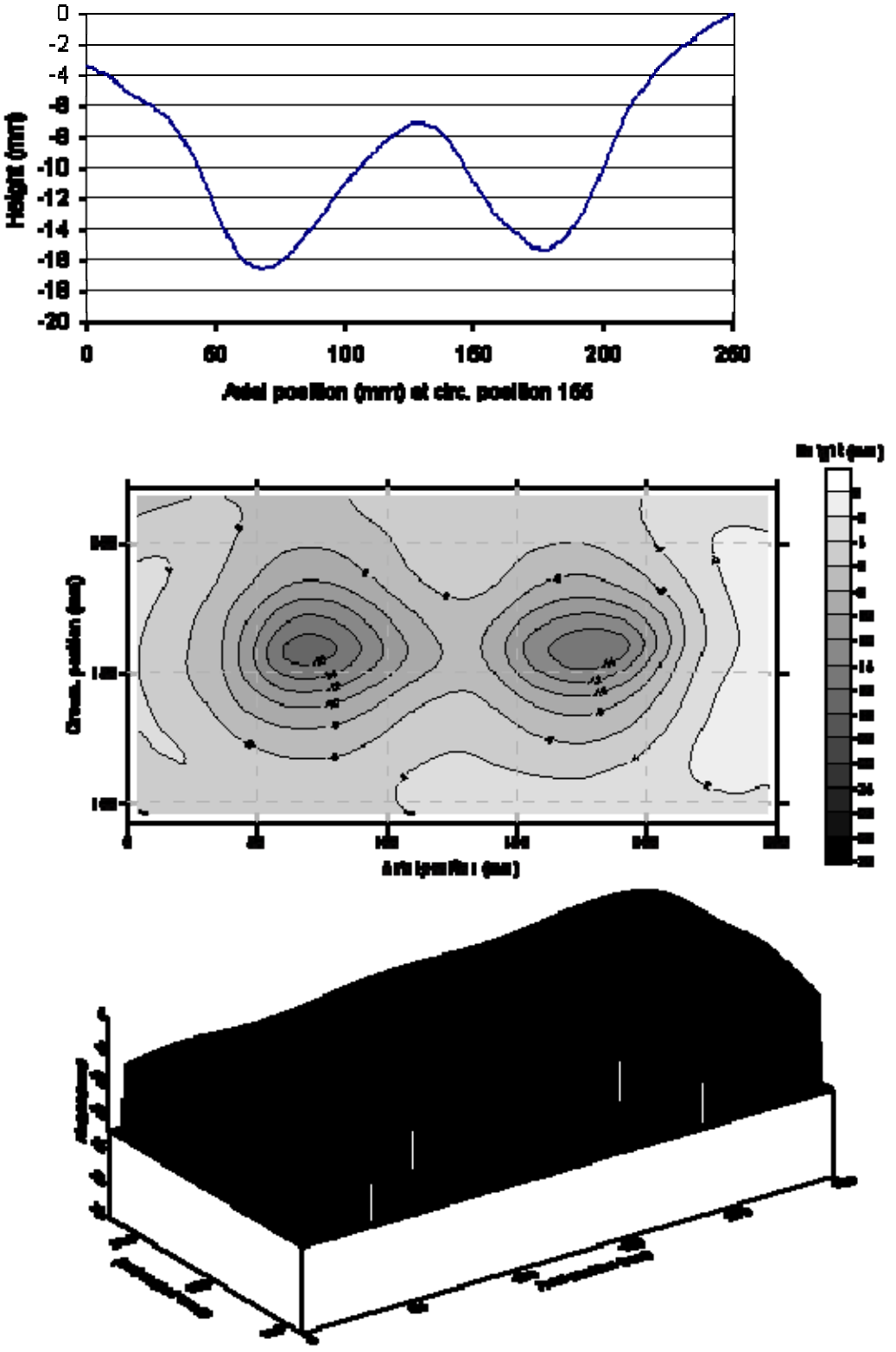

Figure P56:3: Laser geometry scan plots of Sample P56. Line scan through mid-width axial line (top), contour plot (middle), and 3D surface plot (bottom).

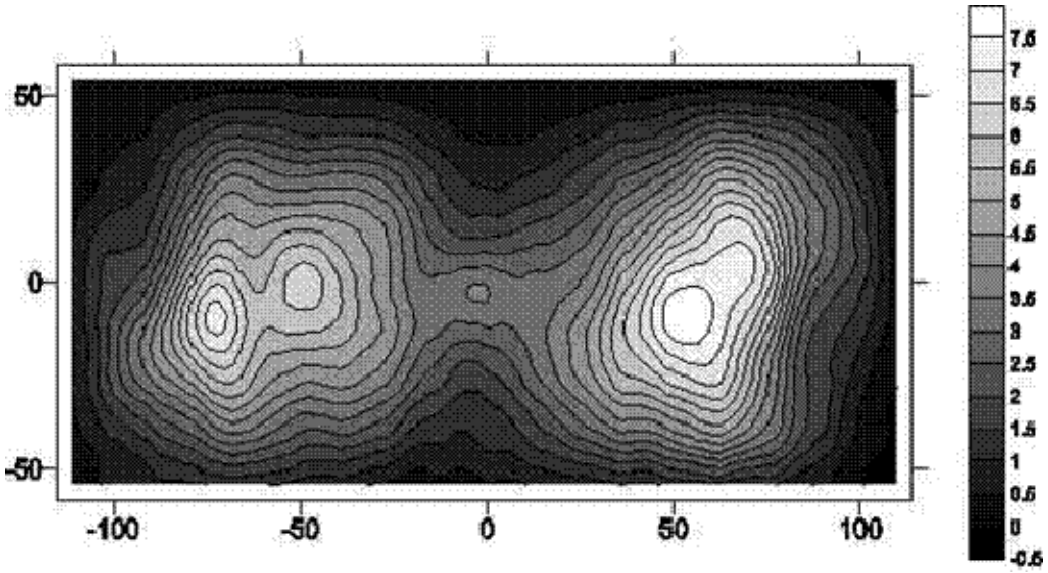

a)

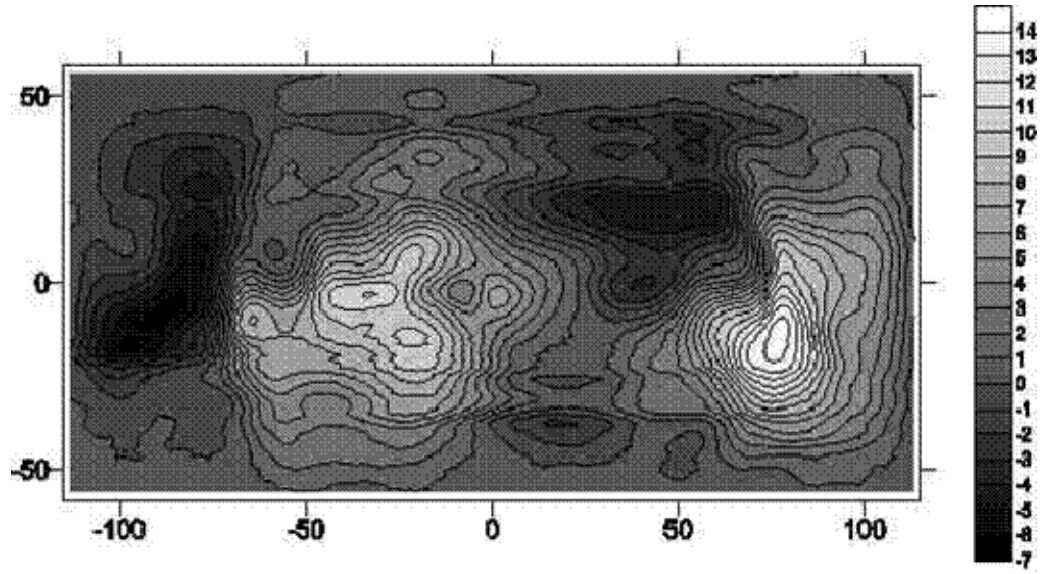

b)

Figure P56:4: MFL (measured) results for Sample P56. a) axial and b) radial.

APPENDIX II

Gaz de France Gouge sample – preliminary measurements

Sample P22

Identifying marks
P22 (also 110/1, also in chalk BEA110)

Sample description:
Sample size: 17cm x 38 cm.
There is a long significant gouge of 17 cm length – but with almost no indication on the inner surface of the pipe. So this is an excellent example of a 'gouge without a dent'. At one end of the gouge there is material exfoliated but still clinging to the surface. On the inside surface there is no apparent geometrical perturbation, except a very slight 'bump' near the end of the gouge that has the exfoliated metal.

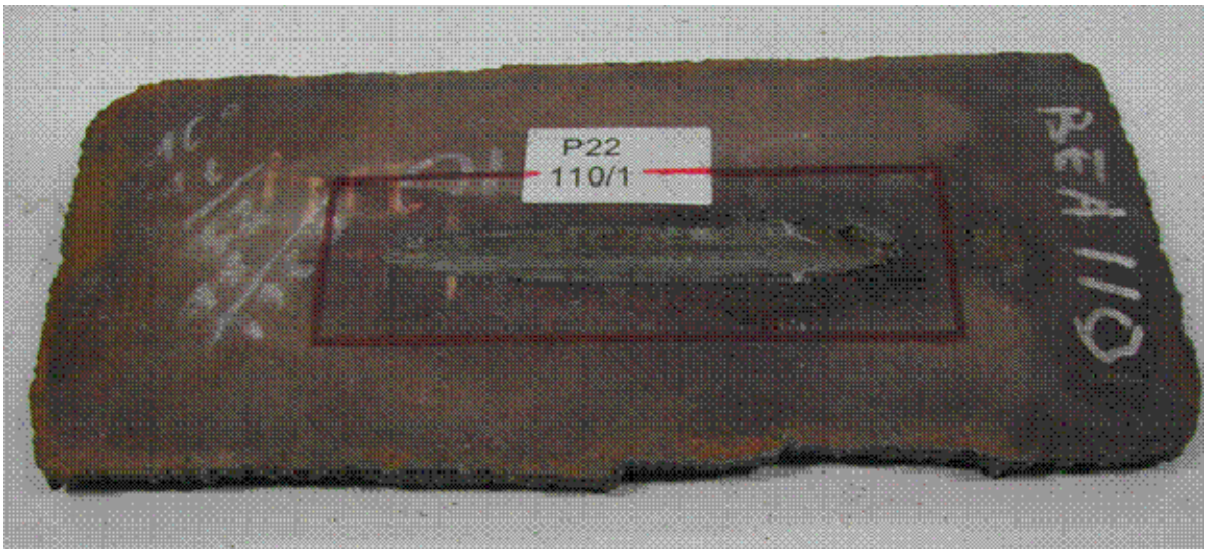

(a)

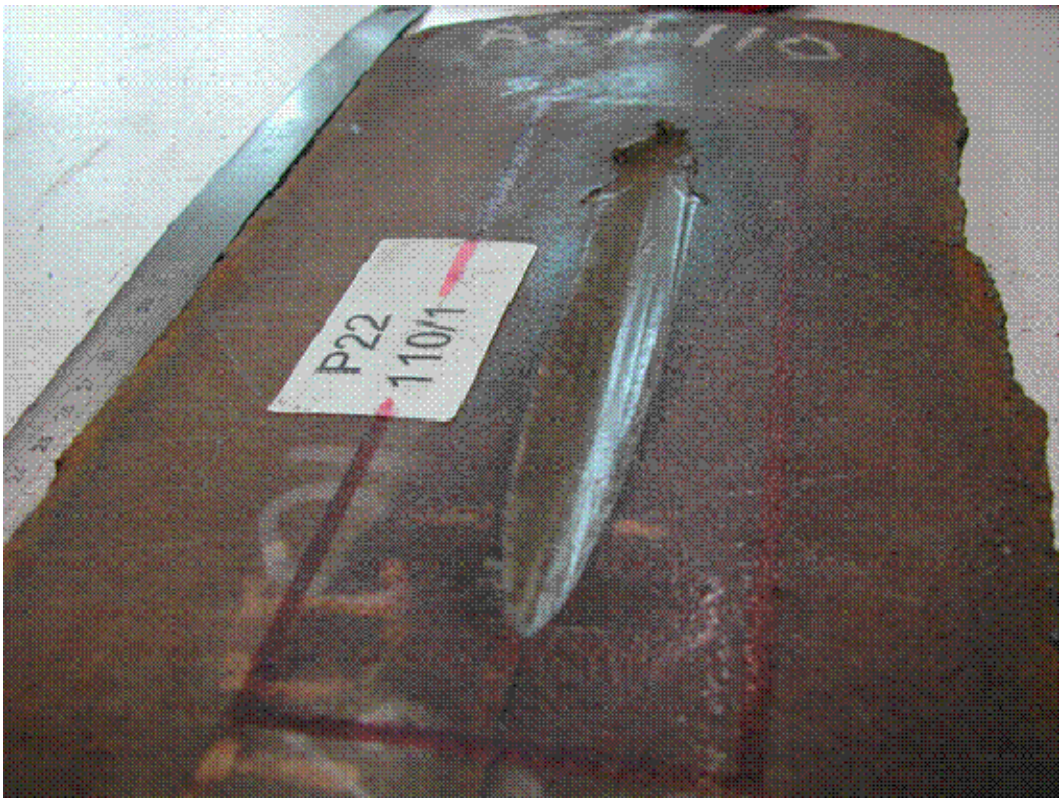

(b)

Figure P22:1: Outer pipe wall – a) top view and b) end-on view of P22 gouge.

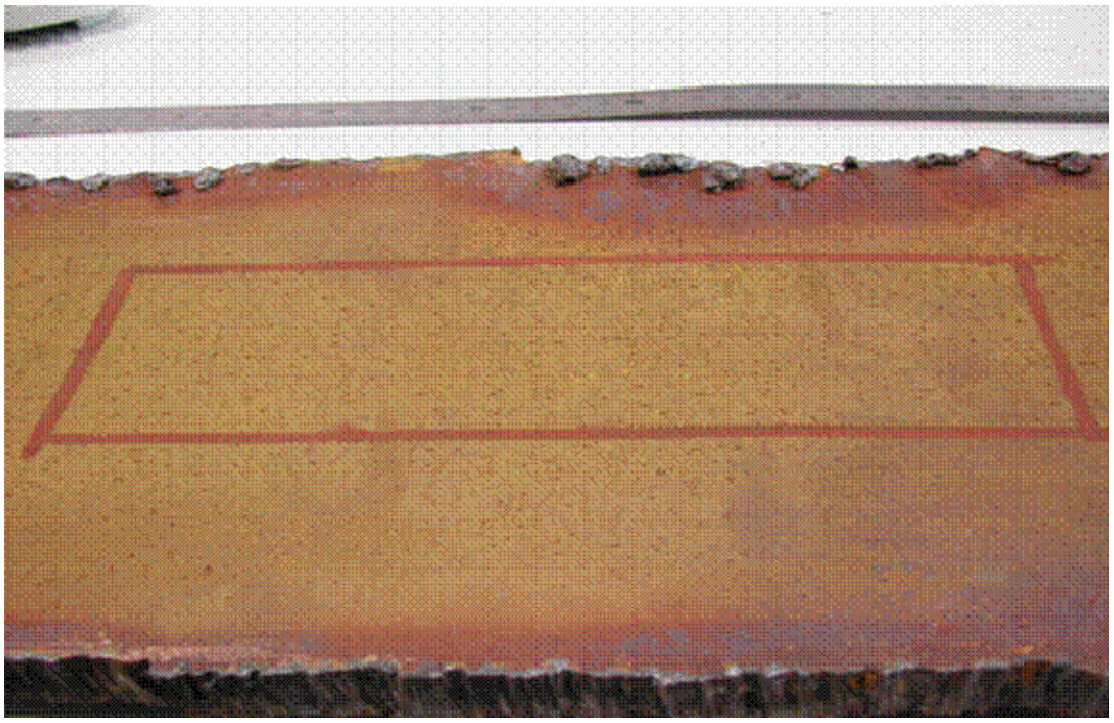

(a)

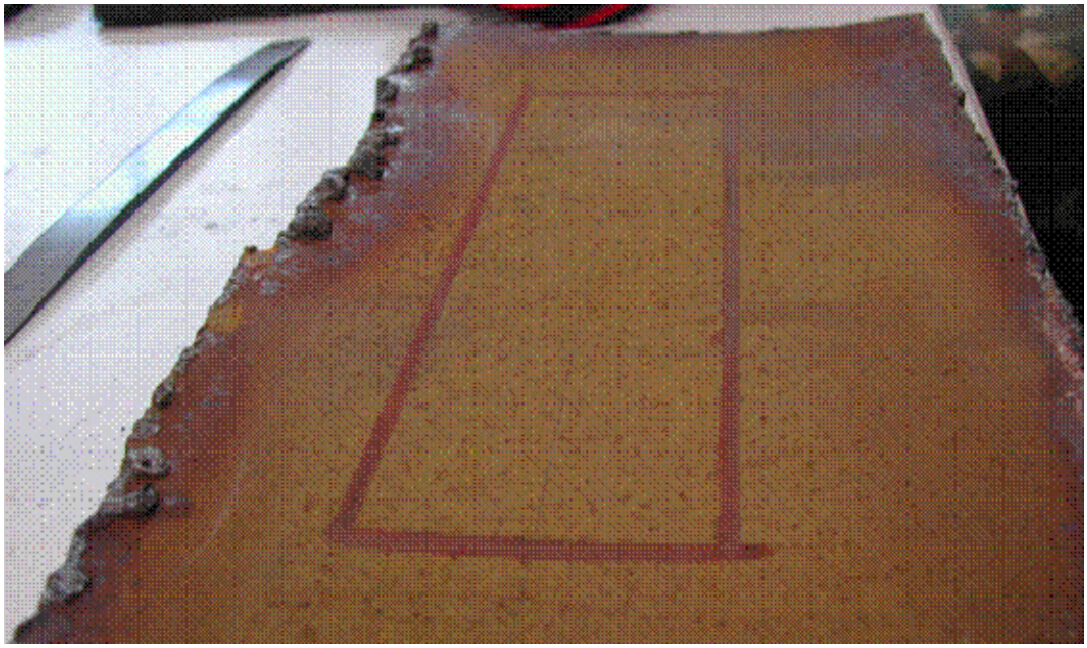

(b)

Figure P22:2: Inner pipe wall – a) top view and b) end-on view of scan area in red. There is essentially no geometry change on the inner wall.

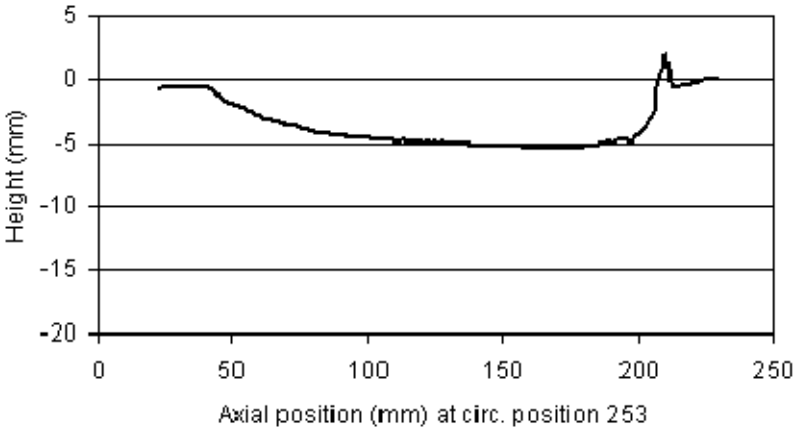

……

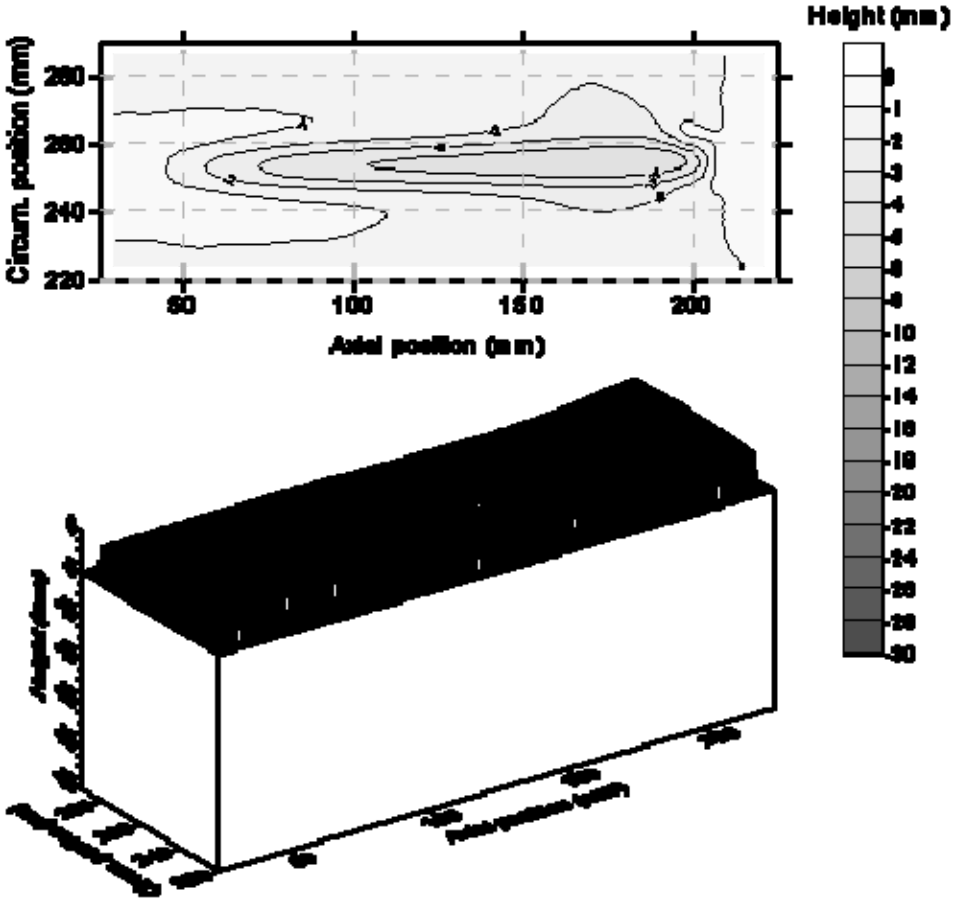

Figure P22.3: Laser geometry scan plots of Sample P22 (gouge). Line scan through mid-width axial line (top), contour plot (middle), and 3D surface plot (bottom).

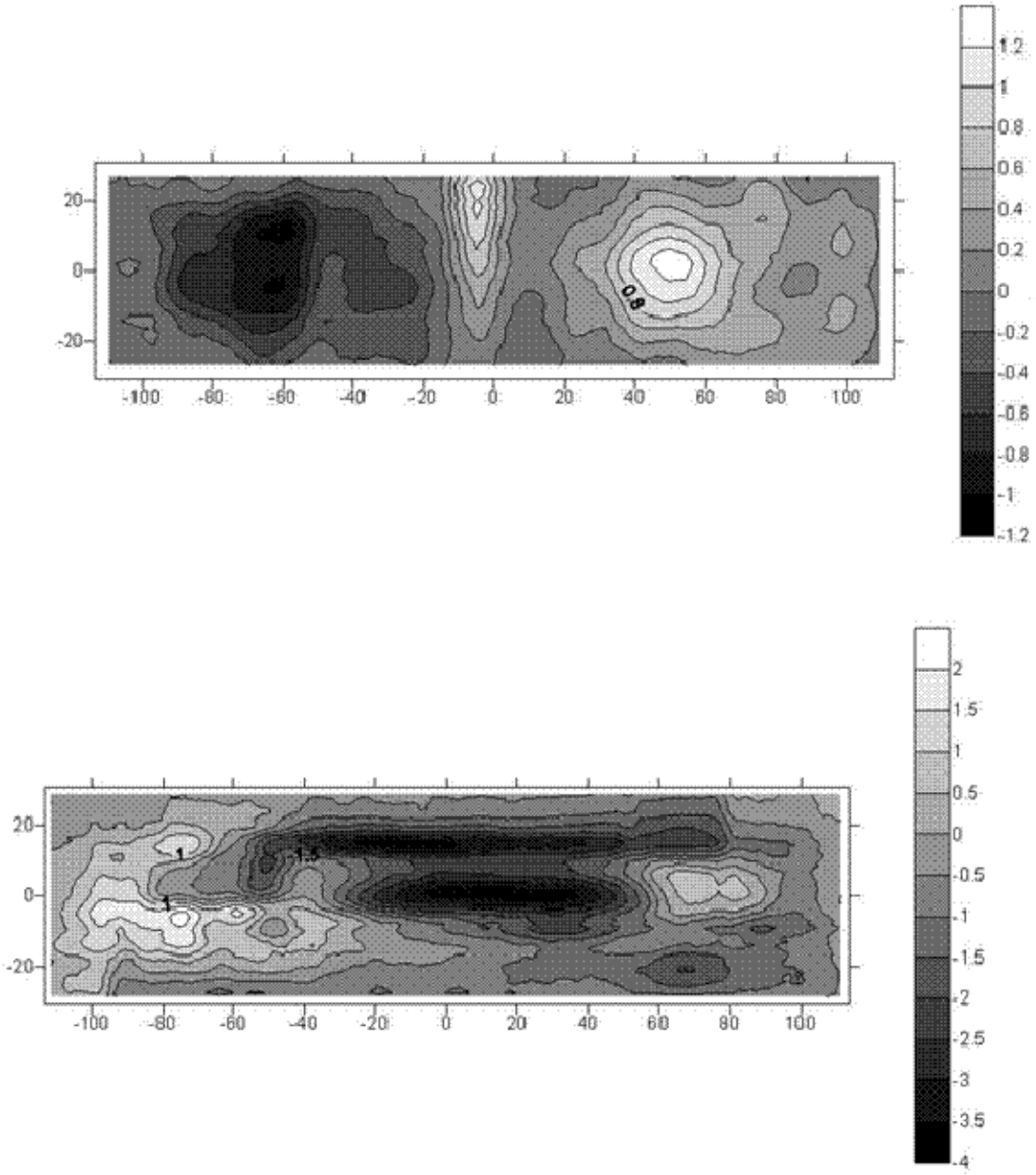

Figure P22:4: MFL (measured) results for Sample P22 (a) MFL_{axial} and (b) MFL_{radial} components.